Of Cells and Surfaces
for Bone Tissue Engineering

Ana Margarida Cravo Barradas

2012

Members of the Graduation Committee:

Chairman: Prof. Dr. G. van der Steenhoven	University of Twente
Promoter: Prof. Dr. C.A. van Blitterswijk	University of Twente
Co-Promoter: Prof. Dr. Jan de Boer	University of Twente
Members:	
Dr. P. Dankers	Technical University of Eindhoven
Prof. Dr. N. Geijsen	Hubrecht Institute
Dr. P. Habibovic	University of Twente
Prof. Dr. D.B.F. Saris	University of Twente
Dr. J. Schrooten	Catholic University of Leuven
Prof. Dr. L.W.M.M. Terstappen	University of Twente

Of Cells and Surfaces *for Bone Tissue Engineering*

Ana Margarida Cravo Barradas

PhD thesis, University of Twente, Enschede, The Netherlands

ISBN: 978-94-6191-325-8

Cover image and art work on page 129 by Lígia M.B.C. Barradas, inspired from tissue section images from Chapter 5 of this book.

Design and layout by Alexandre Paternoster and Ana M.C. Barradas

Press by Ipskamp Drukkers B.V.

The research described in this thesis was performed at the Department of Tissue Regeneration of the University of Twente, Enschede, The Netherlands, and financially supported by the Smart Mix Program of The Netherlands Ministry of Education, Culture and Science.

The publication of this thesis was financially supported by Metalúrgica António Barradas & Filhos Lda., Netherlands society for Biomaterials and Tissue Engineering, Netherlands society for Bone and Calcium, Xpand Biotechnology B.V. and Anna Fonds te Leiden.

OF CELLS AND SURFACES

FOR BONE TISSUE ENGINEERING

DISSERTATION

to obtain
the degree of doctor at the University of Twente,
on the authority of the rector magnificus,
Prof. Dr. H. Brinksma,
on account of the decision of the graduation committee,
to be publicly defended
on Thursday, June 21st, 2012, at 16:45

by

Ana Margarida Cravo Barradas
born on 9th February 1984
in Vila Viçosa, Portugal

Promoter:
Prof. Dr. C.A. van Blitterswijk (University of Twente)

Co-Promoter:
Prof. Dr. Jan de Boer (University of Twente)

À Lígia e ao Firmino,
por todo o amor

Summary

Bone Tissue Engineering (BTE) emerged from the need to find alternatives for the autologous bone graft, that despite many drawbacks is still the prime choice to heal bone defects (Chapter 1). Due to its multidisciplinary nature, BTE bridges subjects such as cell biology and materials sciences. This challenge requests strong communication between scientists from all fields to ensure safe, efficacious and efficient therapies for patients. The work described in this thesis tackles the interaction between cells and materials in BTE strategies, or more specifically, how particular physico-chemical properties of biomaterials influence the osteogenic differentiation of cells *in vitro* and bone formation *in vivo*. A general discussion and main conclusions are provided in Chapter 7.

Chapters 2, 3, 4 and 5 deal with a common subject: osteoinduction of calcium phosphate (CaP) ceramics. A literature review (Chapter 2) provides a general background on the topic, listing CaP ceramics tested, animal models used and discussing the most recent advances in the field. Although CaP ceramics with osteoinductive potential hold promise as bone graft substitutes, the biological mechanism that leads to bone formation is not understood but possibly related to specific physico-chemical properties.

The release of calcium (Ca^{2+}) from CaP ceramics into the body fluids is supposed to be part of the osteoinductive mechanism triggered by these materials. This hypothesis was tested with two *in vitro* models that explored the effect of Ca^{2+} in osteogenic differentiation of human bone marrow derived mesenchymal stromal cells (MSCs). In Chapter 3, MSCs were cultured on tissue culture polystyrene with different Ca^{2+} concentrations ($[Ca^{2+}]$). MSCs cultured with the highest $[Ca^{2+}]$ revealed highest expression of osteogenic markers such as osteopontin, osteocalcin, bone sialoprotein and bone morphogenetic protein 2. In Chapter 4, MSCs cultured in two different CaP ceramics exhibited higher expression of those markers in the ceramic of highest solubility (in a saline physiological solution), β-tricalcium phosphate (TCP), compared with the ceramic of lowest solubility, hydroxyapatite (HA), possibly correlating the extent of Ca^{2+} release from the ceramics with the extent of MSCs osteogenic differentiation.

Chapter 5 revealed a mouse model suitable for the study of osteinductive CaP ceramics *in vivo*. After a screen of mice from 11 different inbred mouse strains subjected to subcutaneous implantation of TCP, FVB arose has the most responsive mouse strain to the osteoinductive potential of TCP. This result not only shows the influence of genetic factors on osteoinductive potential of these ceramics, but it also opens the door for research possibilities not considered before, since until now large animals, such as goats, dogs and baboons, were preferred models. Chapter 6 revealed a polylactic acid (PLA)-gas plasma treated surface that favoured

osteogenic differentiation of MC3T3-E1 cells that could hold potential for the development of novel generation of bone graft substitutes. PLA disks subjected to different gas plasma treatments were altered in terms of their surface chemical composition, wettability and topography. Biological performance of the resulting disks was tuned accordingly. Interestingly the surface that favoured osteogenic differentiation of MC3T3-E1 cells induced the poorest cellular adhesion and lower cell numbers throughout the culturing period.

Samenvattig

Bot Tissue Engineering (BTE) is voortgekomen uit de behoefte om alternatieven te vinden voor autologe bot transplantatie, hetgeen nog altijd de behandeling van eerste keus is om botdefecten te overbruggen ondanks de vele nadelen die hiermee gepaard gaan (Hoofdstuk 1). Door de multidisciplinaire aard van BTE wordt een brug geslagen tussen onderwerpen als celbiologie en materiaalkunde. Deze uitdaging vergt goede communicatie tussen wetenschappers van alle vakgebieden om zodoende veilige, effectieve en efficiënte behandelingen voor patiënten te bewerkstelligen. Het werk dat in dit proefschrift wordt beschreven, gaat over de interactie tussen cellen en materialen in BTE-aanpak, of om meer specifiek te zijn, hoe bepaalde fysiek-chemische eigenschappen van biomaterialen de osteogene differentiatie van cellen *in vitro* en botvorming *in vivo* beïnvloeden. Een algehele discussie en voornaamste conclusies staan in Hoofdstuk 7.

Hoofdstukken 2,3,4 en 5 hebben een gemeenschappelijk onderwerp: osteoinductie van calciumfosfaat (CaP) keramieken. Een review (Hoofdstuk 2) biedt achtergrondinformatie over dit onderwerp, een opsomming van CaP keramieken die getest zijn, dierenstudies die gebruikt zijn en een discussie van recente ontwikkelingen in dit vakgebied. Hoewel CaP keramieken veelbelovend zijn als vervanging voor autologe bottransplantaten, is het biologische mechanisme dat leidt tot botvorming nog onduidelijk maar heeft mogelijk te maken met de specifieke fysiek-chemische eigenschappen. Het vrijkomen van calcium (Ca^{2+}) uit CaP keramieken in lichaamsvloeistoffen is waarschijnlijk een onderdeel van het osteoinductieve mechanisme waartoe deze materialen aanzetten. Deze hypothese is met twee *in vitro* modellen getest die het effect van Ca^{2+} op de osteogene differentiatie van humane mesenchymale stamcellen (MSCs) uit beenmerg onderzochten. In hoofdstuk 3 werden MSCs gekweekt op celkweek polystyreen met verschillende Ca^{2+} concentraties ($[Ca^{2+}]$). MSCs die gekweekt werden met de hoogste $[Ca^{2+}]$ toonden de hoogste expressie van osteogene markers zoals osteopontin, osteocalcine, bone sialoprotein en bone morphogenetic protein 2. In hoofdstuk 4 toonden MSCs die gekweekt waren op twee verschillende calcium keramieken de grootste expressie van deze markers bij het keramiek met de grootste oplosbaarheid (in een fysiologische zoutoplossing), tricalcium fosfaat (TCP) vergeleken met het keramiek met de laagste oplosbaarheid, hydroxyapatiet (HA), mogelijk is er een correlatie tussen de mate van Ca^{2+} die vrijkomt van de keramieken en de mate van de osteogene differentiatie van de MSCs.

In hoofdstuk 5 wordt een muismodel beschreven dat geschikt is om de osteoinductiviteit van CaP keramieken *in vivo* te onderzoeken. Na een screen van 11 verschillende inteelt muizenlijnen, waarbij TCP subcutaan geïmplanteerd was, kwam de FVB muis als beste responder lijn naar voren om het osteoinductieve potentie van TCP aan te tonen. Dit toont

niet alleen de invloed van genetische factoren op de osteoinductieve potentie van TCP, maar opent ook de deur naar nieuwe onderzoeksmogelijkheden die tot voor kort niet voor mogelijk werden gehouden, want grote diermodellen met geiten, honden en bavianen waren tot nu toe de standaard.

Hoofdstuk 6 onthult een polymelkzuur (PLA) oppervlak dat behandeld is met gasplasma, hetgeen gunstig is voor de osteogene differentiatie van MC3T3-E1 cellen waardoor dit de potentie heeft als nieuwe generatie van bottransplantaat vervangers. PLA schijven die aan verschillende gasplasma behandelingen waren blootgesteld, waren verschillend in chemische samenstelling, bevochtbaarheid en topografie. De biologische prestatie van de schijven werd overeenkomstig afgesteld. Interessant om te vermelden is dat het oppervlak dat de beste osteogene differentiatie gaf van MC3T3-E1 cellen, de slechtste hechting van cellen en het laagste aantal cellen gaf gedurende de kweekperiode.

Sumário

A Engenharia de Tecidos do Osso (ETO) surge da necessidade de encontrar alternativas à actual terapêutica do enxerto ósseo autólogo, que apesar de todas as suas desvantagens, continua a ser a principal escolha para a reconstrução de defeitos ósseos (Capítulo 1). Devido à sua natureza multidisciplinar, a ETO estabelece a ponte entre várias disciplinas, nomeadamente a Biologia Celular e a Engenharia de Materiais. Este desafio requer uma forte comunicação entre cientistas das várias áreas para assegurar que as novas terapêuticas propostas são seguras, eficazes e eficientes para o doente.

Esta tese aborda a interacção entre células de origens animal e humana e os materiais utilizados em estratégias de ETO, mais especificamente, como determinadas propriedades físico-químicas dos biomateriais podem influenciar a diferenciação osteogénica das células *in vitro* e a formação de osso *in vivo*. O trabalho experimental é descrito nos capítulos 3, 4, 5 e 6 e a discussão geral e as principais conclusões são apresentadas no Capítulo 7. Os Capítulos 2, 3, 4 e 5 tratam de um tópico comum: a capacidade osteoinductiva de cerâmicos de fosfatos de cálcio (CaF). No Capítulo 2, sumarizam-se conteúdos importantes para compreensão dos capítulos subsequentes através de uma revisão literária do tema. Aqui listam-se os principais materiais cerâmicos testados, os modelos animais utilizados e discutem-se os mais recentes desenvolvimentos científicos na área.

Apesar de os cerâmicos de CaF serem promissores substitutos do enxerto ósseo autólogo, o mecanismo biológico que leva à formação de osso ainda não foi compreendido, mas estará possivelmente relacionado com a sua natureza e organização estrutural, ou noutras palavras, com as suas propriedades físico-químicas. A libertação de cálcio (Ca^{2+}) dos cerâmicos de CaF nos fluídos corporais foi proposto por outros autores como uma parte importante na activação dos mecanismos de osteoinducção. Esta hipótese foi testada em dois modelos *in vitro* que exploraram os efeitos de Ca^{2+} na diferenciação osteogénica de células humanas mesenquimais derivadas da medula óssea (MMOs). No Capítulo 3, as MMOs foram cultivadas em frascos de poliestireno, em meio de cultura contendo diferentes concentrações de Ca^{2+}. As MMOs cultivadas com a concentração de Ca^{2+} mais alta revelaram expressão mais elevada de genes típicos da diferenciação osteogénica, tais como osteopontina, osteocalcina, sialoproteina óssea e proteina morfogenética óssea 2 (BMP-2). No Capítulo 4, as MMOs cultivadas em diferentes cerâmicos de CaF exibiram uma expressão mais elevada daqueles genes no cerâmico de maior solubilidade (em solução fisiológica), fosfato tricálcico (FTC), comparativamente com os resultados da expressão no cerâmico de menor solubilidade, hidroxiapatite (HA), possivelmente correlacionando a extensão da libertação de Ca^{2+} dos cerâmicos com a extensão da diferenciação osteogénica das MMOs.

No Capítulo 5 identificou-se um modelo de murganho adequado ao estudo *in vivo* dos cerâmicos de CaF osteoinductivos, depois de terem sido testados ratinhos de 11 estirpes *inbred* sujeitas a implantação subcutânea do FTC, tendo surgido a FVB como a mais permissiva ao potencial osteoinductivo do FTC. Este resultado mostrou a influência dos factores genéticos no potencial osteoinductivo destes cerâmicos e alargou o potencial de investigação, uma vez que até agora, grandes animais como cabras, cães e babuínos eram tidos como modelos preferencialmente utilizados.

No Capítulo 6 estuda-se a superfície de poli (ácido láctico) (PLA) tratada com gás plasma que favoreceu a diferenciação de células pré-osteoblásticas MC3T3-E1, indicando o seu potencial para o desenvolvimento de uma nova geração de substitutos do enxerto ósseo. Discos de PLA foram tratados com gás plasma e consequentemente a sua superfície foi alterada em termos de composição química, ângulo de contacto e topografia. O desempenho biológico dos discos foi alterado de acordo com essas modificações. Verificou-se também que a superfície que favoreceu a diferenciação osteogénica das células MC3T3-E1 foi também aquela que induziu a adesão celular mais fraca e a menor proliferação celular durante o período de cultura.

Contents

Chapter 1

Introduction

Bone composition and structure

Bone is a type of connective tissue that supports our body and in addition, protects vital organs. It consists of minerals (60%), organic components (30%) and we ter (10%) [1]. Due to this high mineral content, mainly calcium and phosphate, it plays an important role in calcium homeostasis [2, 3]. Structure wise, most bones are composed of an external layer of compact bone surrounding the inner trabecular bone. Compact bone is dense and less metabolically active than the spongy trabecular bone [4]. Bone marrow resides among the trabeculae, where haematopoiesis takes place (blood cells and platelets production) [5]. Firstly, when bone is deposited, it constitutes an unorganized form of bone, so called woven bone. It appears early in the fetus and after fracture healing and is later substituted by lamellar bone, an organized form of bone with aligned collagen fibers deposited in concentric sheets (osteon) [6]. Bone remodelling comprises of bone resorption and deposition of new bone, the orchestrated work of osteoclasts and osteoblasts cells respectively [7]. Osteoblasts deposit the organic matrix of the bone that later will be calcified to originate the mineral phase (ossification). They border areas where new bone is being formed. When entering a resting state they are called flat-bone lining cells. When incorporated in the matrix, they reside in lacunae and are called osteocytes. Osteoclasts are responsible for removing the bone mineral phase and to break down the organic components. Osteoclast activity can be triggered by osteoblast secretion of specific molecules such as NF-kB-ligand (RANK-L) and osteoprotegerin (OPG).

Bone formation

To arrive at the level of structural and functional complexity described above, two routes exist: intramembranous and endochondral bone formation [8]. Long bones of the skeleton form via the latter route, in which mesenchymal cells differentiate into chondrocytes in an avascular environment, producing a cartilage matrix. Before ossification, chondrocytes become hypertrophic and secrete collagen type X instead of II [9]. The cartilaginous template is then invaded by blood vessels, bringing along osteoprogenitor cells, concomitant with chondrocyte death. Ossification takes place except in the growth plates, located in the centre and

extremities of the bone that will remain throughout the first 20 years of life to enlarge the bones [2, 10]. The flat bones of the skull, by contrast, do not grow longitudinally. Here, intramembranous bone formation takes place during which mesenchymal cells aggregate and form condensates of loose mesenchymal tissue, prefiguring the skeletal elements. Within these aggregates, cells differentiate into osteoblasts when associated with adequate vasculature, directly initiating ossification. During fracture healing, both mechanisms can take place to repair the bone [11]. When a fracture is stable and with unchanged anatomy (e.g. a crack), intramembranous repair will occur. Otherwise, a cartilage template will initially stabilize the fracture and later be replaced by bone.

Transcriptional regulation of osteogenesis

The main events of transcriptional regulation of osteogenesis will be discussed here and are summarized in figure 1. In both endochondral bone formation and intramembranous ossification, osteoblasts differentiate from mesenchymal precursors [8]. Several molecules coordinate the differentiation process of which, undoubtedly, core binding factor alpha 1 (**cbfa-1**), also known as runt-related transcription factor 2 (**Runx-2**), is considered the master regulator [12]. Cbfa-1/Runx-2 expression is the earliest and most specific marker of osteogenesis [13]. Mice lacking this transcription factor develop a skeleton that is made of cartilage, as osteoblastic differentiation never occurs, and lack osteoclasts as well [14, 15].

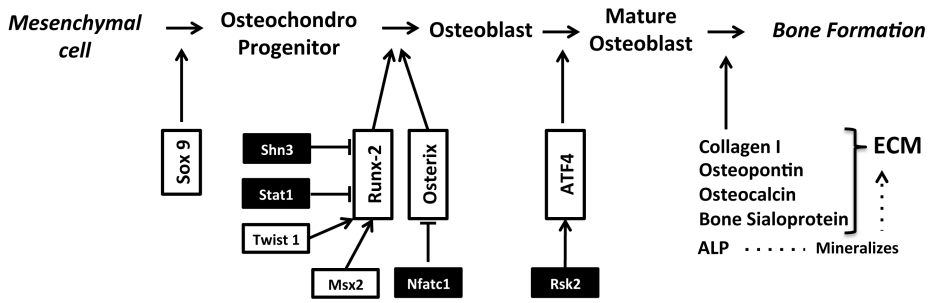

Figure 1: Schematic representation of the mesenchymal cell differentiation process leading to bone formation. Molecules in white boxes regulate at the transcriptional level and those in black boxes at the posttranscriptional level. Lines with arrows indicate activation whereas lines with bars indicate inhibition. For details see text. Adapted from Karsenty; Annu. Rev. Genomics Hum. Genet.; 2008.

Several transcription factors have been suggested to act upstream of Runx-2, such as Twist-1, that has been shown to delay osteogenesis via inhibition of Runx-2 [16]. Another inhibitor of Runx-2 is the homeobox protein encoded by **Hoxa-2** gene. Hoxa-2 deficient mice display ectopic bone formation associated with Runx-2 expression in the second branchial arches [17]. By contrast, mice lacking the muscle segment homeobox gene 2 (**Msx-2**) express less Runx-2 and osteocalcin (OC) and display defective ossification of the skull and bones that form via endochondral ossification [18]. Also mice lacking signal transducer and activator of transcription 1 (**Stat-1**) develop high bone mass. It has been suggested that

Stat-1 function is to inhibit Runx-2 translocation into the nucleus [19]. A similar function has been proposed for schnurri 3 (**Shn-3**), a zinc finger adapter protein, whose deletion in mice leads to an increase in bone matrix deposition [20]. **Osterix** is another transcription factor essential for osteoblast differentiation but believed to act downstream of Runx-2. Together with nuclear factor of activated T cells 1 (**Nfat-1**), osterix can activate transcription of osteoblast specific α1 (I) collagen [21]. In osterix-deficient mice, only bones formed via intramembranous ossification lack a mineralized matrix. Bones formed via the endochondral route show some mineralization degree although it resembles calcified cartilage [22]. Activating transcription factor 4 (**ATF4**) is required for efficient import of amino acids into osteoblasts in order to have proper synthesis of collagen type I [23]. Furthermore, it can also activate transcription of OC [24]. ATF4 deficient mice have a delayed skeletal development and low-bone mass phenotype caused by decreased bone formation [25]. Finally, ATF4 also regulates osteoclast differentiation and hence bone resorption through its expression in osteoblasts [26]. The activity of ATF4 is regulated by p90 ribosomal S6 protein kinase 2 (**RSK2**) [25]. RSK2 deficient mice also show decreased bone mass owing to impaired bone formation and reduced collagen type I synthesis. **Collagen type I** expression is therefore a phenotypical characteristic of mature osteoblasts. Collagen type I accounts for 90% of the extracellular matrix (ECM) and has a structural as well as mechanical role in the bone [27]. Patients suffering from mutations affecting the structure or abundance of collagen type I, as in the case of Osteogenesis Imperfecta, suffer from bone abnormalities ranging from bone fragility to high bone mineralization [28-31]. Besides collagen type I, mature osteoblasts are characterized by the ability to synthesize membrane associated bone-kidney-liver alkaline phosphatase (**ALP**). Although not bone tissue specific, this enzyme is believed to be involved in ECM mineralization through cleavage of pyrophosphate [32, 33] and is already expressed in pre-osteoblasts, prior to the mineralization process [34]. Among the non-collagenous proteins secreted by mature osteoblasts, the most specific one is **OC**, also known as bone Gla protein. This protein is undectatable in preosteoblasts and detected only in mature osteoblasts [34]. Together with Runx-2, they constitute the most specific markers for osteogenesis [35]. OC is in fact an inhibitor of bone formation. Mice lacking OC showed higher bone mass without impaired bone resorption [36]. Osteopontin (**OP**) and bone sialoprotein (**BSP**) are two other non-collagenous components of the ECM that share some structural features. The first accounts for 15% of all non-collagenous proteins in the bone [27]. After fracture healing, OP is upregulated in osteoblasts and mice lacking this protein presented a delay in several bone fracture healing stages [37]. BSP is almost exclusively produced by skeletal related cells, including osteoblasts, osteocytes and hypertrophic chondrocytes. It plays an important role as nucleator of mineralization [38] and increases osteoblast differentiation [39].

G-Protein Coupled Receptor signaling

G-Protein Coupled Receptors (GPCRs) mediate cellular responses to extracellular signals, including hormones, neurotransmitters and local mediators. There are about 500 GPCRs in humans, making them promising drug targets [40]. An example is parathyroid hormone (PTH) ligand that targets PTH receptor 1 (PTHR1) [41] and is effective in the treatment of osteoporosis [42]. All GPCRs have a similar structure, consisting of a single polypep-

tide chain that threads back and forth across the lipid bilayer seven times. Ligand binding alters the receptor conformation which activates trimeric GTP-binding protein (G protein). G proteins are composed of three subunits: α, β and γ. Upon ligand binding, the GDP bound to the α subunit is replaced by GTP inducing conformational changes in the G protein that leads to interaction with the intracellular targets, which are either enzymes or ion channels in the plasma membrane. Inactivation of the α subunit reverses the GPCR activity [43, 44]. This can be controlled by regulator of G-protein signaling (RGS) protein that acts as a α-subunit-specific GTPase-activating protein, shutting off the initial response to the ligand [45-47]. GPCRs can be coupled to different types of G proteins. Depending on the type of G protein, different downstream signaling events will occur. In the case of inhibitory G proteins (Gi), ligand binding will lead to inhibition of adenylyl cyclase. On the other hand, if the G protein is a stimulatory G protein (Gs), activation of adenylyl cyclase will lead to conversion of cyclic adenosine monophosphate (cAMP) from adenosine triphosphate (ATP). Accumulation of cAMP in the cytoplasma will activate protein kinase A (PKA) to release its catalytic subunits. A-kinase anchoring proteins (AKAPs) bind both to regulatory subunits and to a component of the cytoskeleton or membrane of an organelle to allocate the enzyme to a particular subcellular compartment [48]. PKA can enter in the nucleus and phosphorylate a gene regulatory protein called cAMP response element (CRE) binding (CREB) protein that binds to a short DNA sequence known as CRE. In the past we have highlighted the influence of cAMP/PKA pathways in osteogenic differentiation in vitro and bone formation in vivo [49-51].

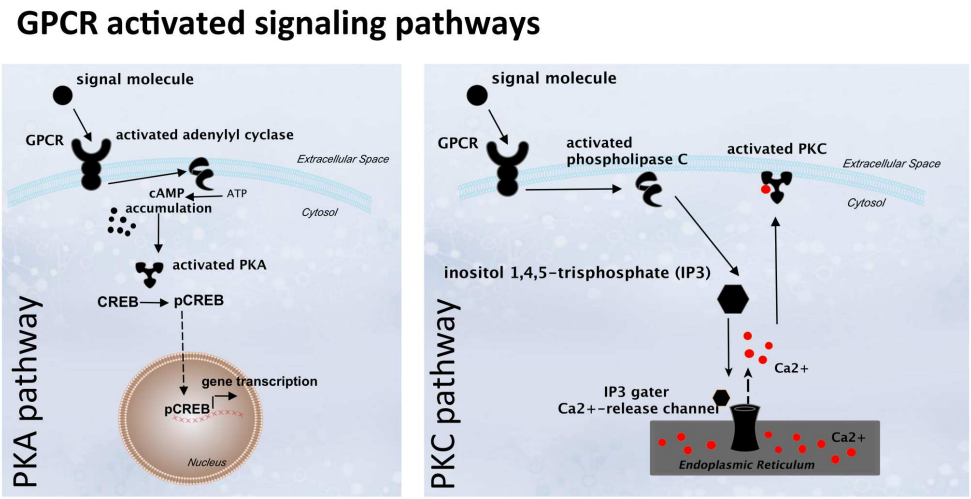

Figure 2: Schematic depiction of GPCR activated signaling pathways. When a signal molecule binds to a GPCR, it alters the receptor conformation which in turn activates G proteins. This leads to activation of downstream signaling events, such as PKA (left diagram) or PKC (right diagram) pathways. For details, see text.

GPCRs can also stimulate the plasma-membrane-bound phospholipase C-β (PLC β), mainly via Gq proteins, which in turn leads to release of Ca^{2+} from the endoplasmic reticu-

lum, through inositol 1,4,5-trisphosphate (IP3)-gated Ca^{2+} release channels. Ca^{2+} concentration increases in the cytosol and together with diacylglycerol and phosphatidylserine activate PKC [52]. PKA and PKC signaling pathways are schematically represented in figure 2.

Bone graft substitutes

Nowadays there are 893×10^6 people older than 60 years. By the end of this decade that number will raise to 2.4×10^9 [53] because fortunately we have a platelet of cares that we didn't have before that allows us to live longer. But growing older means a weaker body, prone to tissue and organ failure, and the increase in the amount of old people will be concomitant with the increase in the number of associated joint disorders, injuries and treatments needed.

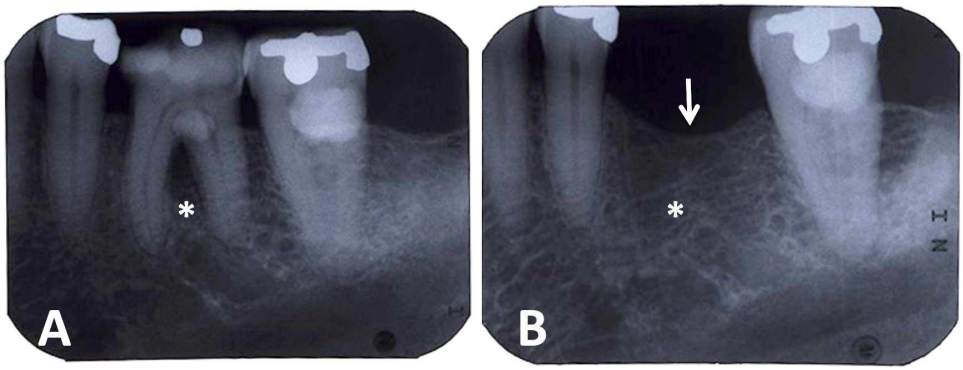

Figure 3: Bone resorption after tooth extraction. A) Notice the original bone (*) level. B) Two years after tooth extraction, bone has been resorbed and the original level lowered down. Courtesy of Mr. Tiago Cruz de Sousa Braga.

When the bone's own repair mechanisms fail, e.g. in non-union fractures after tumour removal or when maxillary augmentation is needed after teeth extraction (figure 3), for instance, bone grafts are the preferable treatment [54-56]. This implies the use of bone collected from other anatomical locations in the patient (if autologous) than the one to be repaired, usually the iliac crest, and placing it to fill the void space. However, this procedure implies an additional surgery to the patient, with associated tissue morbidity, pain. Additionally only a limited amount of tissue can be harvested. Although effective and efficient, it has drawbacks and alongside an ageing population, alternatives are rapidly needed. As a consequence, the market for bone graft substitutes (BGS) has largely expanded, boosting research along. It has been estimated to be $1.9 billion in 2010 and is forecast to reach $3.3 billion in 2017 (http://www.globaldata.com/reportstore). BGS can be synthetic materials and among those, ceramic- and polymer- based will be briefly described here. BGS can also be synthetic materials combined with biological substances or formulations in between, such as the case of demineralized bone matrix (DBM) [57-59]. DBM has a biological origin (bone derived from cadavers or animals) but is further processed to provide a demineralized matrix without losing key biological components thought to render it osteoinductive [60-62]. Furthermore, BGS are

usually defined in terms of their *osteoconductivity*, *osteoinductivity* and *osteogenicity*, which are characteristics that autologous bone grafts posses [63-66]:

- **osteoconductivity** is the property that allows migration of potentially osteogenic cells to the site of future matrix formation at the site of orthotopic implantation;
- **osteoinductivity** refers to the ability to trigger osteogenesis (bone formation);
- **osteogenicity** is the presence of bone forming cells (applicable in the case of cell-based therapies, which will be discussed later).

Ceramic-based BGS can be made from calcium phosphate (CaP) (e.g. tricalcium phosphate (TCP), hydroxyapatite (HA), biphasic calcium phosphate), calcium sulphate or glass [54]. Most CaP ceramics are osteoconductive and some are also osteoinductive [67]. It is suggested but not fully understood that the physico-chemical properties of such materials are at the origin of their ability to induce bone formation [68-70]. Chemical composition, macro-architecture and surface micro- and nano-structure are among those properties. These can be tailored during chemical synthesis and manufacturing. Hence, different formulations will influence the bone grafting potential of such materials. Although osteoinductive CaP ceramics are promising BGS, the exact mechanism via which osteoinductive materials trigger bone formation is unknown. Chapter 2 reviews extensively the latest developments in this research field. Polymers are attractive options as BGS due to their mechanical properties. Commercial BGS are either based on resorbable polyesters, such as polylactic acid (PLA) and polyglycolic acid (PGA), or on polymethyl metacrylate (PMMA). However, due to their poor osteointegration and lack of osteoinductive properties, products based on these polymers are often combined with CaP derivatives in order to overcome those hurdles. Examples are OsteoScaf^{TM}(Tissue Regeneration Therapeutics Inc. Toronto, Canada), which consists of PLGA (PLA/PGA) coated with a CaP layer [71] and Cortoss^{TM}(Stryker Corporation, Kalamazoo, Michigan, U.S.), consisting primarily of bis-GMA (2,2-bis[4-(2-hydroxymethacryloxypropyl) phenyl]propane) and glass ceramic particles, mainly used for spine surgery [72].

Cell-Based therapies in Bone Tissue Engineering

Other alternatives to the autologous bone grafts are cell-based therapies. In this approach, stem cells are used as bone forming units and/or signaling vehicles that transmit molecular instructions among them or to the patient's tissue surroundings. Stem cells are, per definition, cells with capacity of self-renewal and ability to differentiate into multiple lineages of adult tissues, making them an attractive choice for different clinical applications. In general, cell-based therapies comprise of harvesting stem cells from the patient, in vitro processing and implantation of the resulting product back into the patient. During in vitro processing, cells are expanded, exposed to signaling molecules and/or seeded onto carrier materials (e.g. ceramic or polymeric scaffolds) [73, 74]. Multiple formulations of cells, signaling molecules and scaffold materials have been tested, owing to the multidisciplinary aspect of the tissue engineering field, which gathers knowledge from several sciences such as biology, chemistry, medicine and engineering [75]. HEALOS® Bone Graft Replacement (Depuy Orthopeadics

Inc, Warsaw, Indiana, U.S.) is an example of a bone tissue engineering product, composed of cross-linked type I bovine collagen fibers coated with hydroxyapatite and intended to be used in combination with bone marrow aspirates.

Bone marrow derived cells have been widely used as a source of mesenchymal stem cells (MSCs) for tissue engineering applications. Traditionally bone marrow aspirates are placed in tissue culture plastics and the fraction of MSCs corresponds to that of adherent cells [76]. These cells are also referred to as bone marrow derived stromal cells and are able to differentiate into osteogenic, chondrogenic, adipogenic and myogenic lineages [77], but in contrast to what the term *stem cells* suggests, MSCs undergo replicative senescence, which can have implications at the therapeutical level [78, 79]. Induction into the osteogenic lineage, as well as into any other lineage, can be achieved through specific culture medium formulations. Soluble factors such as dexamethasone, cAMP, bone morphogenetic proteins (BMPs), Ca^{2+} and vitamin D3 can differentiate MSCs into osteoblasts [50, 80-85].

Outline of this thesis

The aim of this thesis is to relate specific physico-chemical properties of materials to the biological responses they elicit in *in vitro* and *in vivo* models, particularly regarding the osteogenic differentiation of stem cells and bone formation.

Chapter 2 gives a comprehensive overview of osteoinductive CaP ceramics. It debates questions such as the significance of currently used *in vitro* and *in vivo* models to the study of these ceramics as well as the physico-chemical properties identified in literature as key elements necessary to trigger bone formation. One of such properties is the chemical composition of these materials, of which Ca^{2+} has been postulated to play a determinant role in the biological response of the host.

Chapter 3 demonstrates that MSCs exhibit an osteoblastic phenotype when exposed to a high extracellular Ca^{2+} concentration. The cellular response to such environment is characterized regarding morphological features, proliferation and gene expression. Finally a signaling pathway is proposed to explain how Ca^{2+} triggers BMP-2 expression.

Chapter 4 demonstrates that BMP-2 expression in MSCs is also induced when cells are cultured in β-TCP compared to HA. MSCs attachment and differentiation are compared between these two ceramics, which are distinct in their chemical composition, microstructural properties and bone inductive capacity *in vivo*.

β-TCP also induces bone formation in a mouse model, which is revealed in *Chapter 5*. It further explores the physiological response of mice to different CaP ceramics and the role of blood vessel formation.

Chapter 6 presents the use of PLA treated with gas plasma to guide osteogenic differentiation of osteoprogenitor cells in vitro. Resulting PLA surfaces exhibit differences at the topographical, chemical and wettability levels. Protein and cell adhesion are tuned as well as osteogenic differentiation.

Chapter 7 is where the general discussion and main conclusions of this thesis are presented.

References

[1] Athanasiou KA, Zhu C, Lanctot DR, Agrawal CM, Wang X. Tissue Eng. 2000; 6(4):361-81.
[2] Erlebacher A, Filvaroff EH, Gitelman SE, Derynck R. Cell. 1995;80(3):371-8.
[3] Zaidi M. Skeletal remodeling in health and disease. Nat Med. 2007;13(7):791-801.
[4] Seeman E, Delmas PD. N Engl J Med. 2006;354(21):2250-61.
[5] Wilson A, Trumpp A. Nat Rev Immunol. 2006;6(2):93-106.
[6] Gorski JP. Crit Rev Oral Biol Med. 1998;9(2):201-23.
[7] Rosen CJ. Cell Metab. 2008;7(1):7-10.
[8] Karsenty G. Nature. 2003;423(6937):316-8.
[9] Mundlos S. Prog Histochem Cytochem. 1994;28(3):1-47.
[10] Mackie EJ, Ahmed YA, Tatarczuch L, Chen KS, Mirams M. Int J Biochem Cell Biol. 2008;40(1):46-62.
[11] AI-Aql ZS, Alagl AS, Graves DT, Gerstenfeld LC, Einhorn TA. J Dent Res. 2008;87(2):107-18.
[12] Karsenty G. Endocrinology. 2001;142(7):2731-3.
[13] Ducy P, Zhang R, Geoffroy V, Ridall AL, Karsenty G. Cell. 1997;89(5):747-54.
[14] Ducy P. Dev Dyn. 2000;219(4):461-71.
[15] Komori T, Yagi H, Nomura S, Yamaguchi A, Sasaki K, Deguchi K, Shimizu Y, et al. Cell.1997;89(5):755-64.
[16] Bialek P, Kern B, Yang X, Schrock M, Sosic D, Hong N, Wu H, et al. Dev Cell. 2004;6(3):423-35.
[17] Kanzler B, Kuschert SJ, Liu YH, Mallo M. Development. 1998;125(14):2587-97.
[18] Satokata I, Ma L, Ohshima H, Bei M, Woo I, Nishizawa K, Maeda T, et al. Nat Genet. 2000;24(4):391-5.
[19] Kim S, Koga T, Isobe M, Kern BE, Yokochi T, Chin YE, Karsenty G, et al. Genes Dev. 2003;17(16):1979-91.
[20] Jones DC, Wein MN, Oukka M, Hofstaetter JG, Glimcher MJ, Glimcher LH. Science. 2006;312(5777):1223-7.
[21] Koga T, Matsui Y, Asagiri M, Kodama T, de Crombrugghe B, Nakashima K, Takayanagi H. Nat Med. 2005;11(8):880-5.
[22] Nakashima K, Zhou X, Kunkel G, Zhang Z, Deng JM, Behringer RR, de Crombrugghe B. Cell. 2002;108(1):17-29.
[23] Harding HP, Zhang Y, Zeng H, Novoa I, Lu PD, Calfon M, Sadri N, et al. Mol Cell. 2003;11(3):619-33.
[24] Ducy P, Karsenty G. Mol Cell Biol. 1995;15(4):1858-69.
[25] Yang X, Matsuda K, Bialek P, Jacquot S, Masuoka HC, Schinke T, Li L, et al. Cell. 2004;117(3):387-98.
[26] Elefteriou F, Ahn JD, Takeda S, Starbuck M, Yang X, Liu X, Kondo H, et al. Nature. 2005;434(7032):514-20.
[27] Allori AC, Sailon AM, Warren SM. Tissue Eng Part B Rev. 2008;14(3):275-83.
[28] Boyde A, Travers R, Glorieux FH, Jones SJ. Calcif Tissue Int. 1999;64(3):185-90.
[29] Roschger P, Fratzl-Zelman N, Misof B, Glorieux F, Klaushofer K, Rauch F. Calcif Tissue Int. 2008;82(4):263-70.
[30] Roschger P, Paschalis EP, Fratzl P, Klaushofer K. Bone. 2008;42(3):456-66.
[31] Grabner B, Landis WJ, Roschger P, Rinnerthaler S, Peterlik H, Klaushofer K, Fratzl P. Bone. 2001;29(5):453-7.
[32] Murshed M, Harmey D, Millan JL, McKee MD, Karsenty G. Genes Dev. 2005;19(9):1093-104.
[33] Terkeltaub RA. Am J Physiol Cell Physiol. 2001;281(1):C1-C11.
[34] Aubin JE. Biochemistry and cell biology = Biochimie et biologie cellulaire. 1998;76(6):899-910.
[35] Ducy P, Schinke T, Karsenty G. Science. 2000;289(5484):1501-4.
[36] Ducy P, Desbois C, Boyce B, Pinero G, Story B, Dunstan C, Smith E, et al. Nature.1996;382(6590):448-52.
[37] Duvall CL, Taylor WR, Weiss D, Wojtowicz AM, Guldberg RE. J Bone Miner Res. 2007;22(2):286-97.
[38] Tye CE, Rattray KR, Warner KJ, Gordon JAR, Sodek J, Hunter GK, Goldberg HA. J Biol Chem. 2003;278(10):7949-55.
[39] Gordon JAR, Tye CE, Sampaio AV, Underhill TM, Hunter GK, Goldberg HA. Bone. 2007;41(3):462-73.
[40] Koen J D. Drug Discov Today. 2005;10(12):857-64.
[41] Thomas BE, Sharma S, Mierke DF, Rosenblatt M. J Bone Miner Res. 2009;24(5):925-34.
[42] Baron R, Hesse E. J Clin Endocrinol Metab. 2012;97(2):311-25.
[43] Luttrell L. Mol Biotechnol. 2008;39(3):239-64.
[44] Robishaw JD, Berlot CH. Curr Opin Cell Biol. 2004;16(2):206-9.
[45] Roy AA, Baragli A, Bernstein LS, Hepler JR, Hebert TE, Chidiac P. Cell Signal. 2006;18(3):336-48.
[46] Tsingotjidou A, Nervina JM, Pham L, Bezouglaia O, Tetradis S. Bone. 2002;30(5):677-84.
[47] Roman DL, Traynor JR. J Med Chem. 2011;54(21):7433-40.
[48] McConnachie G, Langeberg LK, Scott JD. Trends Mol Med. 2006;12(7):317-23.
[49] Siddappa R, Mulder W, Steeghs I, van de Klundert C, Fernandes H, Liu J, Arends R, et al. Tissue Eng Part A. 2009;15(8):2135-43.

[50] Siddappa R, Doorn J, Liu J, Langerwerf E, Arends R, van Blitterswijk C, de Boer J. J Tissue Eng Regen Med. 2009;4(5):356-65.
[51] Siddappa R, Martens A, Doorn J, Leusink A, Olivo C, Licht R, van Rijn L, et al. Proc Natl Acad Sci USA. 2008;105(20):7281-6.
[52] Liebmann C, Bohmer FD. Curr Med Chem. 2000;7(9):911-43.
[53] The State of World Population 2011: People and Possibilities in a World of 7 billion. New York: Information and External Relations Division of United Nations Population Fund; 2011.
[54] Damien CJ, Parsons JR. J Appl Biomater. 1991;2(3):187-208.
[55] Habal M. and Reddi A. (eds). Bone grafts & bone substitutes. W. B. Saunders, New York, 1992.
[56] Calori GM, Mazza E, Colombo M, Ripamonti C. Injury. 2011;42, Supplement 2(0):S56-S63.
[57] Pacaccio DJ, Stern SF. Clin Podiatr Med Surg. 2005;22(4):599-606
[58] Biswas D, Bible JE, Whang PH, Miller CP, Jaw R, Miller S, Grauer JN. Am J Orthop (Belle Mead, NJ). 2010;39(11):531-8.
[59] Tassos I. J Oral Maxillofac Surg. 2011;69(1):134-41.
[60] Urist MR. Science. 1965;150(3698):893-9.
[61] Urist MR, Iwata H. J Theor Biol. 1973;38(1):155-67.
[62] Han B, Yang Z, Nimni M. J Orthop Res. 2008;26(1):75-82.
[63] Albrektsson T, Johansson C. Eur Spine J. 2001;10 Suppl 2:S96-101.
[64] Van der Stok J, Van Lieshout EMM, El-Massoudi Y, Van Kralingen GH, Patka P. Acta Biomater. 2011;7(2):739-50.
[65] Cypher TJ, Grossman JP. J Foot Ankle Surg. 1996;35(5):413-7.
[66] Giannoudis PV, Dinopoulos H, Tsiridis E. Injury. 2005;36(3, Supplement):S20-S7.
[67] LeGeros RZ. Chem Rev. 2008;108(11):4742-53.
[68] Yuan H, Fernandes H, Habibovic P, de Boer J, Barradas AM, de Ruiter A, Walsh WR, et al. Proc Natl Acad Sci USA. 2010;107(31):13614-9.
[69] Habibovic P, Sees TM, van den Doel MA, van Blitterswijk CA, de Groot K. J Biomed Mater Res A. 2006;77(4):747-62.
[70] Ripamonti U, Crooks J, Kirkbride AN. S Afr J Sci. 1999;95(8):335-43.
[71] Lickorish D, Guan L, Davies JE. Biomaterials. 2007;28(8):1495-502.
[72] Pomrink GJ, DiCicco MP, Clineff TD, Erbe EM. Biomaterials. 2003;24(6):1023-31.
[73] Zhang Z. Front Med. 2011;5(4):401-13.
[74] Demirbag B, Huri PY, Kose GT, Buyuksungur A, Hasirci V. Biotechnol J. 2011;6(12):1437-53.
[75] Langer R, Vacanti JP. Science. 1993;260(5110):920-6.
[76] Friedenstein AJ, Chailakhyan RK, Latsinik NV, Panasyuk AF, Keiliss-Borok IV. Transplantation. 1974;17(4):331-40.
[77] Pittenger MF, Mackay AM, Beck SC, Jaiswal RK, Douglas R, Mosca JD, Moorman MA, et al. Science. 1999;284(5411):143-7.
[78] Schellenberg A, Lin Q, Schueler H, Koch CM, Joussen S, Denecke B, Walenda G, et al. Aging (Albany NY). 2011;3(9):873-88.
[79] Banfi A, Muraglia A, Dozin B, Mastrogiacomo M, Cancedda R, Quarto R. Exp Hematol. 2000;28(6):707-15.
[80] Jaiswal N, Haynesworth SE, Caplan AI, Bruder SP. J Cell Biochem. 1997;64(2):295-312.
[81] Mostafa NZ, Fitzsimmons R, Major PW, Adesida A, Jomha N, Jiang H, Uludafu H. Connect Tissue Res. 2012;53(2):117-31.
[82] Jorgensen NR, Henriksen Z, Sorensen OH, Civitelli R. Steroids. 2004;69(4):219-26.
[83] Ogston N, Harrison AJ, Cheung HF, Ashton BA, Hampson G. Steroids. 2002;67(11):895-906.
[84] Fiorentini E, Granchi D, Leonardi E, Baldini N, Ciapetti G. Int J Artif Organs. 2011;34(10):998-1011.
[85] Siddappa R, Fernandes H, Liu J, van Blitterswijk C, de Boer J. Curr Stem Cell Res Ther. 2007;2(3):209-20.

Chapter 2

Osteoinductive biomaterials: current knowledge of properties, experimental models and biological mechanisms

Ana M. C. Barradas, Huipin Yuan, Clemens A. van Blitterswijk, Pamela Habibovic

Abstract

In the past thirty years, a number of biomaterials has shown the ability to induce bone formation when implanted at heterotopic sites, an ability known as osteoinduction. Such biomaterials - osteoinductive biomaterials - hold great potential for the development of new therapies in bone regeneration. Although a variety of well characterized osteoinductive biomaterials have so far been reported in the literature, scientists still lack fundamental understanding of the biological mechanism underlying the phenomenon by which they induce bone formation. This is further complicated by the observations that larger animal models are required for research, since limited, if any, bone induction by biomaterials is observed in smaller animals, including particularly rodents. Besides interspecies variation, variations among individuals of the same species have been observed. Furthermore, comparing different studies and drawing general conclusions is challenging, as these usually differ not only in the physico-chemical and structural properties of the biomaterials, but also in animal model, implantation site and duration of the study. Despite these limitations, the knowledge of material properties relevant for osteoinduction to occur has tremendously increased in the past decades. Here we review the properties of osteoinductive biomaterials, in the light of the model and the conditions under which they were tested. Furthermore, we give an insight into the biological processes governing osteoinduction by biomaterials and our view on the future perspectives in this research field.

Definitions and historical background

One of the first definitions of osteoinduction, as proposed by Friedenstein was "the induction of undifferentiated inducible osteoprogenitor cells that are not yet committed to the osteogenic lineage to form osteoprogenitor cells" [1]. Although the phenomenon of bone formation upon implantation of various tissues heterotopically was described as early as in the beginning of the 20th century [2-6], Urist' seminal discovery that acellular, devitalized, decalcified bone matrix induced bone formation in muscles of mouse, rat, guinea pig and rabbit [7], and subsequent identification of Bone Morphogenetic Proteins (BMPs) as sole inducers of heterotopic bone formation [8, 9], set a landmark in this field of research. Based on his studies, Urist defined the process of bone formation by autoinduction, or osteoinduction as "the mechanism of cellular differentiation towards bone of one tissue due to the physicochemical effect or contact with another tissue" [8]. More recently, in a definition proposed by Wilson-Hench, osteoinduction was described as the process by which osteogenesis is induced [10]. It is now generally accepted that a conclusive evidence for osteoinduction can only be given by heterotopic implantation, i.e. implantation in the tissues or organs where bone does not naturally grow.

Heterotopic bone induction as induced by Demineralized Bone Matrix (DBM) and BMPs has been well described by Urist and others. When BMPs, loaded onto insoluble collagenous bone matrix, or DBM are implanted heterotopically in rodents, a cascade of events is initiated: the chemotaxis of undifferentiated mesenchymal cells followed by cell proliferation; differentiation into chondroblasts and chondrocytes, followed by the formation of cartilaginous extracellular matrix containing type II collagen and proteoglycans; chondrocytes maturation, hypertrophy, and cartilage calcification; blood vessels and osteoprogenitor infiltration, removal of cartilage and osteoid apposition and bone matrix production; bone marrow formation and bone remodeling [11]. Although it is generally thought that heterotopic induction of bone formation by BMPs is indeed endochondral, [11], there have been reports on intramembranous, i.e. direct bone formation without cartilage intermediate, at heterotopic sites. For example, fibrous collagen membrane [12], hydroxyapatite (HA) [13] and biomimetic calcium phosphate coatings [14] in combination with BMP induced bone formation directly, without apparent cartilage intermediate. In contrast, BMP on fibrous glass membrane and insoluble bone matrix showed that heterotopic bone was formed following the process of endochondral ossification [12, 13]. Differences in the pathway by which heterotopic bone is induced by BMPs may be associated with differences in vascularization, and hence oxygen supply as well as with mechanical properties (e.g. micromotion) of the carrier [13].

At the time of Urist's discovery of BMPs as osteoinducive factors, the phenomenon of osteoinduction triggered by a completely synthetic biomaterial, by no means resembling the composition of implants used in Urist's studies, was also reported. In 1960, Selye and coworkers implanted Pyrex® glass tubes, with a diameter of 30 mm and a length of 20 mm, the so-called tissue diaphragms, subcutaneously in rats. Histological analysis of tissue formed inside the diaphragms 60 days following implantation, revealed presence of bone, cartilage and hemopoietic tissue [15]. In 1968, Winter and Simpson described subcutaneous bone formation upon implantation of poly-hydroxyethylmethacrylate (poly-HEMA) in pigs [16]. The authors observed that the implanted sponge had calcified prior to bone formation. Calcification of the sponge was also observed after subcutaneous implantation in rats [17].

The observed phenomenon of bone induction by the polymeric sponge could not be explained by the Urist's theory, as the sponge neither contained nor produced BMPs. Interestingly, in earlier reports it was observed that bone was induced by tendons and arteries only if they were first calcified *in vivo*, as reviewed by de Groot [18]. Although the exact underlying phenomenon was not known, these observations suggested that calcification, and hence calcium phosphates might play an important role in the process of osteoinduction.

In the past decade, a large number of publications illustrated osteoinduction by diverse calcium phosphate biomaterials in the form of sintered ceramics [19-26], cements [27-29], coatings [30, 31], as well as coral-derived ceramics [20, 25, 32-35], in various animal models. Also composites consisting of a polymer and HA have shown to be able to induce bone formation heterotopically [36, 37]. Besides calcium phosphate containing biomaterials, osteoinduction was also observed in alumina ceramic [38], titanium [39, 40] and a porous bioglass [41].

Until now the exact mechanism of osteoinduction by biomaterials is still incompletely understood. It is furthermore questionable whether the mechanisms of osteoinduction by BMPs and osteoinduction by inorganic biomaterials are related and, if so, to which extent. The apparent differences between osteoinduction by BMPs and biomaterials are that **1)** bone induced by biomaterials is always intramembranous [25, 42] while BMP-induced bone is mostly formed via the endochondral pathway [11], **2)** in small animals like rodents bone is very rarely induced by synthetic biomaterials [19, 43-46], but easily by BMPs [47-49], **3)** bone induction by biomaterials in large animals is rather slow, requiring weeks to months [27, 35, 39, 50, 51], whereas osteoinduction by BMP-2 and BMP-7 takes place as early as 2-3 weeks upon heterotopic implantation in rodents [14, 52, 53] and 4) while bone is usually observed inside pores or other "protective" areas of a material [51, 54-56], bone formation by BMPs is regularly seen on the periphery of the carrier and even in the soft tissue distant from the carrier surface [14, 57].

The osteoinductive capacity was one of the main reasons for development of clinical therapies based on BMPs, and both BMP-2 and BMP-7 are currently successfully used in a number of applications [58, 59]. It is therefore not surprising that biomaterials with intrinsic osteoinductivity possess a great potential as alternatives to biological approaches to bone regeneration [60].

As earlier mentioned, it is well established that, to be considered osteoinductive, a material should induce bone formation heterotopically, so that de novo bone origin is solely attributed to its osteoinductive properties rather than to the osteoconductive ones (the latter comprises the migration of potentially osteogenic cells to the site of future matrix formation at the site of (orthotopic) implantation [61]. Studies within the field generally describe the chemical and physical properties of osteoinductive materials, as well as the animal model chosen for experimentation. Analysis is usually based on qualitative and quantitative assessment of bone formation induced by different materials and/or at different time points by which critical properties of the setup can be indentified and results explained. Some of the publications also discuss possible biological mechanisms behind the findings, but the driver for bone formation has not been conclusively proven yet.

In the first part of this review, we will discuss the status of osteoinduction by (mostly synthetic) biomaterials, by denoting those that have been identified as osteoinductive with special emphasis on calcium phosphate based ones, as these are the most extensively investigated.

We will discuss the properties of the materials, which are, in our view, essential for osteoinduction to occur. The experimental conditions in which materials were tested and their implications for the outcome as well as the availability of *in vitro* models to predict osteoinductivity will also be elaborated on. Finally, we will focus on the existing theories regarding the mechanism of osteoinduction by biomaterials and provide our view on the topic.

Osteoinductive biomaterials

As can be seen in figure 1, which is a schematic representation of the biomaterials that have so far been shown osteoinductive, all material types, polymers, metals and both synthetic ceramics and ceramics of natural origin, theoretically possess the osteoinductive potential. Glass cylinders [15] and poly-HEMA [16] were the first synthetic materials associated with heterotopic bone formation and so far, poly-HEMA remains the only osteoinductive polymer. Composites, consisting of polylactide and HA particles have however recently shown to be osteoinductive too [36, 37]. In the family of metals, porous titanium (Ti) has shown osteoinductivity, alone [39, 40], coated with a thin layer of calcium phosphate [31] or in a construct with a calcium phosphate ceramic [62].

In contrast to the limited number of reports on osteoinduction by polymers and metals, ceramics, particularly calcium phosphate based ones, have shown osteoinductive potential in a variety of studies: HA [20, 22, 24-26, 33, 34, 63, 64], β-tricalcium phosphate (β-TCP) [65, 66], biphasic calcium phosphate (BCP), that designates the mixture of HA and TCP [27, 45], dicalcium phosphate anhydrous (DCPA), dicalcium phosphate dihydrate (DCPD) [28], carbonated apatite [54], calcium pyrophosphates (CPP) [26, 67] and HA/calcium carbonate (CC) mixtures [32, 35]. A case of osteoinductive glass ceramic has also been reported [41].

A thorough analysis of the materials described so far as osteoinductive (Table 1), could in theory provide answers about properties relevant to osteoinduction. And yet, we are still unable to describe how exactly an osteoinductive material should be designed and produced. The main reason is that the properties of the end material greatly depend on the processing parameters, which often differ among research groups. For example, two porous HA ceramics, prepared by two different groups, may be equal with regard to chemical composition (both can be phase-pure), but completely different in their macroporosity, grain size and surface roughness, and hence differ in their osteoinductive potential. This phenomenon is not unique to osteoinductivity. The capacity to repair bone defects can differ greatly among materials from the same family, and surgeons can now choose from 13 different calcium phosphate based ceramics/cements in the Netherlands alone for applications in trauma- and orthopaedic surgery [68]. Both the starting materials and processing parameters affect properties of the end product, and hence its bioactivity, i.e. the phenomenon by which a biomaterial elicits or modulates biological activity [69]. However, details of the processing parameters are often missing in publications on osteoinductive materials; furthermore, the level to which material properties can be controlled using classical methods of preparation, remains limited. Therefore, in an attempt to draw conclusions on the properties which render a material osteoinductive, one is dependent on the description of physico-chemical properties of the end product. Furthermore, a comparison should always be made in light of the experimental scenario in which osteoinductive potential is investigated, a topic which will be discussed in the

next section of this review. Table 1 therefore contains information about the material properties which so far have been suggested to play a role in osteoinduction: chemical composition, overall geometry of the implant and porosity. Microstructural surface properties, including grain size, microporosity, surface roughness and specific surface area have been suggested as critical factors in osteoinduction [22, 51, 60, 64], however, these properties have not been described for majority of the materials in Table 1, which is why they were excluded. We will, however, in detail discuss the importance of microstructural surface properties based on the existing literature.

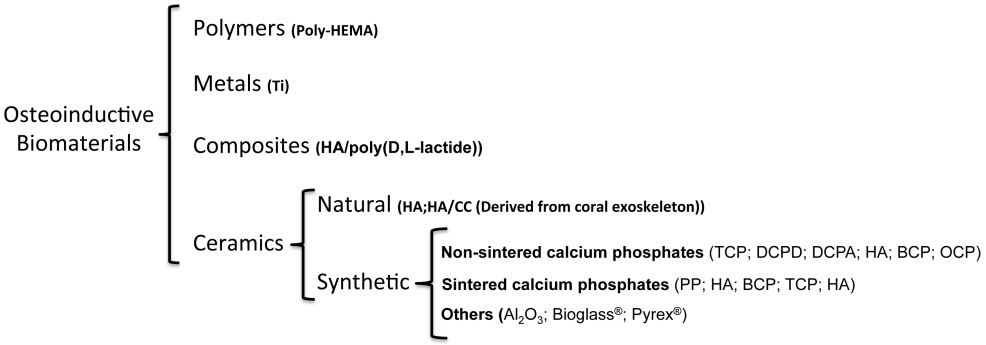

Figure 1: Schematic diagram presenting materials that have been described as osteoinductive, divided according to material family, origin and physico-chemical and structural properties. Poly-HEMA: polyhydroxyethylmethacrylate; Ti: titanium; PP: pyrophosphate; HA: hydroxyapatite; CC: calcium carbonate; BCP: biphasic calcium phosphate; TCP: tricalcium phosphate; DCPD: dicalcium phosphate dihydrate; DCPA: dicalcium phosphate anhydrous; CA: carbonated apatite; OCP: octacalcium phosphate.

Influence of chemical composition

As already mentioned, the majority of materials so far described as osteoinductive contain calcium phosphate. Some of the materials that do not contain calcium phosphate, such as titanium, have been shown to calcify when exposed to simulated body fluid [39, 40], and are therefore expected to undergo a similar calcification *in vivo*. Indeed, in the only publication on osteoinductive polymer, calcification of poly-HEMA *in vivo* was observed before heterotopic bone formation occurred [17]. These data suggest that presence of a calcium phosphate source is a prerequisites for heterotopic bone formation to occur. This observation is not surprising as bioactivity in terms of osteoconduction in an orthotopic environment, has long been recognized for calcium phosphate materials. The liberation of Ca^{2+}, PO_4^{3-}, HPO_4^{2-} from the material into the surrounding may increase the local supersaturation of the biologic fluid causing precipitation of carbonated apatite that incorporates calcium-, phosphate- and other ions (Mg^{2+}, Na^{+}, CO_3^{2-}), as well as proteins, and other organic compounds [51, 70]. The dissolution part of the process is missing in the materials that initially do not contain calcium phosphate; however, their physico-chemical properties are such that they provide nucleation sites for the deposition of a biological apatite layer, containing organics. It is plausible that

similar events occur heterotopically, facilitating bone apposition, but whether precipitation / dissolution-reprecipitation events are also responsible for induction of osteogenic differentiation remains to be elucidated. Related to the expected influence of calcium phosphates, the *in vivo* degradation behaviour of different osteoinductive ceramics requires further discussion. As can be extracted from Table 1, the largest number of studies has been performed with implants consisting of HA, (α- or β-) TCP, and the mixtures of the two, BCP. In addition, in a few studies, osteoinduction was also shown to occur in DCPA- DCPD- cements, carbonated apatite (CA) ceramics and OCP coatings, as well as in some calcium pyrophosphates. It is well known that dissolution properties of calcium phosphates are phase-dependent [71], and in some studies, a direct comparison was made between implants with varying chemical composition. For example, in one of our studies, we compared the performance of an HA and a BCP ceramic, produced at equal conditions, in order to keep other material properties similar (figure 2 A and B). These were implanted intramuscularly in goats and after 6 weeks, bone incidence was higher in the BCP ceramic containing the more soluble TCP, than in the HA ceramic, and so was the amount of bone induced (figure 2 D and E) [51]. In two other studies, higher osteoinductive potential was also observed for the ceramic containing resorbable β-TCP as compared to pure HA [46, 72]. However, in the study by Kurashina and colleagues in rabbits, an increase in the amount of TCP had a negative effect on osteoinduction [73]. These data show that the calcium phosphate phase, and the associated degradation behaviour cannot be appointed as determinant for osteoinduction to occur, without taking into account other material properties. Indeed, as already mentioned, the materials that initially do not contain calcium phosphate, but possess the ability to calcify *in vitro* and *in vivo*, are also able to induce heterotopic bone formation, though to a lesser extent and after a longer period of time than calcium phosphate-containing materials. Based on the current knowledge, it is suggested that an increase in *in vivo* degradation of calcium phosphate materials in general is beneficial for osteoinduction, however, a relatively stable surface is required for the onset of bone formation to take place. In other words, a compromise is to be reached between the level of dissolution/reprecipitation events occuring on the material surface and the rate of material disintegration due to *in vivo* degradation [73, 74]. Apart from physico-chemical dissolution / biological apatite precipitation processes, effect of osteoclastic resorption of biomaterials and therewith accompanied release of calcium ions has also been suggested important in the process of heterotopic bone formation by biomaterials [35]. What still needs to be determined is whether the free calcium, phosphate, or both ions in the vicinity of material surface or the newly formed biological apatite layer on the surface are the trigger of the osteogenic differentiation of the undifferentiated cells, or simply the template where the onset of bone formation can occur, after the osteogenic differentiation has been triggered by different means.

Influence of macrostructural properties

Apart from the chemical composition of the material, the geometry and macrostructural properties have been shown to play an important role. In the case of macrostructure, the most striking example is the importance of porosity. Bone formation has never been observed on a dense sintered ceramic, that does not degrade *in vivo*, whereas a ceramic with the same chemical composition, but containing pores, induced bone formation [19, 22]. Generally, the

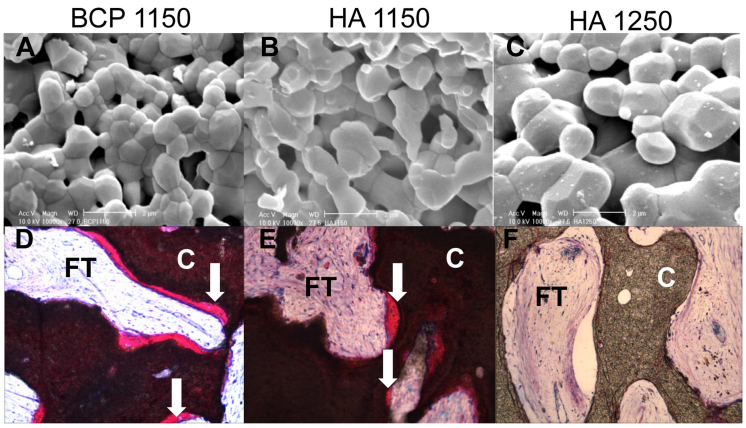

Figure 2: The effect of chemical composition and microstructure of calcium phosphate ceramics on bone formation. Microstructure of BCP1150 (A), HA1150 (B) and HA1250 (C) is shown by Scanning Electron Microscopy images (scale bar = 2 μm). After six weeks of intramuscular implantation in goats, both BCP1150 and HA1150 containing similar microstructure but different chemical composition, induced bone (D and E). However, the incidence in BCP was higher (7/10 versus 5/10) and so was the amount of bone induced. In contrast, no bone was observed in HA1250 (F), with fewer micropores and larger grains than the other two ceramics, but with chemical composition identical to that of HA1150. Light microscopy images of stained non-decalcified sections (scale bar = 100 μm). White arrows point towards bone. C: ceramic; FT: fibrous tissue.

importance of pores inside bone graft substitutes is related to the invasion of the material by blood vessels, that bring along nutrients and oxygen, sustaining therefore the metabolism of cells inside the scaffold [75]. In the case of osteoinductive materials, blood vessels can have the added function of bringing along cells with capacity to differentiate into osteoblasts, which will be discussed in more detail in the section on potential mechanisms behind osteoinduction. Jansen and coworkers suggested that the pore size of the calcium phosphate cement cylinders in their study might have been too small (average 150 μm) when compared to other studies, which could explain why bone formation was not observed after 90 or 180 days of implantation under the skin of goats. They also observed that implant integrity was lost 3 months after implantation and hypothesized that this collapsing of the porous structure might have prevented nutrients supply and decreased the available adsorption areas for protein attachment and cellular adhesion and differentiation [76]. In the study by Fujibayashi and colleagues, titanium blocks with predefined porous structure were able to induce bone formation in dogs, in contrast to titanium fibre meshes, surface-treated in the same way [39]. The importance of a sustainable macrostructure was also appointed by Gosain and coworkers, who did find bone formation after implantation of a calcium phosphate cement paste, but also observed that the rate of material replacement by the newly formed bone increased when macropores were introduced into cement-paste forms of HA, by increasing the ratio TCP/HA. They also concluded that in HA ceramic, with predefined macroporous structure, more heterotopic bone formation was formed than in HA cements, which at the time of implantation

did not contain pores [27]. In one of our studies, it was observed that disintegration of porous macrostructure of the ceramic, due to mechanical fracture, prevented bone formation to occur [74]. In the osteoinductive materials described so far, bone formation was always observed in the pores, and never on the implant periphery or distant from the implant, as is often the case with osteoinduction by BMPs [14, 60], again emphasizing the importance of porous structure. Besides the presence of pores with suitable dimensions, geometry of the implant has been shown important in osteoinduction. In a study by Ripamonti and coworkers, HA ceramic rods and discs containing concavities (figure 3A) varying in height and diameter size, were implanted in the muscle of baboons. The authors observed that bone formation always started in the concave and never on the convex spaces (figure 3B), suggesting that some geometries could be more optimal than others in concentrating BMP and stimulating angiogenesis, as this may be a prerequisite for osteogenesis [55, 77]. We also observed that after implanting bulk cement of DCPA, containing channels (figure 3C), bone was mainly formed in the interior of the peripheral channels, close to their openings, after remaining for twelve weeks in the muscle of goats (figure 3D) [28]. Le Nihouannen and colleagues observed heterotopic bone formation between microporous particles of a BCP ceramic implanted intramuscularly in sheep [56], which reinforces the idea that "protective" areas, such as pores, concavities or channels, are beneficial for bone formation. In order to develop an osteoinductive material, we are of opinion that one ought to pay attention to two aspects of macrostructural properties: (1) macrostructure should be such that there is sufficient supply of nutrients, oxygen and infiltration of cells and tissue, and (2), presence of "protective areas" in the form of pores, channels, concavities, or spaces between individual particles, in which processes leading to heterotopic bone formation can occur without being disturbed by high body fluid refreshments or mechanical forces due to implant movement.

Influence of surface structure

In addition to chemical composition and macrostructural properties, material surface properties at micro- and nanoscale have been shown of great importance for osteoinductive potential. Unfortunately, detailed surface characterization of the materials so far tested for osteoinduction is sparse. Nevertheless, in a few of our studies it has been demonstrated that ceramics with different microstructural properties have different performances when implanted heterotopically. By changing the temperature at which a ceramic is sintered, we were able to vary the grain size and the microporosity of the ceramic, while keeping the chemical composition and the macrostructure constant. We have shown that a decrease in sintering temperature leads to an increase in the number of micropores (defined as pores with a diameter smaller than 10 μm) [51, 60, 64]. This change in surface properties has been shown to have a positive effect on osteoinductive potential of the ceramic. Figure 2 shows examples of microstructure of the two HA ceramics sintered at 1150°C and 1250°C respectively (figure 2B and C) and their behavior heterotopically (figure 2E and F). The number of micropores together with the grain size, will be reflected in the total surface area. By enlarging the surface area, dissolution/reprecipitation events occurring on the ceramic surface as well as mineral deposition from the body fluids are expected to be more pronounced, which may be beneficial for osteoinduction to occur. Fellah and colleagues also compared ceramic implants that differed

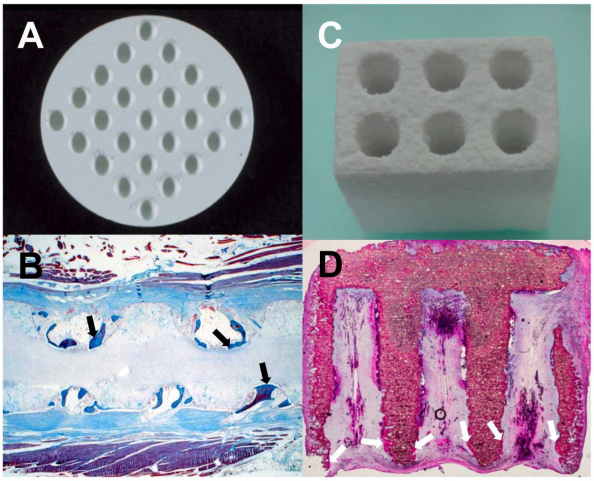

Figure 3: Heterotopic bone formation is influenced by the geometry of the implant. HA implants (Ø=20 mm, height=4 mm), containing concavities (Ø=1600 μm, depth=800 μm) (A) were implanted intramuscularly in the baboon. Bone formation was observed after 90 days only in the concave surfaces of the implant (B). DCPA cement implants ($11.5\times8\times10$ mm^3) containing channels (Ø=2.5 mm, depth=8 mm), open on one and closed on the opposite side of the implant (C) were implanted intramuscularly in the goat and after 12 weeks bone formation occurred only inside the channels, close to the channel opening (D). Black and white arrows point towards bone in B and D respectively. A and B adapted from [55] and [125] respectively. Scale bar = 1 mm.

in surface microstructure. By sintering BCP at three different temperatures, materials with the same chemical composition but different microporosity and specific surface area were obtained and implanted both heterotopically, in paraspinal muscle, and orthotopically, inside polytetrafluoroethylene (PTFE) cylinders in a critical-sized femoral defect in goats, to prevent osteoconduction. Autologous bone chips served as control. Bone formation was not observed heterotopically, whereas orthotopically, an increase in microporosity and specific surface area was shown beneficial for the amount of bone formed. Whereas no de novo bone formation was formed in cylinders containing bone chips, ceramics, particularly the ones sintered at lower temperatures, showed substantial amount of bone formation [78]. Although implantation in femoral epiphysis, even inside a polymeric cylinder is not a heterotopic site, this paper does show the effect of surface properties on the formation of new bone. In the study by Fujibayashi and coworkers, it has been shown that porous titanium was only able to induce bone formation heteretopically following a chemical and thermal surface treatment. This treatment, by which the microstructure of the metal was changed, provided the material with the ability to calcify *in vitro*, and plausibly also *in vivo*, which was, according to the authors, the driving force behind osteoinduction [39]. In addition to the ability to deposit a biological apatite layer on the surface, either through local dissolution/reprecipitation mechanism, or from body fluids, adsorption or coprecipitation of the growth factors (e.g. BMPs) into the newly formed biological apatite layer from the body fluids are also expected to increase

with an increase of the specific surface area, which may be one of the intermediate steps in the initiation of osteogenic differentiation and deposition of de novo bone. Indeed, calcium phosphates, such as HA are well known for their affinity to bind various proteins upon exposure to the *in vivo* environment [79, 80], including BMPs [81-83] and an increase of specific surface area may be required to accumulate sufficient amount of BMPs for osteoinduction to be triggered. Apart from this indirect effect of microstructure on the specific surface area and the related ability to bind proteins or deposit a biological mineral layer, the size and the shape of grains could also exert a direct effect on cells involved in osteoinduction. It has been shown that nanosized surface features can act as a direct physical trigger on Mesenchymal Stromal Cells (MSCs) osteogenic differentiation, without additional osteogenic supplements [84].

Models to study osteoinduction

In vivo *models*

Here, we will concentrate on the factors not directly related to materials properties, but known to be of influence when studying osteoinduction: animal model, implantation site, procedure and study duration. In a number of studies depicted in Table 1, results on bone formation were shown to be animal model dependent. Yang and coworkers tested the performance of sintered BCP ceramics in five different animal models at heterotopic locations, in a single study. Until day 120, in rats, rabbits and goats, only dense fibrous connective tissue encapsulating the ceramics and loose connective tissue inside the pores were observed, without signs of bone formation. However, in dogs and pigs, bone formation was found in implants retrieved as early as 45 days after implantation. Extensive amounts of bone were found at day 120 mainly in the pores of the materials implanted in pigs [45]. This study showed that larger animals yielded more bone than smaller ones, with exception of the goat where no bone formation was observed. Also the only osteoinductive polymer, poly-HEMA, was shown to induce bone formation in pigs [16], but not in rats, where only calcification of the materials occurred, without bone formation [17]. The difference between larger and smaller animals is also seen when evaluating the type of animal models used to perform the studies on osteoinductive materials. Throughout Table 1, the number of published studies concerning small animals is minimal, and the majority involves large ones. The incidence of animal models in the experimentation on calcium phosphate ceramics is illustrated in figure 4. Based on the literature search, there is one single study involving mice, four with rabbits and five with rats, whereas most studies were performed in goats (12) and dogs (17). A number of studies has also been performed in non-human primates (9). This scenario contrasts the studies to test the osteoinductive potential of BMPs or osteogenic potential of tissue engineered constructs, which are mainly performed in mice, rats and rabbits. Figure 4 suggests that the incidence of heterotopic bone formation induced by calcium phosphate ceramics is higher in large animals as compared to small ones, although we do not know how many (unpublished) studies were actually performed in small animals. Overall interspecies variation is characterized by the difference in bone induction between small and large animals. But among large animals differences are also present; for instance, studies involving dogs were in general more successful than those performed in goats. In table I, the number of materials marked with a "+"

in the “Bone” column is higher in studies in dogs as compared with those in goats. Although being a rough comparison, as no other factors regarding the material or animal model were considered, this suggests that a material tested in a dog has higher chances of inducing bone formation than in a goat. This was evident in the study in which the same material was tested under the same conditions in both animal models [45]. Trying to explain these interspecies variations would be at best speculative as long as the exact mechanism behind osteoinduction by biomaterials is incompletely understood, but (patho)physiological and genetic differences are expected to play a role.

Apart from the animal model itself, other factors could influence a material’s ability to induce bone formation heterotopically, which is why ideally, the animals should be of the same strain, age, sex and body weight. For example, in a study by Marusic and colleagues, the authors implanted pieces of bone matrix gelatin intramuscularly in mice from 8 different inbred strains. After four weeks, bone formation was observed only in six out of the eight strains. Within mice from each strain, the number of individuals where bone formation was observed varied and the average amount of bone was also different [85], showing that, even among mice of inbred strain, phenotypical differences are such that results are not only strain but also individual dependent. In the case of larger animals, genetic variability will be even higher, as these are always outbred. The effect of age of the animal was apparent in the two studies by Winter and Simpson in pigs, that showed that heterotopic bone formation by a polymeric sponge was only induced in the younger pig [16].

Whereas mice, rats, rabbits and sometimes minipigs can be obtained with similar or identical genetic makeups, larger animals, such as dogs, sheep and goats are relatively heterogeneous with respect to strain, age and body weight [86]. In general, when choosing an animal model to study osteoinduction, similar considerations are made as for other orthopaedic applications: ethics, availability, housing requirements, ease of handling, cost, susceptibility to disease and available background data of the animal [86]. Considering the described animal model dependence, large animals are usually chosen for assessing osteoinductive potential of biomaterials. Availability is the next important factor determining the choice of the animal model. In the Netherlands, for example, sheep, dogs and goats are used in orthopaedic research, but goats are most widely available. In the majority of studies from our group, we have used young adult Dutch milk goats (age of about 2 years), with the average weight of 65 ± 10 kg. Although such a group of animals is genetically heterogenous, we attempted to limit the effect of age, sex and weight, by performing the follow-up experiments with animals of similar characteristics. Based on papers by others, similar considerations were made in other studies on osteoinductive biomaterials. Despite the fact that we attempted to keep as many parameters of the animal model constant as possible, large variations in the amount and timing of bone induction was observed in different individuals [74], similar to studies in which biological material was tested [85]. It should be mentioned that variations among individuals of the same species are not necessarily a weakness of a study, but potentially tools that will be of help when trying to understand the mechanism behind osteoinduction. We therefore think that in publications on osteoinductive materials, more attention should be paid to the differences observed; for example, instead of providing the mean and standard deviation values for the amount of bone formed, one should also provide information about data distribution, outliers, etc.

Another issue that is possibly related to the size of animals used to study osteoinduction, is the

size of the implant that can be insterted into an animal. We implanted materials with different dimensions (Ø6.5×5 mm^3 versus Ø6.5×10 mm^3) in paraspinal muscles of goats. Similar quality of bone was observed in both types, however bone formation had higher incidence in the larger implants (9/10) as compared to the smaller ones (7/10). Bone formation also started earlier in larger implants [74]. It is obvious that, solely based on this single study, no conclusions can be drawn, however, implant size should be taken into consideration when discussing animal model dependent differences in osteoinductive potential of biomaterials.

Several authors have also investigated the osteoinductive capacity of a material, depending on the implantation site and duration of implantation. Ripamonti and colleagues observed no bone formation in coral-derived ceramics that were partially or fully converted into HA after 60 and 90 days of intramuscular implantation in Papio ursinus, whereas after 365 days, all ceramics showed heterotopic bone formation [34]. Yang and coworkers observed bone formation as early as on day 45 after implantation of BCP cylinders in intramuscular pockets of both dogs and pigs, whereas subcutaneously, bone formation was only observed 60 days after implantation. An increase in implantation time in both animal models was also shown to result in an increased amount of bone [45]. In one of our studies, no bone was found after four months of subcutaneous implantation of a BCP ceramic in goats, whereas intramuscularly, bone was induced in seven out of ten implants in the same animals [74]. These studies suggest that at intramuscular locations, bone formation occurs more frequently, or at least at a higher rate. The results from Gosain and co-workers contrast these findings. They showed no significant differences in the amount of bone formation in implants of HA and BCP between the subcutaneous and intramuscular location in sheep, after 1-year-implantation [27]. The difference in survival time between the studies should however be taken into consideration. It is possible that, at the time of explantation, bone formed intramuscularly had already reached the remodeling phase, whereas subcutaneously, bone, the growth of which was initiated later than intramuscularly, was still in the early formation phase. Related to the implantation site, the level of injury during implantation is a parameter with enormous implications for the *in vivo* response to the implanted material. It is the injury and consequent perturbation of homeostatic mechanisms that leads to the cellular cascades of wound healing. Blood-material interactions, provisional matrix formation, acute inflammation, chronic inflammation, granulation tissue formation, foreign body reaction and development of fibrous capsule are the host reactions following injury due to implantation of a material [87]. In the majority of studies reviewed here, implantation was performed in paraspinal muscles, away from bone, where similar host reactions are expected. Although Zaffe argued that skeletal muscle is not a proper site to study osteoinduction by materials [88], general agreement is that both subcutis and muscle are sites heterotopic to bone formation, and hence suitable to test osteoinductivity of growth factors and materials. In our studies, after opening the skin, blunt dissections were made to create intramuscular pockets after separate fascia incisions, into which materials were placed separately and secured with non-resorbable sutures. Sufficient distance was kept between individual pockets, to avoid that individual implants could affect eachotherÕs behaviour. Pre- and post operative treatment of the animals was performed according to the procedures used for orthotopic implantations.

A note should also be made on the topic of sample analysis following an *in vivo* study. In the majority of studies discussed so far, histological staining of tissue on two-dimensional sections is performed, often followed by quantification based on image analysis. These are

established methods to visualize the character of tissue formed on cellular and matrix level. The fact that the sections are two-dimensional is a disadvantage, especially when quantification is involved, where one can only analyze areas rather than volumes. In addition, depending on the position at which a section is made, one can possibly miss important information. Le Nihouannen and colleagues used X-ray micro-computed tomography (μCT) to quantify the volume of both ceramic material and mineralized bone, distinguishing them based on the gray levels [89]. Although insufficient resolution and inaccurate phase identification are known as important limitations of the μCT technique when studying bone formation in (ceramic) implants, recent studies with high resolution μCT have demonstrated potential of this technique in the field of bone regeneration [90-92].
A thorough histological analysis, that is more extensive than the analysis of quality and quantity of newly formed bone, can also add to the understanding of mechanism of osteoinduction. Presence of inflammatory signs, such as monocytes, mono- and multi- nucleated-macrophages, lymphocytes or fibrous tissue could indicate if and how the immune system contributes to the mechanism of bone formation by biomaterials. For example, Fellah and colleagues extensively characterized the type of white cells present in histological sections of BCP microparticles of varying sizes explanted from rat muscle. They identified and quantified the presence of macrophages, Giant cells and lymphocytes and observed that these amounts varied according to the implanted particle size [93], indicating that macrostructural properties might trigger immune responses accordingly. Similarly, analysis of spatial distribution and quantification of blood vessels inside an implant could provide answers regarding importance of oxygen and nutrient supply as well as cells associated with neovascularization in osteoinduction.
Based on the published work and our experience, we suggest that large animals, such as goats, sheep, dogs or baboons should be used for intramuscular implantation to study material-induced bone formation. Attention should be paid that the group of animals used is controlled for sex, age, weight, and where possible strain, and, considering large differences between individual animals, paired implantations should be performed (comparisons of different materials within each animal of the group). Surgical procedure should be such that minimal damage is caused to the tissue, and the animals should receive the pre- and post-operative treatment according to standard procedures for orthopaedic research. With large animals as animal model, one should be aware that essential biological research tools, such as antibodies, are far less available than for smaller ones, which is one of the delaying factors in the biological comprehension of the mechanism. Therefore, more attention should be paid to methods of histological characterization and quantification of the tissues formed in and around the implanted material.

In vitro *models and choice of cell type*

In the previous section, we have described the complexity of research involving large animals to study osteoinductive biomaterials. Ideally, a simple and reliably predictive *in vitro* assays should be available to screen the osteoinductive properties of biomaterials, and at the same time, accelerate the comprehension of the mechanism behind this phenomenon. Unfortunately, development of such an assay is far from trivial. An important question that needs to be answered is which parameters of the complex *in vivo* environment are relevant to be translated into a simplified *in vitro* system to make it predictive, including cell source and

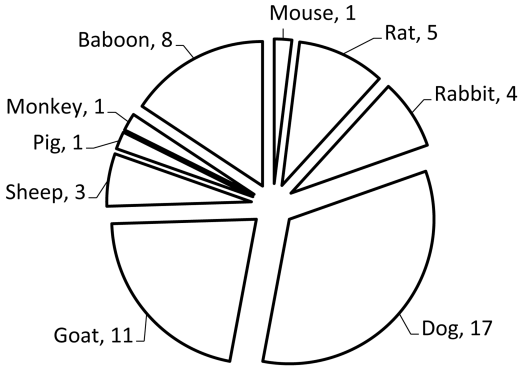

Figure 4: Number of studies performed per animal model to test calcium phosphate materials for their osteoinductive potential. Data derived from the studies presented in table 1. The highest number of studies involved **dog** [19, 20, 22, 29, 32, 45, 46, 64-67, 72, 101, 102, 113, 126, 127] and **goat** [28, 30, 31, 42, 45, 50, 51, 54, 74, 76, 128, 129]; the number of published studies involving **baboon** [20, 25, 33-35, 55, 130, 131], **sheep** [27, 56, 60], **rabbit** [20, 45, 46, 73], rat [15, 19, 45, 46, 132], **mouse** [46], **monkey** [26], and **pig** [45] was lower.

type, culturing conditions and output parameters. The complexity of this question is also evident from the fact that, despite the established clinical use of DBM for decades, assays that are able to reliably predict osteoinductive capacity of DBM *in vivo* are still largely missing. Adkisson et.al. developed a "rapid quantitative bioassay of osteoinduction" by using SaOS-2 osteosarcoma cells and studied cell proliferation rates under influence of DBM. However, correlation between cell proliferation and osteoinduction was not strong [94]. Zhang et.al. and Wolfinbarger and Zhang used human periosteal cells and human dermal fibroblasts to relate cellular ALP activity to DBM osteoinductivity [95, 96]. In these studies, the authors failed to show a clear correlation between *in vitro* assays and *in vivo* bone formation. Carnes et.al. used an immature osteoprogenitor cell line, 2T9 to investigate the effect of DBM on the cell differentiation [97]. They failed to show any effect on differentiation and concluded that there are no soluble factors being released from DBM into the culture medium. Han et.al. assessed the ALP activity of the C2C12 cells in a culture in presence of DBM, and found a correlation with heterotopic bone formation [98]. However, when we repeated a similar study with osteoinductive ceramics, the *in vitro* ALP expression of C2C12 cells could not be correlated to the heterotopic bone formation induced by the ceramics [99]. When studying material-cell interactions and comparing different materials *in vitro*, the material-medium interactions add an additional variable to the equation. In the case of calcium phosphate containing materials, for example, ion exchange between the material and the medium may significantly modify the composition of the latter, and hence the environment for cells to grow and differentiate. Furthermore, changes that take place in the medium will vary depending on the properties of the material, resulting in a study where same cells are cultured in different environments [99], making a comparison difficult and little reliable. These *in vitro* interactions can be very different from the *in vivo* material-body fluid interactions, where there is a continuous refreshment of body fluids around the implant. Although the fact that the situation of a ceramic

implanted in, for example, a goat muscle cannot be mimicked in a culture dish, investing into development of simplified predictive systems is necessary to aid the understanding of the mechanism and accelerate the improvement of the existing materials for bone regeneration. In our recent work, we have described an *in vitro* model with human bone marrow stromal cells (hBMSCs) and four different types of calcium phosphate ceramics: HA, BCP sintered at 1150°C (BCP 1150) and at 1300°C (BCP 1300) and TCP. We showed that after seven days in culture on the different ceramics in osteogenic differentiation medium, genes encoding for proteins characteristic of an osteogenic profile, were differentially expressed by hBMSCs. A trend was observed in the degree of differentiation, with cells on TCP exhibiting higher expression of most genes, followed by those on BCP 1150, BCP 1300 and HA. This trend correlated with the amount of bone obtained when the materials were implanted without cells, intramuscularly in sheep [60]. It is to be further investigated whether this system is only valid for the group of ceramics tested in our study, or it is applicable to other osteoinductive materials as well.

Other *in vitro* models have given insights into the possible role of inflammatory cells on bone formation. Fellah and coworkers investigated the expression of TNF-α and IL-6 by a mouse macrophage cell line when cultured on BCP particles with different size ranges. They observed that expression of these cytokines was highest when macrophages were cultured on microparticles smaller than 20 μm, as compared to 40-80 μm and 80-200 μm particles. Next they cultured pre-osteoblast mouse cells in presence of IL-6 and TNF-α and demonstrated that the expression of some osteogenic markers was higher when cells were cultured in presence of IL-6 than when cultured in osteogenic medium. Based on these data, the authors attempted to correlate microstructural properties of a ceramic directly with inflammatory response and indirectly, with osteogenic response and hence osteoinduction [100]. Studies in which macrophages and pre-osteoblasts are co-cultured on ceramics with different osteoinductive potential would provide a direct insight into the role of inflammation in osteoinduction *in vitro*.

The ability to induce bone formation: where does it originate from?

We have mentioned before that the mechanism behind osteoinduction by biomaterials is not completely understood yet. Nevertheless, a number of hypotheses have been proposed by different researchers. On the basis of current knowledge of material properties so far shown to be relevant for osteoinduction to occur, and biological processes occurring around and in the material upon implantation in, e.g. a muscle, we will discuss different hypotheses and give our view on the phenomenon.

Host response to a biocompatible material implanted in vascularized tissues such as muscle is associated with the events of injury formation, followed by inflammatory cell infiltration, acute and chronic inflammation, granulation tissue formation and foreign body reaction. In general, the polymorphonuclear leukocytes predominant inflammatory response and the leukocytes/ monocytes predominant chronic inflammatory response resolve quickly, within 2 weeks. The process of granulation tissue formation, characterized by the action of monocytes and macrophages, and the subsequent foreign body reaction, consisting either of fibrous capsule formation or macrophage and foreign body giant cell action is highly dependent on

the chemistry and topographical surface properties of the implanted material [87]. In a number of studies, response to heterotopically implanted osteoinductive materials was followed in time based on histology. Yang and coworkers studied the host response to a porous BCP ceramic in muscle of dogs 7-45 days post implantation. On day 7, they observed blood clot and some fibrous tissue inside the pores of the ceramic. On day 15, granulation tissue, with fibroblasts, macrophages and some newly formed blood vessels, was observed. At 30 days, denser fibrous tissue, parallel to the pore walls was observed, with polymorphic cell aggregates in association with capillaries and small venules in the vicinity of ceramic surface, some of which were positive for the ALP staining. Finally, on day 45, presence of similar cell aggregates was obvious, some multinucleated giant cells were found and osteoblasts aligned the newly formed bone, that was in close contact with the ceramic surface [101]. Yuan and colleagues identified similar processes leading to bone formation as Yang and colleagues upon intramuscular implantation in dogs of an HA and a BCP ceramic between 7 and 360 days of implantation. They observed aggregates of large cuboidal cells on the material surface in close association with capillaries, before osteoblasts were observed, that deposited osteoid, leading to bone apposition, remodeling and bone marrow formation. The sequence of processes observed were similar for the two ceramics, however they all occurred at an earlier time point in the BCP than in the HA ceramic, and the amount of bone formed in HA was lower than in BCP at the last time point [72]. Kondo and colleagues showed similar processes upon implantation of β-TCP in dog dorsal muscles: red blood cells, fibroblast-like spindle-shaped cells, few multinucleated cells and some blood vessels at 14 days, loose connective tissue consisting of sparsely distributed reticular collagen fibrils on day 28 and a larger number of TRAP and Cathepsin-K positive multinucleated cells, and newly formed bone on the ceramic surface after 56 days that continued growing until the last analysis point at 168 days [102]. Following intramuscular implantation of HA in baboons for 3, 6 and 9 months, Ripamonti first observed fibrous connective tissue with pronounced cellular and vascular components, then the collagen fibers condensation in fibrous connective tissue at the interface of the HA, and finally morphogenesis of bone, with subsequent remodeling, formation of lamellar bone and differentiation of bone marrow [25]. In all these studies, a natural host response to the material implanted in soft tissue was observed, however, in contrast to many others, these materials eventually led to heterotopic bone formation.

The main questions that remain to be answered are **(1)** what is the identity of the cells which are triggered to differentiate into the osteogenic lineage and **(2)** what triggers their accumulation on the material surface and subsequent osteogenic differentiation.

Considering the first question, Ripamonti and coworkers, who implanted HA heterotopically in baboons, observed that before and during bone formation, laminin staining (for vascular endothelial cells) was localized around capillaries in close proximity to the ceramic, as well as around individual cells that seemed to migrate out of the vascular compartment [103]. Yang and colleagues further commented that in dogs, polymorphic cells that appeared first close to capillaries and microvessels were likely to be migrating towards the ceramic and that osteoblast differentiation was occurring directly within the cell clusters which aggregated at the interface with the ceramics, especially where capillaries were in close proximity to the material [45]. They hypothesized that cells appearing close to the vasculature, those aggregating and those differentiating could be interrelated and could have origin in the proliferation, differentiation or migration of pericytes or endothelial cells.

In the formation of the skeleton, mesenchymal cells aggregate and form condensates of loose mesenchymal tissue, prefiguring the skeletal elements. Within these aggregates, cells may differentiate into osteoblasts, when in association with adequate vascularization, thereby directly initiating ossification, which eventually results in either compact or cancellous bone (intramembranous bone formation). Alternatively, condensates of mesenchymal cells can differentiate into chondrocytes in an avascular environment, producing cartilage which is eventually replaced by bone (endochondral bone formation) [104]. Heterotopic bone formation induced by biomaterials always occurs via the intramembranous pathway, indeed suggesting the importance of the newly formed blood vessels, and the associated cells, such as endothelial cells and pericytes, in the vicinity of the ceramic, as observed in the chronological studies into the process of osteoinduction.

Pericytes derive from multiple cell types and are capable of acquiring various phenotypes [105]. They are mural cells that lie on the abluminal side of blood vessels, immediately opposed to endothelial cells. They have been reported as capable of synthesizing ALP, osteocalcin and formation of colonies that mineralized *in vitro* [106]. Furthermore they deposit a matrix that resembles the one found in calcified blood vessels [105]. Using an experimental model of wound repair in the skull, Sato and Urist demonstrated that BMP induced the osteogenic differentiation of pericytes resulting in the formation of chondroid and woven bone [107]. *in vivo* studies in rats showed that a vascular staining, incorporated in the walls of vessels of the microcirculation that initially stained endothelial cells and pericytes, was found in some of the osteoblasts during bone tissue development after a small periosteum strip was raised from the femur, suggesting that pericytes are a supplementary source of osteoblasts in periosteal osteogenesis [108]. More recently, it has been suggested that an ancestor of the MSC is natively associated with the blood vessel wall, and more precisely, belongs to a subset of perivascular cells, although some MSCs may originate in other cell subsets [109, 110]. Furthermore the authors suggested that pericytes are released upon vessel damage or inflammation, to provide activated MSCs that will in turn stimulate tissue-intrinsic progenitors to regenerate the damaged area among other functions. The *in vivo* data demonstrating close association of heterotopic bone onset on the ceramic surface with capillaries and microvessels, together with our *in vitro* and *in vivo* data showing osteogenic response of bone marrow derived MSCs on osteoinductive ceramics [60] has created our working hypothesis that pericytes contribute to the process of bone formation at the surface of an osteoinductive material, either by undergoing the osteogenic differentiation or by providing activated MSCs as osteoprogenitors. Recently, Ripamonti and coworkers postulated that myoendothelial cells in skeletal muscle may be the cells that differentiate into osteoblasts when in contact with osteoinductive biomaterials [35]. Indeed, clonally derived myoendothelial cells have been shown to differentiate into myogenic, osteogenic and chnodrogenic lineage in cell culture [111]. Early work by Urist and colleagues on osteoinduction by DBM and identification of BMPs, as well as their demonstration of BMP-induced osteogenic differentiation of pericytes, logically poses endogenous BMPs as a possible trigger of osteinduction by biomaterials. By detecting BMP-3 and BMP-7 on the interface of tissue-HA substrate, where bone was observed after implantation in the muscle of primates, Ripamonti and coworkers hypothesized that the intrinsic osteoinductivity of these materials is intimately related to BMPs [55]. The authors proposed that these smart materials act as solid substrata for the adsorption, storage and controlled release of BMPs, for which probably a concentration threshold has to be

reached in order to induce bone formation. These ideas are shared by de Groot, who proposed the rational design and development of BMP concentrators that, after implantation in the patient, are capable of concentrating and immobilizing endogenous BMP complex [112]. Nasu and coworkers further showed that injections of an EP4 agonist in animals that received TCP intramuscularly accelerated bone formation, as compared to the control group that received the biomaterial alone, highlighting the role of these materials as BMP concentrators. EP4 is a prostaglandin E2 (PGE2) receptor which has been proven to enhance the effect of rhBMP in a spinal fusion rabbit model, reducing to half the required dose of rhBMP alone [113]. Ripamonti and coworkers recently argued the hypothesis that materials may concentrate endogenous BMPs, resulting in turn in heterotopic bone formation, because circulating BMPs are bound to protein carriers which inhibits or reduces the osteogenic activity of BMPs [34]. Instead, the authors suggested that first, osteoclastic resorption of the osteoinductive substrate occurs, accompanied with release of calcium ions, that in turn stimulate angiogenesis and osteogenic differentiation of stem cells. Upon osteogenic differentiation, stem cells are then suggested to express and secrete BMPs, which are incorporated into the biomaterial surface to eventually induce heterotopic bone formation [34]. Although it certainly is plausible that endogenous BMPs (either circulating or locally produced by the differentiating cells) are accumulated on the surface of osteoinductive biomaterials, it is difficult to explain why not all materials, or at least all calcium phosphate ceramics, with their high affinity to bind BMPs [114-116] are osteoinductive. In other words, if BMPs are involved in osteoinduction by biomaterials, their role is, in our opinion, dependent on, or at least related to other processes occurring upon implantation of a material, such as the deposition of a biological apatite layer. The ability of a material to form a biological apatite layer on its surface, either through dissolution/reprecipitation or through nucleation from biological fluids, is namely the only property that is characteristic of all materials so far shown osteoinductive. Deposition of the biological apatite layer is accompanied by the co-precipitation of organic factors such as osteogenic proteins, which may trigger the osteogenic differentiation of the relevant cells; however, if the deposition of the biological apatite does not occur, osteoinduction will not occur either, despite the possible adsorption of osteogenic proteins on the material surface. This is possibly related to the amount of proteins that needs to be accumulated in order for osteoinduction to take place. Other theories concentrate on a material's ability to trigger secretion of factors leading to bone formation, rather than to their ability to accumulate them on the surface. Endothelial cells are known to express cytokines such as BMP-2, BMP-4 and BMP-7 [105], and the expression of BMP-2 and BMP-7 has been shown to be markedly upregulated in response to inflammatory stresses [117, 118]. This specific inflammatory response of tissues to the osteoinductive ceramics has been proposed by some researchers as the factors that renders a material osteoinductive. Le Nihouannen and coworkers, for example, elaborated that the induction of bone formation by microporous ceramics was intimately related with the inflammatory response. They hypothesized that particles smaller than 5 ţm are released from the ceramics and provoke an inflammatory reaction, with consequent release of cytokines that promote the differentiation of circulating stem cells into osteoblasts [89]. Micrometer sized particles can also be released from other materials, like metals and polymers, as is often seen in cases of periprosthetic osteolysis, which could extend the theory to these classes of materials as well. However not only particles released from the implants can influence the activity of macrophages but also the surface topography/roughness. De Bruijn and colleagues

suggested the effect of prostaglandin E2 (PGE2) in osteoinduction [119]. PGE2 is a factor that is produced by macrophages around biomaterials during inflammation phase, in particular on micro-rough surfaces [120, 121]. In the study by de Bruijn et.al. is was shown that macrophages produced higher quantities of PGE2 in response to micro-rough surfaced HA, unique for osteoinductive materials, as compared to cells cultured on smooth HA surfaces. Furthermore, PGE2 was shown to be chemotactic for hMSCs and to stimulate their osteogenic differentiation [119]. Based on these findings, the authors proposed that processes leading to heterotopic bone formation start with injury due to implantation, followed by inflammation and invasion of the material by macrophages, that, when osteoinductive stimulates production of inflammatory cytokines, including PGE2, which in turn causes chemotaxis of MSCs, their osteogenic differentiation and eventually bone formation [119]. The role of the immune system is also frequently debated in pathologies that involve spontaneous calcification and/or heterotopic ossification. For example, in a study by Kan and colleagues, it was shown that, when macrophages were depleted in an established mouse model for Fibrodysplasia Ossificans Progressiva, Nse-BMP4 mice, the onset of heterotopic ossification upon tissue injury was delayed and the number of mice that developed ossification decreased. When the Nse-BMP4 mice were lacking mature B and T lymphocytes, the onset of heterotopic ossification occurred without delays, but the spreading and overall amount of ossification were smaller than in mice with B and T lymphocytes, suggesting that the adaptive immune system plays a role in spreading of heterotopic ossification. The authors proposed that the macrophage responses to tissue injury stimulate local inducible / progenitor cells to differentiate into bone, through accumulation of osteogenic factors including BMPs [122]. Furthermore, there is an extensive list of signaling pathways involved in bone metabolism that were also described in association with arteries- and/or plaque calcification, such as extracellular matrix proteins (osteopontin, osteonectin, bone sialoprotein), several BMPs, RANK/RANKL, TNF-α and HA. However, like for material-induced heterotopic bone formation, questions remain regarding the origin of cells that are involved in mechanisms leading to, for example, plaque ossification: smooth muscle cells, pericytes and circulating progenitor cells are possible candidates for osteblasts precursors and monocytes/macrophages for osteoclasts [123]. Although inflammation may be relevant for the onset of heterotopic bone formation by biomaterials, one cannot neglect that the time point at which heterotopic bone formation occurs varies among different materials and different animal models between a few weeks and a year (Table 1), which is long after the initial inflammatory response of the tissue to the implanted material, suggesting that other processes also determine the initiation of heterotopic bone formation. Although no conclusive evidence exists for any of the hypotheses proposed so far for osteoinduction by biomaterials, in the schematic in Figure 5 we have summarized the processes occurring during and possibly determining osteoinduction by biomaterials.

Future perspectives

It is well accepted that certain materials used in bone regeneration are bioactive in terms of osteoconductivity. However, the appreciation of the fact that some of these materials possess intrinsic osteoinductivity by broad audience needs a paradigm shift that can only be achieved with complete comprehension of the mechanism behind this phenomenon [124]. And al-

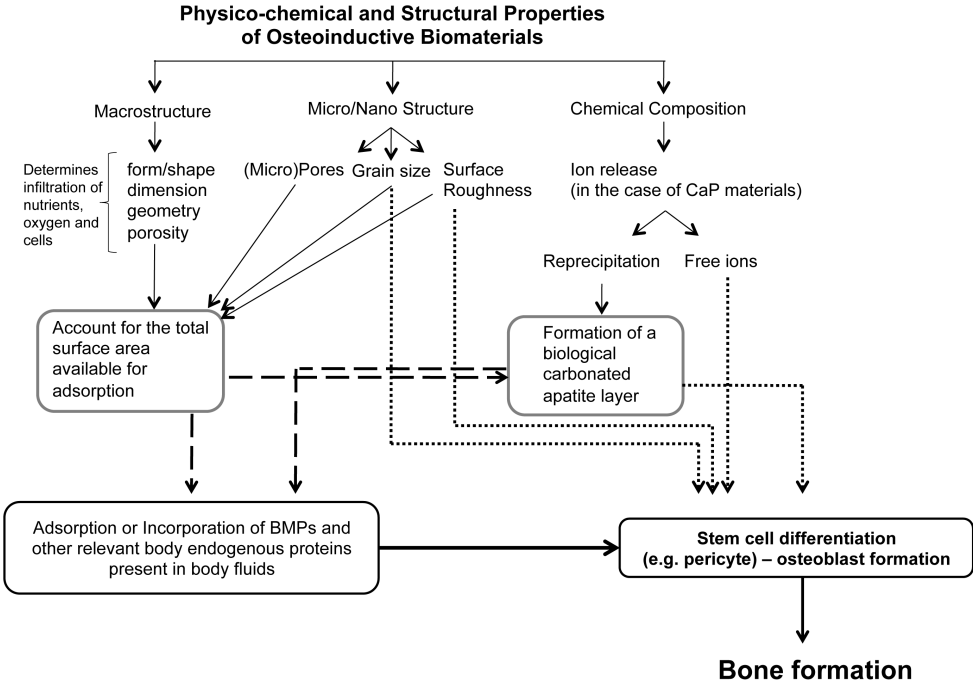

Figure 5: Schematic summarizing hypothesized mechanisms behind osteoinduction by biomaterials. Physico-chemical and/or structural properties of osteoinductive biomaterials may trigger the process of heterotopic bone formation directly or indirectly. Micro and nano structural properties can favor the interaction with BMPs and other essential endogenous proteins that in turn trigger stem cell differentiation into osteoblasts and hence bone formation. But surface topography and inorganic ion release release (in the case of calcium phosphate based ceramics), may also be a direct trigger of the process of osteoblast formation and bone formation.

though the mechanism is still not fully understood, in this review we have shown that the knowledge of material properties relevant for osteoinduction has tremendously increased in the past decade, despite the limitations in available models to test osteoinductivity. More importantly, some osteoinductive materials have shown equal performance to that of BMP-2 and autologous bone in a number of clinically relevant orthotopic *in vivo* models [60]. To provide conclusive evidence that osteoinductive biomaterials can act as a valid alternative to autologous bone and osteogenic growth factors, more studies in which a direct comparison between bone grafts / various growth factors and bone graft substitutes should be performed. Finally, it should be noted that all studies performed so far with osteoinductive biomaterials have been performed in preclinical animal models. Although these models were chosen in such a way that they resembled the clinical situation as closely as possible, only clinical trials will be able to provide the proof for the relevance of osteoinductivity in human patients. In order to accept or reject the existing hypotheses regarding the mechanism of osteoinduction, we are of opinion that the researchers should use the existing knowledge of relevant material

properties to design materials with closely controlled properties, rather than to rely on the processing parameters, which can only be controlled to a limited extent. By such a rational design, one can vary a single parameter, while keeping the others constant, in order to pinpoint which property or properties are essential for osteoinduction to occur. Furthermore, we believe that investing in novel techniques to identify biological processes occurring upon implantation of an osteoinductive material *in vivo* may be more efficient than the search for predictive *in vitro* assays.

Table 1: Overview of the publications referring to osteoinductive materials, divided into material families (polymers, metals, ceramics and composites/hybrids) and sub-categories in the case of ceramic materials (natural and synthetic calcium phosphate ceramics and cements, calcium phosphate coatings, other ceramics, containing glass (ceramic) and alumina ceramic). In addition, information is provided about animal model and implantation site, implantation time and material physico-chemical characteristics, such as chemical composition, form/shape, porous (P), dense (D) or hollow (H) structure and whether bone formation (B) was observed, according to the original descriptions. IM: intramuscular implantation; SC: subcutaneous implantation; CaPP: calcium pyrophosphate; HA: hydroxyapatite; BCP: biphasic calcium phosphate; TCP: tricalcium phosphate; xHA/yTCP: x and y are the fraction (in %) of HA and TCP phases respectively in BCP; CaP: calcium phosphate; CC: calcium carbonate; DCPD: dicalcium phosphate dihydrate; DCPA: dicalcium phosphate anhydrous; PLA: polylactic acid; PDLLAL poly(D,L) lactide; CA: carbonate apatite; OCP: octacalcium phosphate; Ti: titanium; Ta: tantalum; I/II/...: each number represents a different manufacturer or different origin of the powder; STx (x=1,2,3,...): each value of x represents a different ST (sintering temperature); CMT: cement (otherwise it is a sintered ceramic); PH: pre-hardened; *: refers to the surface of the disc; COS: concavities on the surface; O&CC: open and closed channels; +/-: whether a certain material induced/did not induce bone formation in that particular study in at least one of the investigated time points (bone incidence among individuals or bone amounts are not compared); NM: not mentioned in the original article; shape can be a cylinder, disc, rod, block and cube, when implanted in the form of solid pieces of material (in the case of calcium phosphate ceramics).

Authorship, Publication Year	Animal model	Implantation time (days)	Materials			
			Chem Comp/ Commer name	Form/Shape	P/D /H	B
CERAMICS						
Calcium Phosphate Ceramics						
Ripamonti, 1991	Baboon; IM	30/60/120	HA	Cylinder	P	+
Vergervik, 1992	Monkey; SC; IM	28/98	HA	Block	P	+
Yamasaki and Sakai, 1992	Dog; SC	30/90/180	HA	Granules	D P	- +
Toth et.al., 1993	Dog; SC	180	60HA/40βTCP αCaPP βCaPP	Granules	P	+ + +
Klein et.al., 1994	Dog; IM	30/90/ 150/210	HA (I)	Cylinder	D	-
			HA (I) HA (II) HA/αTCP (I) HA/αTCP (I)		P	+ + + +

	Rat; SC	21/42/84	HA (II) 70HA/30βTCP (II) 30HA/70βTCP (II) βTCP (II)	NM	P	- - - -
Pollick et.al., 1995b	Dog; IM, SC	120	HA HA/CC	Rod	P	+ +
Magan and Ripamonti, 1996	Baboon; IM	90	HA	Disc	P	+
Ripamonti et.al., 1996	Dog, Baboon, Rabbit; IM	90	HA	Rod	P	+ + +
Yang et.al., 1996	Rat, Rabbit, Goat; IM, SC	15·/30·/45/ 60/90/120 ·implanted only in dogs and rabbits	63HA/37TCP	Cylinder	P	-
	Dog, Pig; IM, SC					+
Yang et.al., 1997	Dog; IM	7/15/30/ 45/60/90/120	65HA/35βTCP	Cylinder	P	+
Yuan et.al., 1998	Dog; IM	90/180 30/45/60/ 90/180	HA (I) HA_{ST2} (II) HA_{ST1} (II)	Cylinder	P	- + +
		30/45/90/150/ 180 30/45/60 30/45/150	HA/TCP αTCP βTCP			+ - +
		37/60/180 90/180	αTCP/DCPD/HA	PH CMT CMT paste		+ +
Yuan et.al., 1999	Dog; IM	90/180	HA I HA II	Rod	P	+ -
Ripamonti et.al., 1999	Baboon; IM	30/90	HA I HA II HA III HA IV HA V	Rod	P	+ + + + +
Yuan et.al., 2000	Dog; IM	90/180 30/60/180	HA/αTCP/DCPD HA/αTCP/DCPD	CMT paste PH CMT paste	P	+ +
Yuan et.al., 2001	Dog; IM	30/45/150	αTCP βTCP	Disc	P	- +
Yuan et.al., 2001	Dog; IM	913	HA 63HA/37βTCP	Disc	P	+ +

			βTCP			-
			αTCP			-
Eid et.al., 2001	Rat; SC	7	HA	Particles	NM	-
			βTCP			-
			65HA/35βTCP			-
Kurashina et.al., 2002	Rabbit; IM	120	70HA/30TCP	Rod	P	+
			20HA/80TCP			-
			TCP			-
Yuan et.al., 2002	Goat; IM	84	HA	Cube	P	-
			80-90HA/20±10βTCP	Cube	P	+
Gosain et.al., 2002	Sheep; IM,SC	365	60HA/40βTCP	Disc	P	+
			60HA/40βTCP	CMT paste		+
			20HA/80βTCP	Disc		+
			HA	CMT paste		+
			HA	Disc		+
				Disc		+
				CMT paste		
				Disc		
Kruyt et.al., 2004b	Goat; IM	84	HA	Granules	P	+

Habibovic et.al., 2005	Goat; IM	42/84	HA_{ST1}	Cylinder	P	+
			HA_{ST2}			-
			$12HA/88\beta TCP_{ST3}$			+
			$12HA/88\beta TCP_{ST1}$			+
			$12HA/88\beta TCP_{ST4}$			+
Le Nihouannen et.al., 2005	Sheep; IM	180	60HA/40βTCP	Granules	P	+
Habibovic et.al., 2006a	Goat; IM,SC	84	$80HA/20\beta TCP_{ST1}$ I	Cylinder	P	+
			$60HA/40\beta TCP_{ST2}$ I			-
			70HA/30βTCP II			-
			70HA/30βTCP II			+
			CA			-
Habibovic et.al., 2006c	Goat; IM	90	$80HA/20\beta TCP_{ST1}$	Disc	P	+
			$80HA/20\beta TCP_{ST2}$			+
Kondo et.al., 2006	Dog; IM	14/28/42/56/ 112/168	βTCP	Block	P	+
Yuan et.al., 2006	Rat; IM	90	HA	Cylinder	P	-
			62HA/38βTCP			-
	Dog, Rabbit; IM Mouse; SC		HA			+ only dog
			62HA/38βTCP			

						+
Yuan et.al., 2006a	Dog; IM	7/14/21/30/45/ 60/90/180/360	HA 62HA/38βTCP	Cylinder	P	+ +
Bodde et.al., 2007	Goat; SC	90/180	CP (61% αTCP)	CMT cylinder	P	-
Ripamonti et.al., 2007	Baboon; IM	90/180	HA 77HA/33βTCP HA HA	Disc Disc (coarse*) Disc (fine*)	COS	+ + + +
Habibovic et.al., 2008	Goat; IM	84	DCPD DCPA	Cube Cube	OCC OCC	+ +
Habibovic et.al., 2008	Goat; IM	84	80HA/20βTCP ST1 80HA/20βTCP ST2 70HA/30βTCP ST3 70HA/30βTCP ST3 +PLA HA CA	Cylinder	P	+ - + + - -
Ripamonti et.al., 2008	Baboon; IM	90/365	HA 19HA/81βTCP 14HA/86βTCP	Disc	COS	+ + +
Nasu et.al., 2009	Dog; IM	21/42/84	βTCP	Cylinder	P	+
Ripamonti et.al., 2009	Baboon; IM	60/90/365	5HA/95CC 13HA/87CC HA	Rod	P	+ + +
Ripamonti et.al., 2010	Baboon; IM	90	7HA/93CC	Rod	P	+
Habibovic et.al., 2010	Goat; IM	84	CA I CA II	Disc	P	+ -
Yuan et. al., 2010	Sheep; IM	84	10HA/90βTCP ST1 10HA/90βTCP ST2 TCP	Particles	P	+ + +
Calcium phosphate coatings						
De Bruijn et.al., 2000	Dog; IM	90	Ta Ta OCP-coated	Cylinder	P	- +
Barrere et.al., 2003	Goat; IM	84/168	Ti6Al4V OCP-coated Ti6Al4V Ta OCP-coated Ta	Cylinder	P	+ - + -
Habibovic et.al., 2004	Goat; IM	42/84	Ti6Al4V Ti6Al4V OCP-coated	Cylinder	P	- +

Other Ceramics						
Seyle et. al., 1960	Rat; SC	60	Pyrex®	Disc	H	+
Yuan et.al., 1998	Dog; IM	37/60/180	TiO_2	Cylinder	P	-
Yuan et.al., 2001c	Dog; IM	90	Al_2O_3	Cylinder	P	+
Yuan et.al., 2001b	Dog; IM	90	Bioglass®	Cylinder	P	+
METALS						
Fujibayashi et.al., 2004	Dog; IM	90/360	Ti	Block	P	-
			Ti chemically treated			+
			Ti	Mesh Cylinder		-
			Ti chemically treated			-
Takemoto et.al., 2006	Dog; IM	90/180/360	Alkali-heat treated Ti	Cylinder	P	+
			Water/Alkali-heat treated Ti			+
			Dilute HCL/ Alkali-heat treated Ti			+
HYBRIDS/COMPOSITES						
Li et.al., 2007	Goat; IM	84	Ti6Al4V	BCP Cylinders inside a Ti6Al4V cylinder	P	-
			Ti6Al4V + BCP hybrid			+
Hasegawa et.al., 2007	Dog; IM	30/45/60/90/180/360	PDLLA	Cylinder	P	-
			70HA/30PDLLA			+
Barbieri et.al., 2010	Dog; IM	84	PDLLA	Block	P	-
			10HA/90PDLLA			-
			20HA/80PDLLA			-
			40HA/60PDLLA			+
POLYMERS						
Winter and Simpson, 1969	Pig; IM	5/10/26/62	Poly-HEMA	Disc	P	+

Acknowledgments

The authors gratefully acknowledge the financial support of the TeRM Smart Mix Program of the Netherlands Ministry of Economic Affairs and the Netherlands Ministry of Education, Culture and Science (AB) and Innovative Research Incentives Scheme Veni of the Netherlands Organisation for Scientific Research (PH). Hugo Fernandes and Charlène Danoux are acknowledged for critical reading of the manuscript.

References

[1] Friedenstein AY. Clin Orthop Relat Res. 1968;59:21-37
[2] Bertelsen A. Acta Orthop Scand. 1944;15:139-81
[3] Huggins C. Arch Surg. 1931;22:377-408
[4] Levander G. Acta Chir Scand. 1934;74:425-6
[5] Urist MR, McLean FC. J Bone Joint Surg Am. 1952;34-A:443-76
[6] Moss ML. Science. 1958;127(3301):755-6
[7] Urist MR. Science. 1965;150(3698):893-9
[8] Urist MR, Silverman BF, Buring K, Dubuc FL, Rosenberg JM. Clin Orthop. 1967;53:243-83
[9] Urist MR, Strates BS. J Dent Res. 1971;50(6):1392-406
[10] Wilson-Hench J. Osteoinduction. In: Williams D, ed. Progress in biomedical engineering: Definitions in biomaterials. Elsevier, Amsterdam, 1987
[11] Reddi AH. Coll Relat Res. 1981;1(2):209-26
[12] Sasano Y, Ohtani E, Narita K, Kagayama M, Murata M, Saito T, Shigenobu K, et al. Anat Rec. 1993;236(2):373-80
[13] Kuboki Y, Saito T, Murata M, Takita H, Mizuno M, Inoue M, Nagai N, et al. Two distinctive Connect Tissue Res. 1995;32(1-2):219-26
[14] Liu Y, de Groot K, Hunziker EB. Bone. 2005;36(5):745-57
[15] Selye H, Lemire Y, Bajusz E. 1960;151:572-85
[16] Winter GD, Simpson BJ. Nature. 1969;223(5201):88-90
[17] Winter GD. Proc R Soc Med. 1970;63(11 Part 1):1111-5
[18] de Groot K. Calcif Tissue Res. 1973;13(4):335-7
[19] Klein C, de Groot K, Chen W, Li Y, Zhang X. Biomaterials. 1994;15(1):31-4
[20] Ripamonti U. Biomaterials. 1996;17(1):31-5
[21] Yamasaki H. Jpan J Oral Biol. 1990;32:190-2
[22] Yamasaki H, Sakai H. Biomaterials. 1992;13(5):308-12
[23] Zhang X. A study of porous block HA ceramics and its osteogenesis. In: Bioceramics and the human body. Ravaglioli A, Krajewski A, eds. Elsevier, Amsterdam; 1991
[24] Pollick S, Shors EC, Holmes RE, Kraut RA. J Oral Maxillofac Surg. 1995;53(8):915-22
[25] Ripamonti U. J Bone Joint Surg. 1991;73(5):692-703
[26] Vargervik K. Critical sites for new bone formation. In: Bone grafts and bone substitutes. Habal MB, Reddi AH, eds. WB Saunders, Philadelphia; 1992
[27] Gosain AK, Song L, Riordan P, Amarante MT, Nagy PG, Wilson CR, Toth JM, et al. Plast Reconstr Surg. 2002;109(2):619-30
[28] Habibovic P, Gbureck U, Doillon CJ, Bassett DC, van Blitterswijk CA, Barralet JE. Biomaterials. 2008;29(7):944-53
[29] Yuan H, Li Y, de Bruijn JD, de Groot K, Zhang X. Biomaterials. 2000;21(12):1283-90
[30] Habibovic P, van der Valk CM, van Blitterswijk CA, De Groot K, Meijer G. J Mater Sci Mater Med. 2004;15(4):373-80
[31] Barrere F, van der Valk CM, Dalmeijer RA, Meijer G, van Blitterswijk CA, de Groot K, Layrolle P. J Biomed Mater Res. A. 2003;66(4):779-88
[32] Pollick S, Shors EC, Holmes RE, Kraut RA. J Oral Maxillofac Surg. 1995;53(8)915-22
[33] Magan A, Ripamonti U. J Craniofac Surg. 1996;7(1):71-8
[34] Ripamonti U, Crooks J, Khoali L, Roden L. Biomaterials. 2009;30(7):1428-39
[35] Ripamonti U, Klar RM, Renton LF, Ferretti C. Biomaterials. 2010;31(25):6400-10
[36] Barbieri D, Renard AJ, de Bruijn JD, Yuan H. Eur Cell Mater. 2010;19:252-61
[37] Hasegawa S, Neo M, Tamura J, Fujibayashi S, Takemoto M, Shikinami Y, Okazaki K, et al. J Biomed Mater Res A. 2007;81(4):930-8
[38] Yuan H, de Bruijn JD, Zhang X, van Blitterswijk CA, de Groot K, editors. Osteoinduction by porous alumina ceramic. European Conference on Biomaterials; 2001; London, UK.
[39] Fujibayashi S, Neo M, Kim HM, Kokubo T, Nakamura T. Biomaterials. 2004;25(3):443-50
[40] Takemoto M, Fujibayashi S, Matsushita T, Suzuki J, Kokubo T, Nakamura T, editors. Osteoinductive ability of porous titanium implants following three types of surface treatment. 51st Annual Meeting of the Orthopaedic Research Society; 2005; Washington DC.
[41] Yuan H, de Bruijn JD, Zhang X, van Blitterswijk CA, de Groot K. J Biomed Mater Res. 2001;58(3):270-6

[42] Yuan H, Van Den Doel M, Li S, Van Blitterswijk CA, De Groot K, De Bruijn JD. J Mater Sci Mater Med. 2002;13(12):1271-5
[43] Ohgushi H, Goldberg VM, Caplan AI. J Orthop Res. 1989;7(4):568-78
[44] Ohgushi H, Dohi Y, Tamai S, Tabata S. J Biomed Mater Res. 1993;27(11):1401-7
[45] Yang Z, Yuan H, Tong W, Zou P, Chen W, Zhang X. Biomaterials. 1996;17(22):2131-7
[46] Yuan H, van Blitterswijk CA, de Groot K, de Bruijn JD. Tissue Eng. 2006;12(6):1607-15
[47] Reddi AH. Curr Opin Cell Biol. 1992;4(5):850-5
[48] Reddi AH. Curr Opin Genet Dev. 1994;4(5):737-44
[49] Wozney JM. Eur J Oral Sci. 1998;106 Suppl 1:160-6
[50] Habibovic P, Yuan H, van den Doel M, Sees TM, van Blitterswijk CA, de Groot K. J Orthop Res. 2006;24(5):867-76
[51] Habibovic P, Yuan H, van der Valk CM, Meijer G, van Blitterswijk CA, de Groot K. Biomaterials. 2005;26(17):3565-75
[52] Ono I, Gunji H, Kaneko F, Saito T, Kuboki Y. J Craniofac Surg. 1995;6(3):238-44
[53] Kato M, Toyoda H, Namikawa T, Hoshino M, Terai H, Miyamoto S, Takaoka K. Biomaterials. 2006;27(9):2035-41
[54] Habibovic P, Kruyt MC, Juhl MV, Clyens S, Martinetti R, Dolcini L, Theilgaard N, et al. J Orthop Res. 2008;26(10):1363-70
[55] Ripamonti U, Crooks J, Kirkbride AN. South African J Sci. 1999;95(8):335-43
[56] Le Nihouannen D, Daculsi G, Saffarzadeh A, Gauthier O, Delplace S, Pilet P, Layrolle P. Bone. 2005;36(6):1086-93
[57] Yuan H, de Bruijn JD, Zhang X, van Blitterswijk CA, de Groot K. J Mater Sci Mater Med. 2001;12(9):761-6
[58] Boakye M, Mummaneni PV, Garrett M, Rodts G, Haid R. J Neurosurg Spine. 2005;2(5):521-5
[59] Vaccaro AR, Patel T, Fischgrund J, Anderson DG, Truumees E, Herkowitz HN, Phillips F, et al. Spine. 2004;29(17):1885-92
[60] Yuan H, Fernandes H, Habibovic P, de Boer J, Barradas AM, de Ruiter A, Walsh WR, et al. Proc Natl Acad Sci USA. 2010;107(31):13614-9
[61] Davies JE, Hosseini MM. Histodynamics of endosseous wound healing. In: Bone engineering. Davies JE, editor. Toronto, Canada: em squared Inc.; 2000. p. 1-14.
[62] Li J, Habibovic P, Yuan H, van den Doel M, Wilson CE, de Wijn JR, van Blitterswijk CA, et al. Biomaterials. 2007;28(29):4209-18
[63] van Eeden SP, Ripamonti U. Plast Reconstr Surg. 1994;93(5):959-66
[64] Yuan H, Kurashina K, de Bruijn JD, Li Y, de Groot K, Zhang X. Biomaterials. 1999;20(19):1799-806
[65] Yuan H, Yang Z, de Bruijn JD, de Groot K, Zhang X. Biomaterials. 2001;22(19):2617-23
[66] Yuan H, de Bruijn JD, Li Y, Feng Z, Yang K, de Groot K, Zhang X. J Mater Sci Mater Med. 2001;12(1):7-13
[67] Toth J, Lynch K, Hackbarth D. Bioceramics. 1993;6:9-13
[68] Van der Stok J, Van Lieshout EM, El-Massoudi Y, Van Kralingen GH, Patka P. Acta Biomater. 2011;7(2):739-50
[69] Williams DF, editor. The Williams dictionary of biomaterials. Liverpool, UK: Liverpool University Press; 1999.
[70] LeGeros RZ. Chem Rev. 2008;108(11):4742-53
[71] Elliot JC. Structure and chemistry of the apatites and other calcium orthophosphates. Amsterdam: Elsevier; 1994
[72] Yuan H, van Blitterswijk CA, de Groot K, de Bruijn JD. J Biomed Mater Res A. 2006;78(1):139-47
[73] Kurashina K, Kurita H, Wu Q, Ohtsuka A, Kobayashi H. Biomaterials. 2002;23(2):407-12
[74] Habibovic P, Sees TM, van den Doel MA, van Blitterswijk CA, de Groot K. J Biomed Mater Res A. 2006;77(4):747-62
[75] Muschler GF, Nakamoto C, Griffith LG. The Journal of bone and joint surgery. 2004;86-A(7):1541-58
[76] Bodde EW, Cammaert CT, Wolke JG, Spauwen PH, Jansen JA. J Biomed Mater Res B Appl Biomater. 2007;83(1):161-8
[77] Ripamonti U, van den Heever B, Crooks J, Tucker MM, Sampath TK, Rueger DC, Reddi AH. J Bone Miner Res. 2000;15(9):1798-809
[78] Fellah BH, Gauthier O, Weiss P, Chappard D, Layrolle P. Biomaterials. 2008;29(9):1177-88
[79] Wallwork M, Kirkham J, Zhang J, Alastair Smith D, Brookes S, Shore R, Wood S, et al. Langmuir. 2001;17(8):2508-13
[80] Kandori K, Horigami N, Kobayashi H, Yasukawa A, Isikawa T. J Colloid Interface Sci. 1997;191(2):498-502
[81] Zhou H, Wu T, Dong X, Wang Q, Shen J. Biochem Biophys Res Commun. 2007;361(1):91-6

[82] Boix T, Gomez-Morales J, Torrent-Burgues J, Monfort A, Puigdomenech P, Rodriguez-Clemente R. J Inorg Biochem. 2005;99(5):1043-50
[83] Uludag H, D'Augusta D, Palmer R, Timony G, Wozney J. J Biomed Mater Res. 1999;46(2):193-20
[84] Dalby MJ, Gadegaard N, Tare R, Andar A, Riehle MO, Herzyk P, Wilkinson CD, et al. Nature materials. 2007;6(12):997-1003
[85] Marusic A, Katavic V, Grcevic D, Lukic IK. Bone. 1999;25(1):25-32
[86] An YH, Friedman RJ. Animal models of bone defect repair. In: An YH, Friedman RJ, editors. Animals models in orthopaedic research. Boca Raton, USA: CRC Press LLC; 1999. p. 241-60.
[87] Anderson J. The cellular cascades of wound healing. In: Davies J, editor. Bone engineering. Toronto: Em squared; 2000. p. 81-93.
[88] Zaffe D. Micron. 2005;36(7-8):583-92
[89] Le Nihouannen D, Saffarzadeh A, Gauthier O, Moreau F, Pilet P, Spaethe R, Layrolle P, et al. J Mater Sci Mater Med. 2008;19(2):667-75
[90] Castellani C, Zanoni G, Tangl S, van Griensven M, Redl H. Clin Oral Implants Res. 2009;20(12):1367-74
[91] Jones AC, Arns CH, Hutmacher DW, Milthorpe BK, Sheppard AP, Knackstedt MA. Biomaterials. 2009;30(7):1440-51
[92] Komlev VS, Mastrogiacomo M, Pereira RC, Peyrin F, Rustichelli F, Cancedda R. Eur Cell Mater. 2010;19:136-46
[93] Fellah BH, Josselin N, Chappard D, Weiss P, Layrolle P. J Mater Sci Mater Med. 2007;18(2):287-94
[94] Adkisson HD, Strauss-Schoenberger J, Gillis M, Wilkins R, Jackson M, Hruska KA. J Orthop Res. 2000;18(3):503-11
[95] Wolfinbarger L, Jr., Zheng Y. *in vitro* Cell Dev Biol Anim. 1993;29A(12):914-6
[96] Zhang M, Powers RM, Jr., Wolfinbarger L, Jr. J Periodontol. 1997;68(11):1076-84
[97] Carnes DL, Jr., , De La Fontaine J, Cochran DL, Mellonig JT, Keogh B, Harris SE, Ghosh-Choudhury N, et al. J Periodontol. 1999;70(4):353-63
[98] Han B, Tang B, Nimni ME. J Orthop Res. 2003;21(4):648-54
[99] Habibovic P, Woodfield T, de Groot K, van Blitterswijk C. Adv Exp Med Biol. 2006;585:327-60
[100] Fellah BH, Delorme B, Sohier J, Magne D, Hardouin P, Layrolle P. J Biomed Mater Res A. 2010;93(4):1588-95
[101] Yang ZJ, Yuan H, Zou P, Tong W, Qu S, Zhang XD. J Mater Sci Mater Med. 1997;8(11):697-701
[102] Kondo N, Ogose A, Tokunaga K, Umezu H, Arai K, Kudo N, Hoshino M, et al. Biomaterials. 2006;27(25):4419-27
[103] Ripamonti U, van den Heever B, van Wyk J. Matrix. 1993;13(6):491-502
[104] van Gaalen S, Kruyt M, Meijer G, Mistry A, Mikos A, van den Beucken J, Jansen J, et al. Tissue engineering of bone. In: Van Blitterswijk C, Thomsen P, Lindahl A, Hubbel J, Williams D, Cancedda R, et al., editors. Tissue Engineering. London: Academic Press; 2008. p. 559-610.
[105] Collett GD, Canfield AE. Circ Res. 2005;96(9):930-8
[106] Brighton CT, Lorich DG, Kupcha R, Reilly TM, Jones AR, Woodbury RA, 2nd. Clin Orthop Relat Res. 1992;(275):287-99
[107] Sato K, Urist MR. Clin Orthop Relat Res. 1985;(197)301-11
[108] Diaz-Flores L, Gutierrez R, Lopez-Alonso A, Gonzalez R, Varela H. Clin Orthop Relat Res. 1992;(275):280-6
[109] da Silva Meirelles L, Caplan AI, Nardi NB. Stem Cells. 2008;26(9):2287-99
[110] Crisan M, Yap S, Casteilla L, Chen CW, Corselli M, Park TS, Andriolo G, et al. Cell Stem Cell. 2008;3(3):301-13
[111] Zheng B, Cao B, Crisan M, Sun B, Li G, Logar A, Yap S, et al. Nat Biotechnol. 2007;25(9):1025-34
[112] De Groot J. Tissue Eng. 1998;4(4):337-41
[113] Nasu T, Takemoto M, Akiyama N, Fujibayashi S, Neo M, Nakamura T. J Biomed Mater Res A. 2009;89(3):601-8
[114] Urist MR, Huo YK, Brownell AG, Hohl WM, Buyske J, Lietze A, Tempst P, et al. Proc Natl Acad Sci U S A. 1984;81(2):371-5
[115] Luyten FP, Cunningham NS, Ma S, Muthukumaran N, Hammonds RG, Nevins WB, Woods WI, et al. J Biol Chem. 1989;264(23):13377-80
[116] Wang EA, Rosen V, Cordes P, Hewick RM, Kriz MJ, Luxenberg DP, Sibley BS, et al. Proc Natl Acad Sci U S A. 1988;85(24):9484-8
[117] Cola C, Almeida M, Li D, Romeo F, Mehta JL. Biochem Biophys Res Commun. 2004;320(2):424-7
[118] Sorescu GP, Song H, Tressel SL, Hwang J, Dikalov S, Smith DA, Boyd NL, et al. Circ Res. 2004;95(8):773-9

[119] de Bruijn J, Shankar K, Yuan H, Habibovic P. Osteoinduction and its evaluation. In: Kokubo T, editor. Bioceramics and their clinical applications. Cambridge, UK: Woodhead Publishing Ltd; 2008. p. 199-219.
[120] Refai AK, Textor M, Brunette DM, Waterfield JD. J Biomed Mater Res A. 2004;70(2):194-205
[121] Thomsen P, Gretzer C. Curr Opin in Solid State and Mater Sci 2001;5:163-76
[122] Kan L, Liu Y, McGuire TL, Berger DM, Awatramani RB, Dymecki SM, Kessler JA. Stem Cells. 2009;27(1):150-6
[123] Doherty TM, Asotra K, Fitzpatrick LA, Qiao JH, Wilkin DJ, Detrano RC, Dunstan CR, et al. Proc Natl Acad Sci U S A. 2003;100(20):11201-6
[124] Yuan H, Fernandes H, Habibovic P, de Boer J, Barradas AMC, De Ruiter A, Walsh WR, et al. Nat Rev Rheumatol. 2011;7(4):8-9
[125] Ripamonti U. Smart biomaterials with intrinsic osteoinductivity: geometric control of bone differentiation. In: Davies JM, editor. Bone engineering. Toronto, Canada: em squared Corporation; 2000. p. 215-21.
[126] de Bruijn JD, Yuan H, Dekker R, Layrolle P, de Groot K, van Blitterswijk CA. Osteoinductive biomimetic calcium-phosphate coatings and their potential use as tissue-engineering scaffolds. In: Davies JE, editor. Bone engineering. Toronto, Canada: em squared; 2000. p. 421-31.
[127] Yuan H, Yang Z, Li Y, Zhang X, De Bruijn JD, De Groot K. J Mater Sci Mater Med. 1998;9(12):723-6
[128] Kruyt MC, de Bruijn JD, Yuan H, van Blitterswijk CA, Verbout AJ, Oner FC, Dhert WJ. Transplantation. 2004;77(3):359-65
[129] Habibovic P, Juhl MV, Clyens S, Martinetti R, Dolcini L, Theilgaard N, van Blitterswijk CA. Acta Biomater. 2010;6(6):2219-26
[130] Ripamonti U, Richter PW, Thomas ME. Plast Reconstr Surg. 2007;120(7):1796-807
[131] Ripamonti U, Richter PW, Nilen RW, Renton L. J Cell Mol Med. 2008;12(6B):2609-21
[132] Eid K, Zelicof S, Perona BP, Sledge CB, Glowacki J. J Orthop Res. 2001;19(5):962-9

Chapter 3

A calcium-induced signaling-cascade leading to osteogenic differentiation of human bone marrow-derived mesenchymal stromal cells

Ana M. C. Barradas, Hugo Fernandes, Nathalie Groen, Yoke Chin Chai, Jan Schrooten, Jeroen van de Peppel, Johannes P.T.M. van Leeuwen, Clemens A. van Blitterswijk, Jan de Boer

Abstract

The response of osteoprogenitors to calcium (Ca^{2+}) is of primary interest for both normal bone homeostasis and the clinical field of bone regeneration. The latter makes use of calcium phosphate-based bone void fillers to heal bone defects, but it is currently not known how Ca^{2+} released from these ceramic materials influences cells in situ. Here, we have created an in vitro environment with high extracellular Ca^{2+} concentration and investigated the response of human bone marrow derived mesenchymal stromal cells (hMSCs) to it. Ca^{2+} enhanced proliferation and morphological changes in hMSCs. Moreover, the expression of osteogenic genes is highly increased. A 3-fold up-regulation of BMP-2 is observed after only 6 hours and pharmaceutical interference with a number of proteins involved in Ca^{2+} sensing showed that not the calcium sensing receptor, but rather type L Voltage Gated Calcium Channels are involved in mediating the signaling pathway between extracellular Ca^{2+} and BMP-2 expression. MEK1/2 activity is essential for the effect of Ca^{2+} and using microarray analysis, we have identified c-fos as an early Ca^{2+} response gene. We have demonstrated that hMSC osteogenesis can be induced via extracellular Ca^{2+}, a simple and economic way of priming hMSCs for bone tissue engineering applications.

Introduction

Calcium phosphate (CaP) biomaterials are frequently used as bone graft substitutes, mostly because their chemical composition resembles that of the bone mineral phase. For purely synthetic bone graft substitutes a balance between different physico-chemical properties that maximizes the osteoconductive and osteoinductive behavior in the host's tissue is desired [1]. For instance, it is assumed that calcium ions (Ca^{2+}) released from the materials plays a role in their bioactive properties, but the molecular mechanism is currently unknown. In bone tissue engineering, however, CaP biomaterials are applied as scaffolds for delivery of mesenchymal stromal cells (MSCs) to the injury site to trigger formation of new bone [2]. Clinical trials have shown proof of principle for the combination of CaP ceramics and human MSCs (hMSCs) in healing bone defects [3-5]. In order to achieve a successful combination of cells and materials, attention has been devoted to certain scaffold parameters, such as porosity (micro and/or macro) [6-8], chemical composition or topography [9, 10] of the scaffold.

Both in the case of bone graft substitutes and as scaffold in bone tissue engineering, dissolution of Ca^{2+} and phosphate ions ($PO_4{}^{3-}$) from the solid phase of CaP biomaterials into the surrounding environment should be considered. Ca^{2+} participates in many cellular functions but its role in those functions remains elusive. In bone, Ca^{2+} has a structural role, since osteoblasts deposit an extracellular matrix (ECM) that contains nucleation sites for mineral deposition. Ca^{2+} and $PO_4{}^{3-}$ are constituents of that mineral phase, being constantly interchanged to the surrounding extracellular environment as free ions during bone remodeling. This dynamic process is finely tuned by parathyroid hormone (PTH), which in turn is secreted in response to Ca^{2+} serum levels. PTH enhances osteoclast-mediated bone resorption, resulting in a local increase in Ca^{2+} concentration ($[Ca^{2+}]$) making it available for several biological functions in the body. As a consequence, osteoblasts and osteoprogenitors are locally exposed to high $[Ca^{2+}]$ but how this affects their function is not yet understood.

In vitro studies have shown that Ca^{2+} positively influences osteogenesis of different cell types, such as pre-osteoblasts [11], osteoblasts [12,13], macrophages [13, 14] and human periosteal derived stem cells (hPDCs) [16]. In addition, it has been shown that Ca^{2+}, dose-dependently, enhances proliferation of MC3T3 and hPDCs [17]. Moreover, upon treatment with Ca^{2+}, the morphology of hPDCs was altered from fibroblastic to cuboidal, a hallmark of osteoblasts. Expression of osteopontin (OP) and osteocalcin (OC) was enhanced [13], as well as that of bone morphogenetic protein-2 (BMP-2) [15, 16], by Ca^{2+}. BMP-2 is essential to maintain bone homeostasis and has a prominent role in fracture healing [17]. It is also known to regulate transcription factors implicated in osteogenic differentiation such as Runx-2 [18] and osterix [17, 19]. Unfortunately, BMP-2 regulation via extracellular Ca^{2+} is poorly understood but, if elucidate, could unveil novel strategies for bone tissue engineering. Understanding how hMSCs sense extracellular Ca^{2+} ($[Ca^{2+}]_o$) released by CaP biomaterials and respond to it becomes fundamental to improve cell-based therapies for bone tissue engineering. There are several mechanism by which cells sense $[Ca^{2+}]_o$. For instance, Ca^{2+} is a ligand for several G-protein coupled receptors (GPCRs), can enter the cell via gap junction hemichannels [20] or activate the Notch signaling pathway in the chick embryo during left-right organ asymmetry acquisition [21]. Furthermore, ion channels such as voltage-gated Ca^{2+} channels (VGCCs), acid sensing ion channels (ASIC) - ASIC1a/ASIC1b - and human ether-à-go-go related gene (HERG) K+ channels open in response to variations in $[Ca^{2+}]$

[22]. The best described GPCR involved in Ca^{2+} sensing is the Calcium Sensing receptor (CaSR), first identified in parathyroid cells and involved in the regulation of PTH secretion [23]. This GPCR has been identified in both osteoblasts and hMSCs [24, 25], although its role is still unclear. Several other receptors belonging to the GPCR family are known to respond to Ca^{2+} fluctuations, such as metabotropic glutamate receptors (mGluRs) [26], gamma-aminobutyric acid (GABA), GABAB and GPRC6A [27] and their activity has been correlated to osteoblast function [28]. L-type VGCCs (L-VGCCs) could be activated by biphasic CaP crystals [29] in a mouse embryonic fibroblast cell line and by hydroxyapatite dissolved Ca^{2+} in human embryonic palatal mesenchyme cells, leading to an increase in OP, Bone Sialoprotein (BSP) and Alkaline Phosphatase (ALP) expression [30].

In osteoblasts, Ca^{2+} treatment results in phosphorylation of extracellular signal regulated kinases 1 and 2 (ERK1/2), which was significantly reduced in the presence of a CaSR antagonist [30]. ERK1/2 phosphorylation also occurred when MC3T3-E1 cells were treated with $PO_4{}^{3-}$ in the presence of Ca^{2+}, but not in its absence [13]. In addition, biphasic CaP crystals failed to induce expression of a characteristic set of genes in mouse embryonic fibroblasts when upstream activators of ERKs were blocked [29]. Besides the MAPK/ERK signaling pathway, Protein Kinase A (PKA) signaling has been implicated in Ca^{2+} induced fibroblast growth factor 2 (FGF-2) gene expression [14] in cementoblasts. Here we have investigated how Ca^{2+} regulates osteogenesis and proliferation of hMSCs and proposed a signaling cascade via which BMP-2 expression is triggered.

Materials and Methods

Cell culture and proliferation

We previously characterized hMSCs as multipotent and they comply with the standard surface marker panel that defines hMSCs [31]. Briefly, cells were isolated from bone marrow aspirates (5-20 ml) obtained from donors with written informed consent. Aspirates were resuspended using 20G needles, plated at a density of 5×10^5 cells/cm^2 and cultured in proliferation medium (PM), consisting of basic medium (BM) comprising α-MEM (Gibco), 10% foetal bovine serum (Lonza), 2 mM L-glutamine (Gibco), 0.2 mM ascorbic acid (Sigma), 100 U/ml penicillin and 100 mg/ml streptomycin (Gibco)) supplemented with 1 ng/ml recombinant human basic fibroblast growth factor (AbD Serotec). hMSCs were expanded at initial seeding density of 1000 cells/cm^2 in PM and medium was refreshed every 2 to 3 days. Cells were harvested at approximately 80% confluency for subculture. All experiments were performed in a 5% CO^2 humid atmosphere at 37°C.

Differentiation media

Osteogenic differentiation medium (OM) consisted of BM containing 10 nM dexamethasone (Sigma). Ca^{2+} medium (CaM) was prepared from BM by diluting in it 100× pH Buffer Solution (pHBS) containing 600 mM CaCl (Sigma-Aldrich). pHBS consisted of demineralized water with 25 mM Hepes (Invitrogen) and 140 mM NaCl (Sigma-Aldrich) [16]. CaM final [Ca^{2+}] was 7.8 mM. BM containing 100× diluted pHBS was used as control medium (CM) and its final [Ca^{2+}] was 1.8 mM.

Cell differentiation experiments
For differentiation experiments, passage two to three hMSCs were seeded at 5000 cells/cm^2 and allowed to adhere overnight in BM. The next day, medium was changed to the experimental culture conditions. Neomycin and cycloheximide (Sigma-Aldrich) were added to CM or CaM at the desired concentrations. $MgSO_4.7H_2O$, $SrCl_2.6H_2O$, $GdCl_3$ (Sigma-Aldrich) were added to pHBS and the different culture media were prepared by diluting those solutions 100$\times$ in BM. Stock solutions of Spermine, NPS2390, Nifedipine, A23187, H89 (Sigma Aldrich) and U0126 (Promega) were dissolved following the manufacturer's instructions and added to either BM, CM or CaM.

Cell proliferation assay
Total DNA was measured with the CyQuant Cell Proliferation Assay kit (Molecular Probes) to assess cell proliferation. Briefly, culture medium was aspirated, cells rinsed with PBS and frozen at -80°C. After thawing, 20 μl/cm^2 of lysis buffer (prepared according to manufacturer's instructions) were added to the samples at room temperature (RT) for 1 hour. Afterwards, cell lysate and CyQuant GR dye (1$\times$) were mixed 1:1 in a 96-well microplate and incubated for 5 minutes. Fluorescence was measured at an excitation and emission wavelengths of 480 and 520 nm, respectively, using a spectrophotometer (Perkin Elmer Corporation).

RNA Isolation, cDNA synthesis and Real Time quantitative PCR
Total RNA was isolated using the NucleoSpin® RNA II isolation kit (Macherey-Nagel) in accordance with the manufacturer's protocol. RNA was collected in RNAse-free water and the total quantity analyzed by spectrophotometry. First strand cDNA synthesis was made from total RNA using iScript (Bio-Rad) according to the manufacturer's protocol. One μl of undiluted cDNA was used for quantitative real time PCR performed on a Light Cycler PCR machine (Roche) using SYBR green I master mix (Invitrogen). Data was analysed using Light Cycler software version 3.5.3, using the fit point method by setting the noise band to the exponential phase of the reaction to exclude background fluorescence. Expression of osteogenic marker genes was normalised to GAPDH levels and fold induction were calculated using the comparative ΔCT method. Primers sequences are shown in table 1.

cRNA synthesis and whole-genome microarray analysis
cRNA was synthesized from 500 ng RNA using the Illumina TotalPrep RNA amplification Kit (Ambion/Life Technologies), according to the manufacturer's protocol. Briefly, single stranded cDNA was synthesized using a T7 oligo(dT) primer followed by second strand synthesis to obtain double stranded cDNA. Biotin-labeled cRNA was generated by in vitro transcription using T7 RNA polymerase. RNA 6000 Nano assay was used to assess both RNA and cRNA integrity on a Bioanalyzer 2100 (Agilent Technologies). Microarrays were performed using Illumina HT-12 v4 expression Beadchips (Illumina, Inc), according to the manufacturer's instructions. Briefly, 750 ng of cRNA was hybridized on each array overnight after which the array was washed and blocked. Fluorescent signal was developed by the addition of streptavidin Cy-3 (GE healthcare). Each array was scanned on an Illumina iScan reader and analyzed with GenomeStudio (Illumina, Inc). Background correction of the raw intensity values was performed in GenomeStudio and further data processing and statistical testing were performed with R and Bioconductor statistical software (http://www.bioconductor.org/),

Table 1: Primers sequences for human genes.

Name	*Primer sequence*
ALP	5'-GACCCTTGACCCCCACAAT-3'
	5'-GCTCGTACTGCATGTCCCCT-3'
BMP-2	Commercially bought (SA Biosciences)
BSP	5'-TGCCTTGAGCCTGCTTCC-3'
	5'-CAAAATTAAAGCAGTCTTCATTTTG-3'
GAPDH	5'-CGCTCTCTGCTCCTCCTGTT-3'
	5'-CCATGGTGTCTGAGCGATGT-3'
ID-1	5'-GCAAGACAGCGAGCGGTGCG-3'
	5'-GGCGCTGATCTCGCCGTTGAG-3'
IGF-1	5'-CTTCAGTTCGTGTGTGGAGACAG-3'
	5'-CGCCCTCCGACTGCTG-3'
OC	5'-GGCAGCGAGGTAGTGAAGAG-3'
	5'-GATGTGGTCAGCCAACTCGT-3'
OP	5'-CCAAGTAAGTCCAACGAAAG-3
	5'-GGTGATGTCCTCGTCTGTA-3'
Runx-2	5'-GGAGTGGACGAGGCAAGAGTTT-3'
	5'-AGCTTCTGTCTGTGCCTTCTGG- 3'

using the lumi-package [32]. Background subtracted intensity values were transformed using variance stabilization and quantile normalized. The probes having an Illumina detection p value <0.01 and detected in at least two samples were filtered and considered for further analysis. A linear modeling approach with empirical Bayesian methods, as implemented in the R package "limma" [33], was applied for differential expression analysis of the resulting probe-level expression values. By uploading the Illumina identifiers and resultant log ratios onto the Ingenuity IPA 9.0 software (Ingenuity Systems, Inc.), gene lists were generated, containing only those from molecules or relationships experimentally observed in human cells.

Staining with fluorescent dyes and Cell Profiler analysis

hMSCs were washed with PBS, fixed with 10% formalin (Sigma) for 10 minutes, permeabilized with 0.1% Triton X-100 for 10 minutes and blocked using 10% v/v FBS. Subsequently, 165 nM of Alexa Fluor 594 (Invitrogen) was added to the cells, to stain the cell cytoskeleton, and incubated at 37°C for 30 minutes upon which they were washed and 1 μg/ml of DAPI (Sigma-Aldrich/Fluka) was added for 10 minutes, to stain the cell nucleus. After washing with PBS, cells were imaged using fluorescence microscopy (BD Pathway 435, BD Biosciences). The analysis was performed in images acquired from five different areas of the sample and at least 50 cells were used to measure morphological parameters using CellProfiler using built-in modules (MeasureObjectAreaShape) [34].

Immunostaining

Medium was aspirated from cell culture samples, cells were washed with PBS and fixed for 20 minutes with freshly prepared 4% v/v paraformaldehyde in PBS, at RT. After permeabi-

lization with 0.25% v/v Triton-X in PBS for 10 minutes, cells were incubated with 1% v/v BSA in 0.1% PBS-Tween (PBST) for 30 minutes to block unspecific binding sites. The CaSR and the phospho T888 CaSR (Abcam) antibodies were diluted in 1% v/v BSA in 0.1% PBST. Polyclonal Rabbit IgG was added undiluted and all primary antibodies were incubated for 1 hour at 37°C. Afterwards, cells were incubated with Goat anti-Rabbit IgG Alexa 488 conjugated (Invitrogen) diluted in 1% v/v BSA in 0.1% PBST for 1 hour at RT, in the dark. To visualize the cell structure, cells were incubated for 15 minutes in 1 μg/ml Dapi (Sigma-Aldrich/Fluka) and for 30 minutes with 165 nM Alexa 568-conjugated phalloidin. Both dyes were diluted in PBS.

Statistical analysis

All experiments were performed with triplicate biological samples. Statistical analysis was done using One-way Analysis of Variance (ANOVA) with Tukey's multiple comparison test ($p < 0.05$), unless otherwise indicated in the figure legend. Error bars indicate standard deviation. For all figures the following applies: * = $p < 0.05$; ** = $p < 0.01$; *** = $p < 0.001$.

Results

To understand how $[Ca^{2+}]_o$ can influence hMSC behavior, we compared cell proliferation, morphology and osteogenic differentiation when cells were treated with control medium (CM), containing 1.8 mM, versus Ca^{2+} Medium (CaM), containing 7.8 mM. The latter concentration was chosen because it induced highest cell numbers and expression of osteogenic markers in hPDCs [16].

Ca^{2+} and proliferation of hMSCs

First, we assessed the effect of elevated $[Ca^{2+}]_o$ on hMSC proliferation. For this, cells were seeded on tissue culture plastics and cultured in CM or CaM. Samples were collected for DNA quantification at 1, 3 and 7 days. At early time points, we did not observe differences in cell numbers between treatments (figure 1). However, we observed higher cell numbers at day 7 in samples treated with CaM compared to CM, suggesting that proliferation of hMSCs is dependent on $[Ca^{2+}]_o$.

Ca^{2+} effect on cell morphology

Next, we investigated whether different $[Ca^{2+}]_o$ would affect cell shape, because in some conditions, cell shape is directly linked to cell differentiation [35-38]. Therefore, differences in morphological cellular parameters between cells treated with CM or CaM could indicate whether to expect differences at differentiation level. Thus, 1000 hMSCs were seeded per cm^2 on glass slides and cultured for 6 and 12 hours in CM or CaM. Cells were fixed and stained with fluorescent dyes for the cell nucleus and actin fibers (blue and red respectively in figure 2A). Samples were imaged with a fluorescent microscope and at least 50 cells per condition were investigated for 13 different standard parameters for both the nucleus and actin fibers. The results shown in figure 2B refer only to parameters in which statistical significant differences were observed for the nuclei, actin fibers or both, between the two treatments.

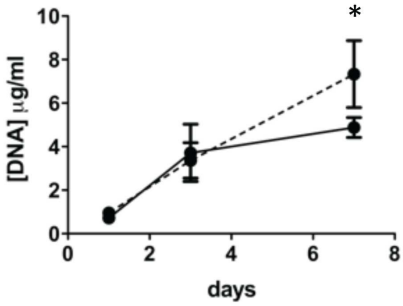

Figure 1: Ca^{2+} induces cell proliferation. DNA concentration was quantified after 1, 3 and 7 days as an indirect measure of cell numbers. At day 7, [DNA] is statistically significantly higher in hMSCs treated with CaM as compared to CM. Statistical analysis was done with Two-Way Anova and Bonferroni post-hoc tests.

After 6 hours, cells treated with CM had a higher nucleus area and higher minor axis length than cells treated with CaM. From 6 to 12 hours, cells from both treatments exhibited decreased nucleus perimeter and were rounder (form factor value closer to 1). After 6 hours, there were no statistical significant differences between the treatments for any of the parameters concerning cell shape (actin fibers). However, after 12 hours, cells treated with CaM were more spread (higher area and larger perimeter) than cells treated with CM. Cells treated with CaM also showed a higher minor axis length. However, cells treated with CM exhibited a rounder morphology (higher form factor value). Evidently, Ca^{2+} induced changes in cellular morphology.

Ca^{2+} effect on gene expression

Differences in the nucleus and cytoskeletal conformation between cells treated with CM and CaM could indicate differentiation. Therefore next we analyzed the actual effects of $[Ca^{2+}]_o$ on hMSCs differentiation. For this, cells were treated with CM and CaM and also with BM and OM as a positive osteogenic control. After 6 hours, 3, 6 and 13 days, we collected samples for RNA isolation and analyzed the expression of several bone related genes (figure 3).

hMSCs cultured in OM exhibited higher expression of Alkaline Phosphatase (ALP) at days 6 and 13 than cells cultured in BM [39] and expression of BMP-2 was lower in OM (figure 3 A), as observed earlier (unpublished data). Expression of ALP and insulin like growth factor 1 (IGF-1) were lower in CaM at most timepoints. No effect was observed on the expression of the transcription factor Runx-2 but in contrast, increased expression of all ECM proteins (OP, BSP and OC) was observed (figure 3 B). Notably OP expression was increased 2000 fold by CaM at day 13.

Furthermore, treatment with CaM increased BMP-2 expression at all time points (figure 4 A). To confirm these data, additional experiments were performed in hMSCs from three different donors and we consistently observed an effect of CaM on BMP-2 gene expression. For

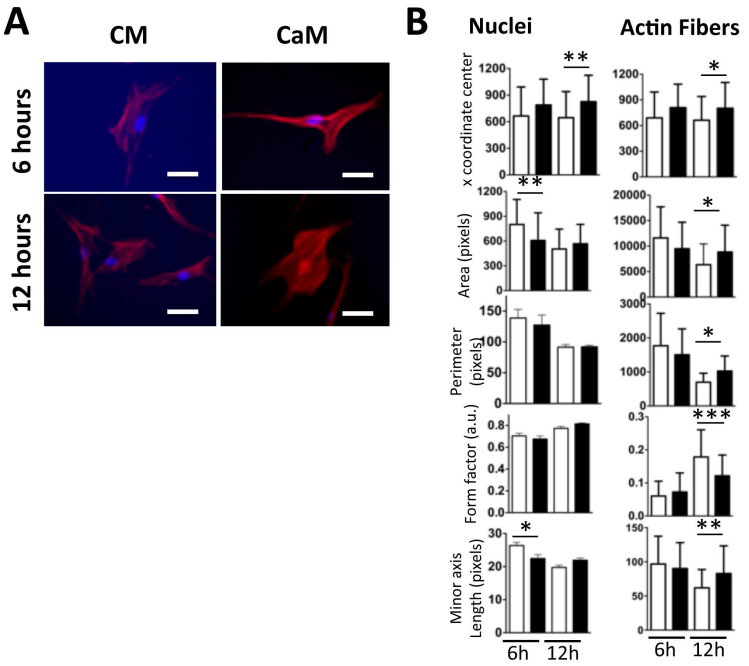

Figure 2: Ca^{2+} induces cell morphological changes. A. Staining of cell nucleus (blue; DAPI) and actin skeleton (red; phaloidin) in cells treated with CM and CaM for 6 and 12 hours. Scale bar is 10 μm. B. Analysis of morphological features of nuclei and actin fibers from dapi and phalloidin stainings respectively in cells cultured in CM (white bars) and CaM (black bars) for 6 and 12 hours. The following parameters were analyzed with the MeasureObjectAreaShape module of Cell Profiler: x coordinate center; area; perimeter; form factor; minor axis length.

instance, BMP-2 expression increased at least 3 fold only 6 hours after initiating the treatment (figure 4 B). Taken together, the observations of higher BMP-2 gene expression, ALP and ECM bone proteins, shows that hMSCs will develop an osteoblastic phenotype due to increased [Ca^{2+}] in the culture medium.

Effect of GPCRs ligands on BMP-2 expression

After disclosing the effects of Ca^{2+} on the expression of bone related genes, we aimed at understanding the signal transduction pathways associated with this interaction. Ca^{2+} sensing via the Calcium Sensing Receptor (CaSR) has been described in vivo [40], as well as in vitro, in some cell types [41, 42]. Since it is known that hMSCs possess this receptor [25], we first hypothesized that the CaSR could be involved in the observed effects of Ca^{2+} on hMSCs that led to BMP-2 gene expression. We selected several well-known CaSR agonists [43], exposed hMSCs to them at different concentrations in CM and after 6 hours we analyzed BMP-2 gene expression. Neither Mg^{2+}, Gd^{3+}, neomycin nor spermine was able to induce BMP-2 expression (figure 5 A and B). In contrast, BMP-2 expression was induced 2 and 3 fold by both 2 and 10 mM Sr^{2+}, respectively which is similar to the effect of CaM. Because

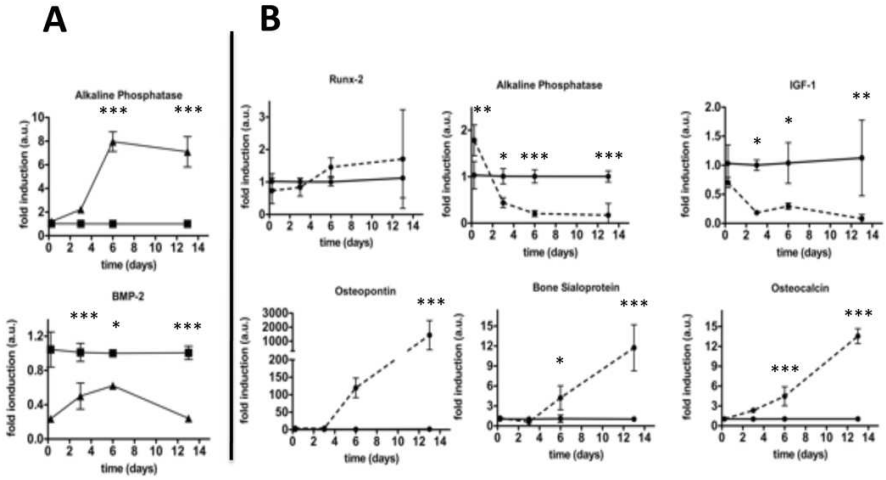

Figure 3: hMSCs osteogenic profile. A. hMSCs were treated with either BM (squares) or OM (triangles). Alkaline Phosphatase and BMP-2 gene expression were measured after 6 hours, 3, 6 and 13 days. B. hMSCs were treated with CM (continuous line) or CaM (dashed line) for 6 hours, 3, 6 and 13 days. CaM increased expression of all bone related extracellular matrix proteins (Osteocalcin, Osteopontin, Bone Sialoprotein) for all late time points but did not have an effect on Runx-2 and decreased expression of IGF-1 and Alkaline Phosphatase relatively to control medium. Statistical Analysis was done with Two-way Anova and Bonferroni post-hoc tests.

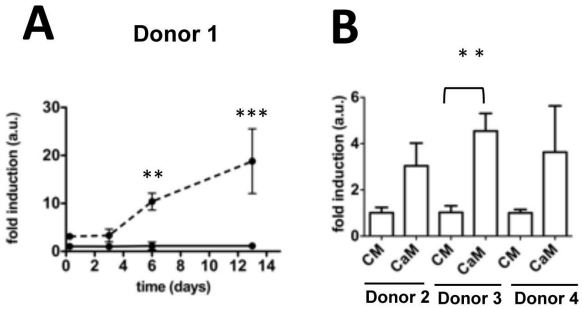

Figure 4: CaM induces expression of BMP-2. hMSCs were treated with CM or CaM. A. BMP-2 expression was analyzed at different time points (6 hours, 3, 6 and 13 days) and was always higher for cells treated with CaM (dashed line) compared to those treated with CM (continuous line), although differences were only statistically significant for 6 and 13 days of culture. Statistical analysis was done with Two-way Anova and Bonferroni post-hoc tests. B. hMSCs from three other donors also showed higher expression of BMP-2 after 6 hours when cultured in the presence of Ca^{2+} as compared to control conditions. Statistical analysis was done for the individual donors with a student's t-test with Welch's correction.

Sr^{2+} was the only CaSR agonist able to induce BMP-2 expression, these data suggests that Ca^{2+}-induced BMP-2 expression in hMSCs is not mediated via the CaSR.

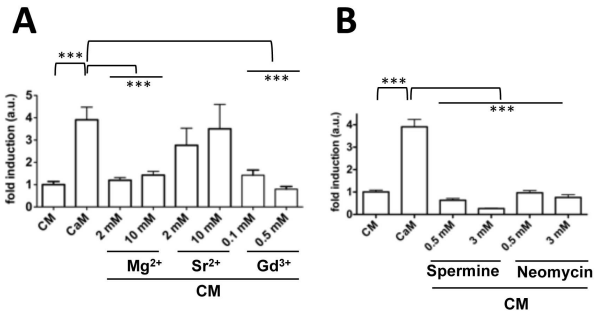

Figure 5: Sr^{2+} induces BMP-2 gene expression. hMSCs were treated with CM, CaM or CM containing different CaSR agonists at various concentrations. BMP-2 expression was analyzed 6 hours later. A. BMP-2 expression increased in the presence of 2 and 10 mM Sr^{2+}, compared to cells in CM. Mg^{2+} and Gd^{3+} did not have an effect on BMP-2 expression. B. BMP-2 expression was not regulated by Spermine nor Neomycin at any of the tested concentrations.

To verify the expression and activity of the CaSR receptor in our hMSCs we stained the CaSr and its phosphorylated form respectively. The CaSR was observed at the cell surface (figure 6), showing that hMSCs express the receptor. The p-CaSR was also detected but there were no apparent differences in the amount of p-CaSR between CM and CaM. This suggested that the receptor can be phosphorylated by both tested $[Ca^{2+}]$s in hMSCs at comparable levels, further suggesting that the CaSR is not involved in mediating BMP-2 expression.

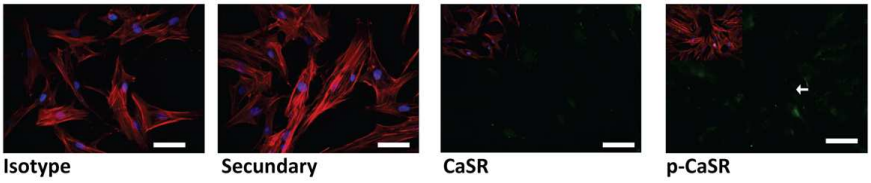

Figure 6: Immunostaining of the Calcium Sensing Receptor (CaSR). hMSCs were treated with CaM for 6 hours and after that fixed and stained with dapi (blue), phalloidin (red) and antibodies against the CaSR and the phosphorilated CaSR (p-CaSR) (green). CaSR and p-CaSR images show only blue and green channel and insight shows all channels. Control stainings with isotype or secundary antibodies alone showed no specific signal. Scale bar is 10 μm.

Next we looked at metabotropic glutamate receptor type 1 (mGluR1), another subclass of Ca^{2+} sensing GPCRs. We pre-treated hMSCs with an antagonist of the mGluR1, NPS2390 [42, 44], for 30 minutes at 1 or 10 μM in CM, followed by 6 hours treatment with the antagonist diluted in CaM (figure 7). BMP-2 expression was not affected by the mGluR1

antagonist after 6 hours, suggesting that this receptor is also not involved in mediating the response of hMSCs to Ca^{2+}.

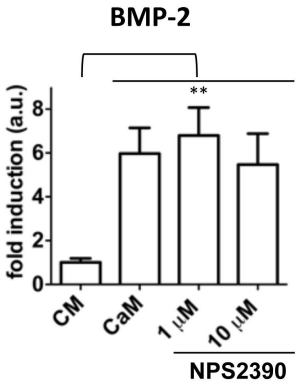

Figure 7: mGluR1 antagonist does not regulate BMP-2 gene expression. hMSCs were treated with either CM, CaM or CaM containing 1 or 10 μM of NPS2390, an antagonist of mGluR1. Before incubation of NPS2390 in CaM, cells were pre-treated with NPS2390 in BM for 30 minutes. BMP-2 expression was measured after 6 hours.

L-VGCCs and BMP-2 expression

Because we did not find evidence for a role of the CaSR and mGluR1 in Ca^{2+} sensing in hMSCs, we looked into the role of L-VGCCs, which upon elevated $[Ca^{2+}]_o$ can transport Ca^{2+} across the cell membrane. To mimick L-VGCC activity, we added a compound, calcium ionophore A23187, which facilitates the transportation of Ca^{2+} via the channels, to both CM and CaM at a final concentration of 10 μM and cultured hMSCs for 6 hours. Interestingly, we observed increased BMP-2 gene expression in the cells treated with both media containing the A23187 when compared to CaM and CM alone, by 1 and 2 fold respectively (figure 8 A). The same experiment was repeated with hMSCs from 2 other donors (figure S1 A), with a positive effect on BMP2 expression in one, but not in the other donor. When hMSCs were cultured in CaM containing 5 μM of Nifedipine, a L-VGCC blocker, BMP-2 expression decreased compared to cells in CaM, although this was not statistically significant (figure 8 B). Additional experiments with two other donors showed no effect of Nifedipine on BMP-2 expression (figure S1 B). Although experiments with A23187 suggest an involvement of L-VGCCs in mediating BMP-2-Ca^{2+} driven expression, Nifedipine data does not fully support it, and additional experiments would have to be performed to verify the role of L-VGCCs in Ca^{2+} induced BMP2 expression.

MEK 1/2 and BMP-2 expression

Next, we investigated whether the PKA signaling pathway could be mediating BMP-2 expression, because it is known that Ca^{2+} is involved in PKA signaling in different cell types [14] and we have previously shown that PKA activation is associated with enhanced BMP2 expression [2]. Therefore, we treated hMSCs with CM and CaM, in the presence or absence

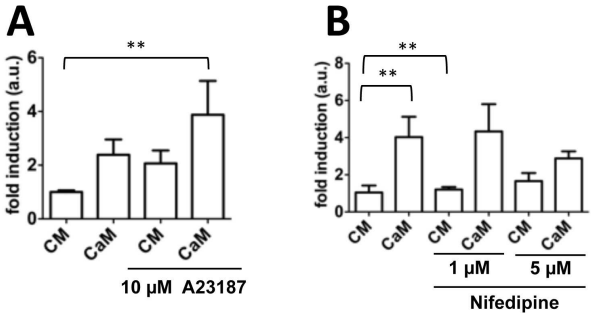

Figure 8: BMP-2 gene expression. hMSCs were treated with either CM, CaM or co-incubated with CM or CaM containing A. Calcium Ionophore A23187 or B. Nifedipine. Before co-incubation, cells were pre-treated with either molecule in BM for 30 minutes. Gene expression was analyzed 6 hours after of co-incubation.

of 1 μM H89, an inhibitor of PKA activity. After 6 hours, we observed a statistically significant decrease in BMP-2 expression in cells cultured in CaM in the presence of H89 compared to cells cultured in CaM alone (figure 9 A). However this effect was not confirmed in other donors (figure S2 A). ERK1/2 is involved in gene expression mediated by calcium in other cell types [11, 45]. To know whether ERK1/2 could be involved in mediating Ca^{2+} induced BMP-2 gene expression, we cultured cells in CM and CaM alone or in the presence of 5 or 20 μM of MEK1/2 inhibitor (U0126), a Map kinase kinase upstream of ERK1/2. After 6 hours, gene expression analysis showed that blocking MEK1/2 results in the abrogation of BMP-2 expression (figure 9 B), showing that MEK1/2 is essential for Ca^{2+} mediated BMP-2 expression, which in this case was confirmed in multiple donors (figure S2 B).

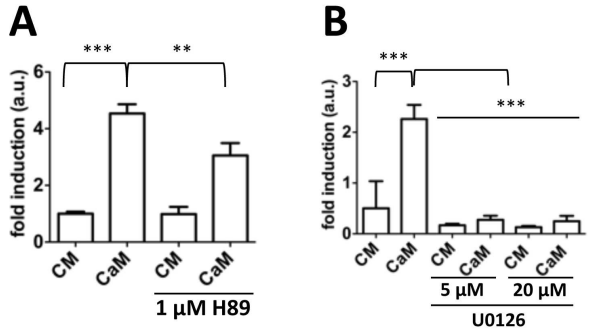

Figure 9: MEK1/2 inhibitors regulate BMP-2 gene expression. hMSCs were treated with either CM or CaM, alone or containing PKA (H89) or Mek 1/2 inhibitors. Before co-incubation, cells were pre-treated with BM containing the respective molecule at the given concentrations for 30 minutes. BMP-2 gene expression was measured 6 hours after co-incubation. A. Treatment with CaM and PKA inhibitor decreased BMP-2 gene expression, compared to CaM alone. B. Treatment with CaM and Mek1/2 inhibitor abrogated BMP-2 expression compared to CaM treatment, at both U0126 concentrations.

Microarray analysis
To understand whether BMP-2 is a direct target gene of Ca^{2+} signaling, not requiring de novo protein synthesis, we exposed hMSCs in CM and CaM to the translation inhibitor cycloheximide (Chx). After 6 hours, BMP-2 gene expression was induced in the control situation, but cycloheximide blocked the Ca^{2+} effect on BMP-2 expression (figure 10), indicating that BMP-2 is not a direct target gene of Ca^{2+} signaling.

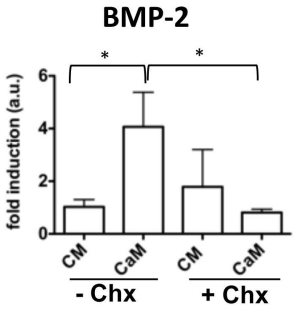

Figure 10: BMP-2 gene expression depends on de novo protein production. hMSCs were treated with either CM or CaM, alone (-Chx) or containing 10 μM of cycloheximide (+Chx). In the presence of cycloheximide, BMP-2 expression was decreased 3 fold compared to CaM alone, after 6 hours.

To further investigate the molecular mechanisms upon treatment with CaM, we performed a microarray analysis. After one and 6 hours of exposure to CaM or CM, samples were collected for RNA isolation and as a control, BMP-2 expression levels compared by qPCR. After 1 hour, no difference in BMP-2 expression was observed, between cells treated with CM or CaM (figure S3), indicating that the BMP-2 promoter was activated between 1 and 6 hours. Therefore, we performed whole genome gene expression analysis on samples treated for 1 hour to analyze the events preceding BMP-2 promoter activation. From the gene expression data, a list of the 38 genes with highest expression in cells treated with CaM is shown in Table 2. Cells treated with CaM showed highest fold change increase for HSPE1 (1.76). Expression of many genes associated with DNA transcription was increased in CaM condition, such as BLZF1, CDK1, EGR1, Fos, HMGB2, KLF6, NFKB1A, NR4A2 and XRCC6.

Discussion

Ca^{2+}-induced osteogenesis and proliferation of several cell types has been previously described but not for hMSCs. Here we have shown that upon treatment of hMSCs with elevated $[Ca^{2+}]_o$, hMSCs exhibited increased proliferation (figure 1) and expression of bone related genes, such as OC, BSP and OP (figure 3 B). As early as 6 hours, expression of BMP-2 is 3-fold induced in cells treated with Ca^{2+} (figure 4), which indicates that Ca^{2+} is a potential osteoinductive trigger in hMSCs.
Interestingly to note are the differences observed between the effects of Ca^{2+} and dexamethasone on hMSCs osteogenesis. Ca^{2+} and dexamethasone seem to have antagonic effects, at least regarding ALP and BMP-2 expressions. Whereas OM decreases BMP-2 expression,

Table 2: Genes regulated in hMSCs by CaM after 1 h.

Symbol	*Entrez gene name*	*Fold Change*
HSPE1	heat shock 10kDa protein 1 (chaperonin 10)	1.75
EGR1	early growth response 1	1.58
RPLP1	ribosomal protein, large, P1	1.45
NR4A2	nuclear receptor subfamily 4, group A, member 2	1.41
STOM	stomatin	1.34
CDK1	cyclin-dependent kinase 1	1.33
RPL22	ribosomal protein L22	1.33
LILRB1	leukocyte immunoglobulin-like receptor, subfamily B (with TM and ITIM domains), member 1	1.32
ELOVL5	ELOVL family member 5, elongation of long chain fatty acids (FEN1/Elo2, SUR4/Elo3-like, yeast)	1.31
SDCBP	syndecan binding protein (syntenin)	1.30
MPST	mercaptopyruvate sulfurtransferase	1.30
CDC42	cell division cycle 42 (GTP binding protein, 25kDa)	1.30
ALDOA	aldolase A, fructose-bisphosphate	1.29
MEST	mesoderm specific transcript homolog (mouse)	1.28
BUB3	budding uninhibited by benzimidazoles 3 homolog (yeast)	1.27
NUSAP1	nucleolar and spindle associated protein 1	1.27
ADD3	adducin 3 (gamma)	1.27
HMGB2	high-mobility group box 2	1.27
NFKBIA	nuclear factor of kappa light polypeptide gene enhancer in B-cells inhibitor, alpha	1.27
KPNA2	karyopherin alpha 2 (RAG cohort 1, importin alpha 1)	1.27
MCL1	myeloid cell leukemia sequence 1 (BCL2-related)	1.26
BLZF1	basic leucine zipper nuclear factor 1	1.26
XRCC6	X-ray repair complementing defective repair in Chinese hamster cells 6	1.26
KLF6	Kruppel-like factor 6	1.26
FOS	FBJ murine osteosarcoma viral oncogene homolog	1.26
ARSA	arylsulfatase A	1.26
FDPS	farnesyl diphosphate synthase	1.25
PTP4A2	protein tyrosine phosphatase type IVA, member 2	1.25
AMY1A	amylase, alpha 1A (salivary)	1.25
PRKAA1	protein kinase, AMP-activated, alpha 1 catalytic subunit	1.25
SMNDC1	survival motor neuron domain containing 1	1.24
ACTA2	actin, alpha 2, smooth muscle, aorta	1.24
SOCS5	suppressor of cytokine signaling 5	1.24
PPT1	palmitoyl-protein thioesterase 1	1.24
PTS	6-pyruvoyltetrahydropterin synthase	1.24
RPS28	ribosomal protein S28	1.24
HNRNPM	heterogeneous nuclear ribonucleoprotein M	1.24
KRIT1	KRIT1, ankyrin repeat containing	1.23
POSTN	periostin, osteoblast specific factor	1.23
CASP6	caspase 6, apoptosis-related cysteine peptidase	1.23
VPS37A	vacuolar protein sorting 37 homolog A (S. cerevisiae)	1.23
LRRFIP1	leucine rich repeat (in FLII) interacting protein 1	1.23
TSNAX	translin-associated factor X	1.23
EIF1AX	eukaryotic translation initiation factor 1A, X-linked	1.23
CRCP	CGRP receptor component	1.22
FXR1	fragile X mental retardation, autosomal homolog 1	1.22
GOLPH3	golgi phosphoprotein 3 (coat-protein)	1.22
PRSS23	protease, serine, 23	1.22

Ca^{2+} enhances it from as early as 6 hours. On the other hand, ALP, whose expression level is increased by OM from day 3 on, in accordance with our data [39] and that of others [46], is decreased by Ca^{2+} from day 3 on. Evidence for the role of Ca^{2+} in hMSCs differentiation was first given based on changes in cell morphology. The onset of Ca^{2+}-induced morphological changes seems to happen first in the nucleus and later in the cytoskeleton. We observed that higher $[Ca^{2+}]_o$ renders the cells with smaller nuclei and enlarged cytoskeletons (increased area and perimeter). Others have shown that cell spreading favors osteogenesis. hMSCs cultured on larger islands of fibronectin committed to osteogenesis whereas those cultured on smaller islands committed to adipogenesis [35].

We further investigated how hMSCs sense $[Ca^{2+}]_o$ that ultimately leads to increased expression of BMP-2. Experiments with GPCR agonists and antagonists, targeting the CaSR and mGluR1 respectively, suggest that these receptors are not involved in BMP-2 expression. However Sr^{2+} did have an effect on BMP-2 expression. Sr^{2+} is known to enhance osteoblasts precursors differentiation [47] and expression of BMP-2 in primary osteoblasts [48]. Furthermore, a link between Sr^{2+}-induced CaSR activation and BMP-2 expression has been proposed in MC3T3 cells [49]. Given our findings, we cannot exclude the possibility that a GPCR similar to the CaSR might be activated and is linked to BMP-2 expression by at least two types of cations: Ca^{2+} and Sr^{2+}.

The hypothesis of an yet unknown calcium sensing mechanism similar to the CaSR has been proposed by others [14]. Kanaya et al. investigated the effects of Ca^{2+} in FGF-2 expression in cementoblasts. Similarly to our findings, some CaSR agonists induced expression of FGF-2, but others didn't. However, their data showed that the signaling pathway upstream of FGF-2 expression required cyclic adenosine monophosphate (cAMP)/PKA activation, excluding the CaSR involvement since cAMP levels are reduced upon activation of the CaSR [42, 50-52]. In our case, the involvement of PKA signaling was suggested in one case, as upon addition of H89 to the culturing medium, BMP-2 expression was decreased. This was not confirmed in other donors and additional experiments have to be performed to clarify the role of cAMP/PKA. However, we have shown in the past that cAMP induces expression of BMP-2 in hMSCs [2]. On the other hand, cAMP also induces ALP in hMSCs and here we have shown that Ca^{2+} decreases expression of ALP (figure 2B).

A23187, a molecule that facilitates Ca^{2+} transportation across L-VGCCs, increased expression of BMP-2, although not in all donors. On the other hand, Nifedipine, a L-VGCC blocker, had only a small effect in one of the donors. The role of L-VGCCs in mediating BMP-2 expression in hMSCs is unclear. However, it should be noticed, that there are four isoforms of L-VGCCs known and affinity to the same blocker varies. For instance, Cav1.3 and Cav1.4, two isoforms of L-VGCCs, show lower affinity for DHP (1,4 dihydropyridine) blockers, such as Nifedipine, than Cav1.2 [53]. We were unable to find literature reporting the expression of isoforms in hMSCs. Furthermore, others have shown that Gd^{3+} blocks L-VGCCs in monocytes [54]. In figure 5A we have shown that Gd^{3+} did not induce BMP-2 expression, which, in light of these findings, could be speculated interpreted as actual inhibition of the expression due to L-VGCCs blockage. Our data clearly shows that MAPK signaling is essential for BMP-2 expression, as a Mek1/2 inhibitor abrogated BMP-2 expression in all donors. Sr^{2+} has been shown to promote osteogenic differentiation of hMSCs via an ERK 1/2 and p38 dependent mechanisms. It was also the only molecule tested that showed an effect on BMP-2 expression (figure 5A). Therefore it seems that Ca^{2+} and Sr^{2+} induced osteogenic

differentiation of hMSCs share a common pathway.

Experiments with cyclohexemide, a protein translation inhibitor, indicated that BMP-2 expression depends on de novo protein synthesis upon treatment with CaM, as its expression was suppressed when cells were treated with that compound. To further understand which molecules could be involved in the expression of BMP-2, we performed a whole genome microarray analysis on cells treated for 1 hour with or without elevated $[Ca^{2+}]_o$. Genes regulated by CaM are shown in Table 2. Among these genes, we identified some that could be involved in the signaling pathways related events activated by Ca^{2+}. Stomatin is present in the vesicles that are usually formed and released at the site of membrane lipid rafts upon elevation of cytosolic levels of Ca^{2+} [55]. Early growth Response 1 (EGR1) is a target of ERK1/2 [56]. Furthermore EGR1 has been related with Ca^{2+} internalization via VGCCs [57]. Jun is a constituent of the activator protein 1 (AP-1) transcription factor dimer, of which the other molecule is Fos, also seen in Table 2. The AP-1 dimer can in turn bind to the AP-1 domain in the promoter region of several genes, such as BMP-2 [58] and BSP [59], which were shown to be both upregulated by CaM. The transcription factor NR4A2 has been shown to activate OP [60] and OC [61] transcription, whose expression was here induced by CaM after 6 and 3 days respectively. Furthermore NR4A2 activity has been linked to MAPK [62]. Taken together these findings suggests a strong involvement of MAPK signaling and Ca^{2+} internalization in mediating the effects of CaM in hMSCs. The data found and discussed above has led us to a proposed mechanism that is summarized in figure 11.

The interaction between degradable ceramic prosthesis or scaffolds, and bone marrow cells, if further understood, can lead to the improvement of regenerative therapies. Although CaP ceramics have been the prime choice in bone tissue regeneration strategies, due to their chemical composition being so close to that of the natural bone, they are not the ideal solution for load bearing applications. Hence, more applicable in these situations would be the use of polymers, which render the scaffold with mechanical properties that can be tuned to match that of the bone. One can envision the combination of polymers and hMSCs for bone tissue engineering in different setups: **1)** enhance osteogenic differentiation of hMSCs in tissue culture plastics with Ca^{2+} (cheaper than any known osteogenic compound) and after a short period of time, seed these cells on polymeric scaffolds; **2)** coat polymeric scaffolds with CaP layers and then seed hMSCs with or without an in vitro culturing period prior to usage in the patient; **3)** a more expensive and sophisticated approach would be to incorporate in the scaffold known molecules that stimulate BMP-2 expression, such as A23187.

Conclusions

We have shown how Ca^{2+} influences the proliferation, morphology and osteogenic differentiation of hMSCs. Furthermore, we have discussed the role of GPCRs, such as CaSR and mGluR1, in mediating the signaling pathway triggered by $[Ca^{2+}]_o$ that results in BMP-2 expression. Our data shows that neither receptor is likely to be part of such molecular mechanism, but we do not exclude the possibility of an unknown GPCR mediating hMSCs BMP-2 expression in response to $[Ca^{2+}]_o$. We also suggest that L-VGCCs play a role in that pathway, but not exclusively. Furthermore, MEK1/2 is essential for BMP-2 expression, probably via Fos expression and AP-1 formation that in turn binds to the AP-1 binding domain of the

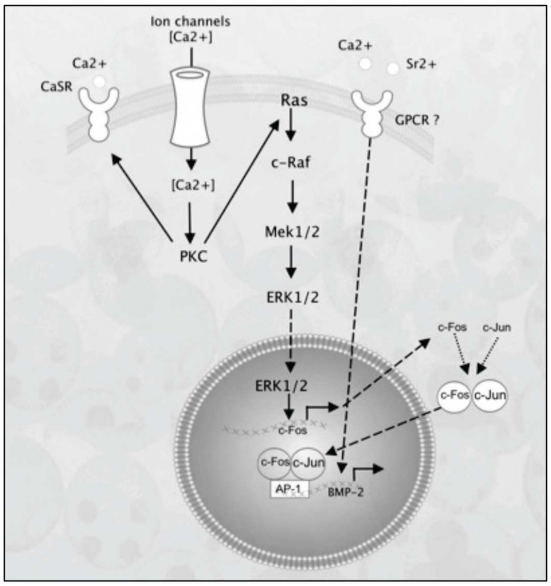

Figure 11: Schematic depiction of the proposed signaling pathway involved in Ca^{2+}-mediated BMP-2 gene expression. Ca^{2+} is internalized possibly via LVGCCs which in turn activates Protein Kinase C. PKC phosphorilates the CaSR at the Thr888 diminishing its sensitivity to Ca^{2+}. At the same time, PKC phosphorilates GDP that activates the GTPase Ras, activating the Ras-MAP-kinase signaling pathway. After phosphorilation, ERK is translocated into the nucleus and activates transcription of c-Fos transcription factor. C-Fos binds to c-Jun forming the AP-1 transcriptional activator. AP-1 translocates to the nucleus and binds to the AP-1 binding site in the promoter region of the BMP-2 gene, activating its transcription. A GPCR similar to the CaSR and sensitive to both Ca^{2+} and Sr^{2+} might also be involved in mediating BMP-2 expression.

BMP-2 promoter region. A better understanding of how hMSCs sense Ca^{2+} could lead the way in the development of new therapies, such as hMSCs pre-treatment with Ca^{2+} prior to cell seeding in scaffolds or incorporation of compounds with Ca^{2+} stimulatory functions that lead to BMP-2 expression.

Acknowledgements

The authors gratefully acknowledge the financial support of the TeRM Smart Mix Program (AB) and STW (HF) of the Netherlands Ministry of Economic Affairs and the Netherlands Ministry of Education, Culture and Science (AB), BioMedical Materials Program (NG) and IDO project 05/009-QuEST (YCC).

Supplementary Information

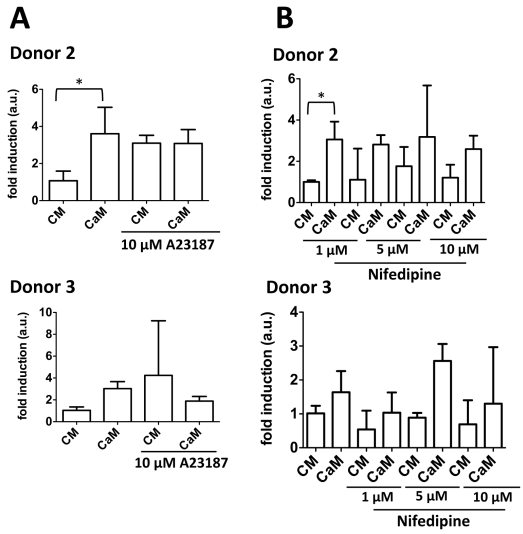

Figure S1: BMP-2 gene expression in different hMSCs donors. hMSCs were treated with either CM, CaM or co-incubated with CM or CaM containing A. Ionophore A23187 or B. Nifedipine. Before co-incubation, cells were pre-treated with either molecule in BM for 30 minutes. Gene expression was analyzed 6 hours after of co-incubation.

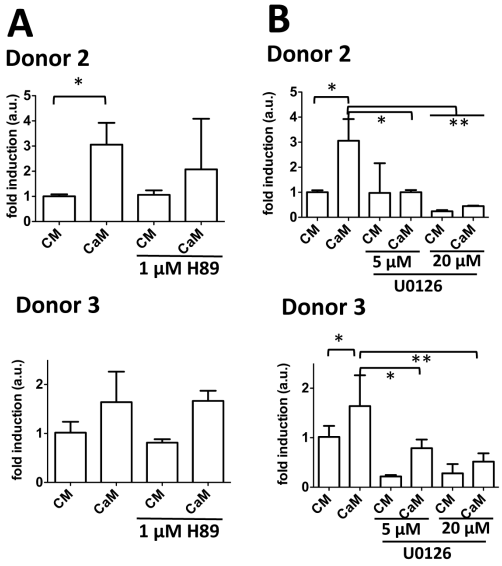

Figure S2: BMP-2 gene expression in different hMSCs donors. hMSCs were treated with either CM or CaM, alone or containing A. Protein Kinase A (H89) or B. MAP Kinase Kinase (Mek 1/2) inhibitors. Before co-incubation, cells were pre-treated with BM containing the respective molecule at the given concentrations for 30 minutes. BMP-2 gene expression was measured 6 hours after co-incubation.

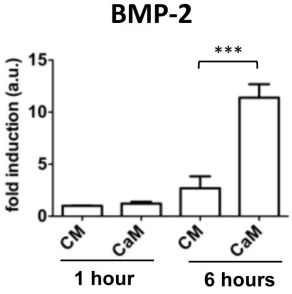

Figure S3: BMP-2 gene expression was not increased in cells treated with CaM after 1 hour.

References

[1] Barradas AMC, Yuan H, van Blitterswijk CA, Habibovic P. Eur Cell Mater. 2011;21:407-29.
[2] Siddappa R, Martens A, Doorn J, Leusink A, Olivo C, Licht R, et al. Proc Natl Acad Sci USA. 2008;105(20):7281-6.
[3] Quarto R, Mastrogiacomo M, Cancedda R, Kutepov SM, Mukhachev V, Lavroukov A, et al. N Engl J Med. 2001;344(5):385-6.
[4] Gan Y, Dai K, Zhang P, Tang T, Zhu Z, Lu J. Biomaterials. 2008;29(29):3973-82.
[5] Yamasaki T, Yasunaga Y, Ishikawa M, Hamaki T, Ochi M. J Bone Joint Surg Br. 2010;92-B(3):337-41.
[6] Okamoto M, Dohi Y, Ohgushi H, Shimaoka H, Ikeuchi M, Matsushima A, et al. J Mater Sci Mater Med. 2006;17(4):327-36.
[7] Rouahi M, Gallet O, Champion E, Dentzer J, Hardouin P, Anselme K. J Biomed Mater Res A. 2006;78A(2):222-35.
[8] Fellah BH, Delorme B, Sohier J, Magne D, Hardouin P, Layrolle P. J Biomed Mater Res A. 2010;93A(4):1588-95.
[9] dos Santos EA, Farina M, Soares GA, Anselme K. J Biomed Mater Res A. 2009;89A(2):510-20.
[10] Yuan H, Fernandes H, Habibovic P, de Boer J, Barradas AM, de Ruiter A, et al. Proc Natl Acad Sci USA. 2010;107(31):13614-9.
[11] Khoshniat S, Bourgine A, Julien M, Petit M, Pilet P, Rouillon T, et al. Bone. 2011;48(4):894-902.
[12] Nakamura S, Matsumoto T, Sasaki J-I, Egusa H, Lee KY, Nakano T, et al. Tissue Eng Part A. 2010;16(8):2467-73.
[13] Dvorak MM, Siddiqua A, Ward DT, Carter DH, Dallas SL, Nemeth EF, et al. Proc Natl Acad Sci USA. 2004;101(14):5140-5.
[14] Kanaya S, Nemoto E, Ebe Y, Somerman MJ, Shimauchi H. Bone. 2010;47(3):564-72.
[15] Honda Y, Anada T, Kamakura S, Nakamura M, Sugawara S, Suzuki O. Biochem Biophys Res Commun. 2006;345(3):1155-60.
[16] Chai YC, Roberts SJ, Schrooten J, Luyten FP. Tissue Eng Part A. 2010;17(7-8):1083-97.
[17] Rosen V. Cytokine Growth Factor Rev. 2009;20(5-6):475-80.
[18] Lee KS, Kim HJ, Li QL, Chi XZ, Ueta C, Komori T, et al. Mol Cell Biol. 2000;20(23):8783-92.
[19] Matsubara T, Kida K, Yamaguchi A, Hata K, Ichida F, Meguro H, et al. J Biol Chem. 2008;283(43):29119-25.
[20] Thimm J, Mechler A, Lin H, Rhee S, Lal R. J Biol Chem. 2005;280(11):10646-54.
[21] Raya A, Kawakami Y, Rodriguez-Esteban C, Ibanes M, Rasskin-Gutman D, Rodriguez-Leon J, et al. Nature. 2004;427(6970):121-8.
[22] Hofer AM, Lefkimmiatis K. Physiology. 2007;22(5):320-7.
[23] Brown EM, Gamba G, Riccardi D, Lombardi M, Butters R, Kifor O, et al. Nature. 1993;366(6455):575-80.
[24] Chang W, Tu C, Chen T-H, Komuves L, Oda Y, Pratt SA, et al. Endocrinology. 1999;140(12):5883-93.
[25] House MG, Kohlmeier L, Chattopadhyay N, Kifor O, Yamaguchi T, Leboff MS, et al. J Bone Miner Res. 1997;12(12):1959-70.
[26] Skerry TM. J Bone Miner Metab. 1999;17(1):66-70.
[27] Pi M, Faber P, Ekema G, Jackson PD, Ting A, Wang N, et al. J Biol Chem. 2005;280(48):40201-9.
[28] Pi M, Zhang L, Lei S-F, Huang M-Z, Zhu W, Zhang J, et al. 2010;25(5):1092-102.
[29] Major ML, Cheung HS, Misra RP. Biochem Biophys Res Commun. 2007;355(3):654-60.
[30] Ma S, Yang Y, Carnes DL, Kim K, Park S, Oh SH, et al. J Oral Implantol. 2005;31(2):61-7.
[31] Alves H, Munoz-Najar U, De Wit J, Renard AJS, Hoeijmakers JHJ, Sedivy JM, et al. J Cell Mol Med. 2010;14(12):2729-38.
[32] Du P, Kibbe WA, Lin SM. Bioinformatics. 2008;24(13):1547-8.
[33] Smyth GK. Stat Appl Genet Mol Biol. February 2004. Available from URL: http://www.ncbi.nlm.nih.gov/pubmed/16646809
[34] Carpenter A, Jones T, Lamprecht M, Clarke C, Kang I, Friman O, et al. Genome Biol. 2006;7(10):R100.
[35] McBeath R, Pirone DM, Nelson CM, Bhadriraju K, Chen CS. Dev Cell. 2004;6(4):483-95.
[36] Dalby MJ, Gadegaard N, Tare R, Andar A, Riehle MO, Herzyk P, et al. Nat Mater. 2007;6(12):997-1003.
[37] Unadkat HV, Hulsman M, Cornelissen K, Papenburg BJ, Truckenmueller RK, Post GF, et al. Proc Natl Acad Sci USA. 2011;108(40):16565-70.
[38] Wang Y-K, Yu X, Cohen DM, Wozniak MA, Yang MT, Gao L, et al. Stem Cells Dev. 2012;21(7):1176-86
[39] Siddappa R, Licht R, van Blitterswijk C, de Boer J. J Orthop Res. 2007;25(8):1029-41.
[40] Brown EM, Lian JB. Sci Signal. 2008;1(35):pe40.
[41] Aguirre A, GonzĞlez A, Planell JA, Engel E. Biochem Biophys Res Commun. 2010;393(1):156-61.
[42] He Y, Zhang H, Teng J, Huang L, Li Y, Sun C. Biochem Biophys Res Commun. 2011;404(1):393-9.

[43] Saidak Z, Brazier M, Kamel S, Mentaverri R. Mol Pharmacol. 2009;76(6):1131-44.
[44] Ara T, Hattori T, Fujinami Y. J Pharmacol. 2011;2(1):30-5.
[45] Tada H, Nemoto E, Kanaya S, Hamaji N, Sato H, Shimauchi H. Biochem Biophys Res Commun. 2010;394(4):1093-7.
[46] Piek E, Sleumer LS, van Someren EP, Heuver L, de Haan JR, de Grijs I, et al. Bone. 2010;46(3):613-27.
[47] Zhu L-L, Zaidi S, Peng Y, Zhou H, Moonga BS, Blesius A, et al. Biochem Biophys Res Commun. 2007;355(2):307-11.
[48] Verberckmoes SC, De Broe ME, D'Haese PC. Kidney Int. 2003;64(2):534-43.
[49] Takaoka S, Yamaguchi T, Yano S, Yamauchi M, Sugimoto T. Horm Metab Res. 2010;42(09):627-31.
[50] Hofer AM, Brown EM. Nat Rev Mol Cell Biol. 2003;4(7):530-8.
[51] He Y-H, He Y, Liao X-L, Niu Y-C, Wang G, Zhao C, et al. Mol Cell Biochem. 2012;361(1):321-8.
[52] Broadhead GK, Mun HC, Avlani VA, Jourdon O, Church WB, Christopoulos A, et al. J Biol Chem. 2011;286(11):8786-97.
[53] Zuccotti A, Clementi S, Reinbothe T, Torrente A, Vandael DH, Pirone A. Trends Pharmacol Sci. 2011;32(6):366-75.
[54] Lacampagne A, Gannier Fo, Argibay J, Garnier D, Le Guennec J-Y. Biochim Biophys Acta. 1994;1191(1):205-8.
[55] Salzer U, Hinterdorfer P, Hunger U, Borken C, Prohaska R. Blood. 2002;99(7):2569-77.
[56] Fu M, Zhang J, Lin Y, Zhu X, Zhao L, Ahmad M, et al. Biochem J. 2003;370(3):1019-25.
[57] Mayer SI, Muller I, Mannebach S, Endo T, Thiel G. J Biol Chem. 2011;286(12):10084-96.
[58] Helvering LM, Sharp RL, Ou X, Geiser AG. Gene. 2000;256(1-2):123-38.
[59] Kim RH, Shapiro HS, Li JJ, Wrana JL, Sodek J. Matrix Biol. 1994;14(1):31-40.
[60] Lammi J, Huppunen J, Aarnisalo P. Mol Endocrinol. 2004;18(6):1546-57.
[61] Pirih FQ, Tang A, Ozkurt IC, Nervina JM, Tetradis S. J Biol Chem. 2004;279(51):53167-74.
[62] Kovalovsky Dn, Refojo Dn, Liberman AC, Hochbaum D, Pereda MP, Coso OA, et al. Mol Endocrinol. 2002;16(7):1638-51.

Chapter 4

Molecular analysis of biomaterial-driven osteogenesis in human mesenchymal stromal cells

Ana M. C. Barradas, Veronica Monticone, Marc Hulsman, Charlène Danoux, Hugo Fernandes, Zeinab Thamasebibirgani, Florence Barrère-de Groot, Huipin Yuan, Marcel Reinders, Pamela Habibovic, Clemens van Blitterswijk, Jan de Boer

Abstract

Calcium phosphate (CaP) based ceramics are used as bone graft substitutes in the treatment of bone defects. The physico-chemical properties of these materials determine their bioactivity, meaning that molecular and cellular responses in the body will be tuned accordingly. In a previous study, we compared two porous CaP ceramics, hydroxyapatite (HA) and β-tricalcium phosphate (TCP), which, among other properties, differ in their degradation behaviour *in vitro* and *in vivo*. Additionally we demonstrated that the more degradable β-TCP induced more bone formation in an heterotopic model in sheep. This correlated to *in vitro* data, where human bone marrow derived mesenchymal stromal cells (MSC) exhibited higher expression of osteogenic differentiation markers, such as osteopontin, osteocalcin and bone sialoprotein, when cultured in β-TCP than in HA. More recently, we also showed that this effect could be mimicked *in vitro* by exposure of MSC to high concentrations of calcium ions (Ca^{2+}). To further correlate surface dynamics of HA and β-TCP ceramics to the molecular response of MSC, we followed Ca^{2+} release and surface changes in time as well as cell attachment and osteogenic differentiation of MSC on these ceramics. Within 24 hours, we observed differences in cell morphology, with MSC cultured in β-TCP displaying more pronounced attachment and spreading than cells cultured on HA. In the same time frame, β-TCP induced expression of G-protein coupled receptor (GPCR) 5 A and regulator of G-protein signaling 2, revealed by DNA microarray analysis. These genes, associated with the protein kinase A and GPCR signaling pathways, may herald the earliest response of MSC to bone-inducing ceramics.

Introduction

In the occurrence of a bone defect due to trauma or tumor resection, bone void fillers are needed to regain the bone's original properties and functions. Autologous bone grafting (autograft), in which healthy bone is collected and transplanted to the defect, is the most frequently applied therapy in such situations. Two properties that determine the autograft successful bone regeneration are osteoinduction (i.e. it induces commitment of undifferentiated cells to become osteoblasts) and osteoconduction (i.e. provides a framework for bone ingrowth), . However, the amount of bone that can be collected is limited, and furthermore, the method may pose severe disadvantages, such as donor-site pain and morbidity [1]. Due to these limitations, and concomitant with an increasing world population, there is an urgent demand for bone graft substitutes (BGS) (2).

Among BGS, synthetic calcium phosphate (CaP) ceramics are widely used because their chemical composition resembles that of bone mineral [3-5]. Besides, the majority of CaP ceramics are osteoconductive, providing excellent osteointegration between the host bone and the implant. Ideally, CaP BGS should also possess intrinsic osteoinductivity, however only a subclass of these materials has been shown to be osteoinductive, as demonstrated by de novo bone formation upon heterotopic implantation in pre-clinical animal models , for example in the muscle [6, 7].

In the past decades, several formulations of CaP ceramics have been developed that vary, in terms of chemical composition, in crystallinity and macro- and micro-scaled structural features. In general, most formulations include macro-scaled pores, which are void spaces in the structure that allow ingrowth of cells, blood vessels and tissue. Furthermore some contain micro-scaled pores as well (defined as having a diameter smaller than 10 μm). Chemical composition of the material is often characterised by the calcium to phosphate ratio (Ca/P). In general, lower Ca/P ratios lead to a higher dissolution rate. For instance, hydroxyapatite (HA), with a Ca/P ratio of 1.67, dissolves slower than tricalcium phosphate (TCP), whose Ca/P ratio is 1.5 [8, 9]. However, all above mentioned properties, together with the mechanical properties and the presence of cells, such as osteoclasts, can affect CaP degradability.

So far, there is no clear link between the physico-chemical properties of CaP BGS and their bioactivity at the molecular level. Further impairing this knowledge is the fact that a stringent comparison between different studies/labs cannot be done. Although a material might bear the same name in different publications, usually following its chemical composition, other properties can be different due to the protocols used for its preparation. Nonetheless, a fundamental understanding of the physico-chemical properties of a particular set of materials that drive specific molecular and cellular responses might improve the design of CaP biomaterials and perhaps unlock other clinical therapies for bone regeneration, not considered so far.

Within limits, *in vitro* models can help understanding how CaP ceramics regulate osteogenic differentiation of cells. As such, CaP based materials and their bioactivity in terms of osteogenic differentiation (*in vitro*) and in some cases, correlation to bone-forming capacity (*in vivo*), has been a subject of intensive research. For instance, Matsushima and colleagues [10] observed that bone marrow-derived mesenchymal stromal cells (MSC) combined with β-TCP formed more bone in a subcutaneous *in vivo* model in nude rats, than MSC grown on HA. Although in both cases MSC were alkaline phosphatase (ALP) positive *in vitro* prior

to implantation, there was no quantitative analysis of ALP staining. Tan et. al. [11] also observed that HA and biphasic calcium phosphate (BCP) induced expression of osteogenic markers in C2C12 cells but did not quantify the differences between the two ceramics. SaOS-2 cells showed higher levels of ALP activity when cultured in HA (Osbone®) granules than when cultured in β-TCP (Cerasorb®) but differences between the two ceramics in gene expression of typical osteogenic differentiation markers, such as osteopontin (OP), bone sialoprotein (BSP) and osteonectin (ON), were not observed [12]. Similarly, HA also induced higher levels of ALP gene expression in SaOS-2 cells than BCP or TCP did, but no statistically significant differences were detected regarding expression of OC, ON and collagen type I (Col I) [13]. In contrast, we showed that MSC cultured in β-TCP did express more OP, OC, Col I and BSP than in HA after 7 days. In addition we also showed that β-TCP, without cells, induced 5 times more bone formation than HA when implanted intramuscularly in dogs [14], further correlating the *in vivo* bone forming capacity and osteogenic differentiation potential *in vitro*.

Since β-TCP and HA in our study showed different *in vitro* dissolution rates, we hypothesized that dissolution of calcium ions dissolution (Ca^{2+}) drives MSC osteogenic differentiation *in vitro* and bone formation *in vivo*. More recently, it was demonstrated that MSC expressed more OP, OC, BSP and in addition more BMP-2 in a high Ca^{2+} concentration ([Ca^{2+}]) milieu than in a low one [15], in accordance with the osteogenic profile of MSC cultured in β-TCP (higher solubility) and HA (lower solubility) (14).

In this study, we used MSC to investigate the biological mechanism that leads to these distinct osteoblastic phenotypes on β-TCP versus HA. At very early time points, MSC gene expression differences was analysed through DNA microarray analysis. Also physico-chemical properties of these ceramics associated with their dissolution/precipitation surface events were investigated.

Materials and Methods

HA and β-TCP fabrication

HA ceramics were prepared from HA powder (Merck) using the dual-phase mixing method and sintered at 1250°C for 8 hours, according to a previously described method [16]. β-TCP ceramics were prepared from TCP powder (Plasma Biotal) and sintered at 1100°C. Ceramic particles were cleaned ultrasonically with acetone, 70% ethanol and demineralized water and dried at 80°C. Particles were sieved to obtain a 1-2 mm sized particle batch, and were autoclaved prior to use. For a detailed physico-chemical characterization of these materials the reader is referred to Yuan et. al. [14].

Inductively Coupled Plasma-Optical Emission Spectrometry

In a previous study, we showed the Ca^{2+} release profile from HA and β-TCP in SPS for approximately 3 hours [14]. Here, we studied the release profiles of Ca^{2+} and $PO_4{}^{3-}$, in a time scale corresponding to cell culturing experiments (days). Fifteen particles of either HA or β-TCP were immersed in 10 ml of either simulated physiological saline (SPS; 0.8% NaCl, 50 mM Hepes, pH 7.3) or minimum essential medium α (α-MEM, Gibco) for four hours, then solutions were refreshed with 500 μl of respective liquid and after four hours, refreshed

again, but this time, with 10 ml. All incubation steps were carried out in a 5% CO2 humid atmosphere at 37°C, according to what is usually done in cell culture experiments: ceramics pre-wetting for 4 hours, followed by cell seeding in low volume and then addition of cell culture medium. For a schematic representation of procedures see figure 1 A. At specific time points, SPS and α-MEM samples were collected for [Ca^{2+}] and [$PO_4{}^{3-}$] measurements by Inductively Coupled Plasma-Optical Emission Spectrometry (ICP-OES, Varian 720 ES, Evisa). Standard samples for Ca^{2+} and $PO_4{}^{3-}$ measurements were prepared by dissolving $CaCl_2.2H_2O$ and $Na_2HPO_2.2H_2O$, respectively, in SPS solution with varying concentrations. Individual samples were prepared for each time point collection, to ensure that concentrations would not be disturbed by incomplete liquid removal for analysis. Each data point represents one measurement (n=1). Due to the technical difficulties associated with ICP-OES analysis, we did not add FBS to α-MEM, which is usually present in a concentration of 10%. It should be noted that SPS does not contain Ca^{2+} or PO43, whereas α-MEM contains 1.8 mM CaCl2 and 1.01 mM NaH2PO4.

Fourier Transformed Infrared Spectroscopy
Ceramic particles that remained in the tubes after removing solutions for ICP-OES analysis were transferred to new tubes and dried at room temperature for analysis with Fourier transformed infrared spectroscopy (FTIR, Perkin-Elmer Spectrum 1000).

Scanning Electron Microscopy
Samples for scanning electron microscopy (SEM) were fixed in 10% formalin (Sigma), dehydrated in an ethanol gradient series and dried using critical point dryer equipment (CPD 030, BAL-TEC). The samples were then gold-sputtered and imaged with SEM in secondary electron mode (XL30 ESEM-FEG, Philips). In the case of samples without cells, only the dehydration and subsequent steps were performed.

Cell culture and proliferation
MSC were previously characterized as multipotent and comply with the standard CD marker panel that defines MSC [17]. MSC were isolated from bone marrow aspirates (5-20 ml) obtained from donors with written informed consent. Aspirates were resuspended using 20 G needles, plated at a density of 5×10^5 cells cm^{-2} and cultured in proliferation medium (PM), consisting of α-MEM (Gibco), 10% foetal bovine serum (Lonza), 2 mM L-glutamin (Gibco), 0.2 mM ascorbic acid (Sigma), 100 U/ml penicillin and 100 mg/ml streptomycin (Gibco) (Basic Medium, BM) supplemented with 1 ng/ml rhbFGF (AbD Serotec). MSC were expanded at an initial seeding density of 1000 cells cm^{-2} in PM and medium was refreshed every 2 to 3 days. Cells were harvested at approximately 80% confluency for subculture. All experiments were performed in a 5% CO2 humid atmosphere at 37°C.

MSC culture on ceramic scaffolds
HA and β-TCP were incubated in BM for 4 hours prior to cell seeding for optimal infiltration of medium into the ceramic pores and protein adsorption to the surface. Three particles of either HA or β-TCP were placed in one corner in squared wells of polystyrene plates. A cell suspension of 100 μl MSC in passage 2 or 3 in BM was pipetted on top of each particle set. To ensure maximum cell adhesion to the ceramic surface, plates were tilted to avoid cell

dispersion throughout the well. Cells were allowed to attach for 4 hours after which 2 ml of osteogenic differentiation medium (OM; BM containing 10 nM dexamethasone (Sigma)) was slowly added to each sample. OM was refreshed every 2 days. MSC cultured in β-TCP or HA are referred to as MSC-TCP and MSC-HA respectively.

RNA isolation and gene expression analysis using quantitative qPCR

Total RNA was isolated from biological triplicates of MSC-TCP or MSC-HA after 12 hours, 2, 3, 5 and 7 days of culturing using a combination of the TRIzol (Invitrogen) method with the NucleoSpin RNA II isolation kit (Macherey-Nagel). Samples were rinsed in PBS and 1ml of TRIzol reagent was added. After 1 freeze/thaw cycle, 200 μl chloroform was added per sample followed by centrifugation to achieve phase separation. The aqueous phase, containing the RNA, was collected, mixed with an equal volume of 75% ethanol and loaded onto the RNA binding column of the NucleoSpin RNA II isolation kit. Subsequent steps were in accordance with the manufacturer's protocol. RNA was collected in RNAse-free water. The quality and quantity of total RNA was analysed by gel electrophoresis and spectrophotometry. First strand cDNA was synthesized using iScript (Bio-Rad) according to the manufacturer's protocol. One μl of undiluted cDNA was used for quantitative real time PCR performed on a Light Cycler PCR machine (Roche) using SYBR green I master mix (Invitrogen). For 18S amplification, cDNA was diluted 100$\times$. The PCR amplifications were run under the following conditions: initial denaturation for 5 minutes at 95°C, then cycled 45 times at 95°C for 15 seconds, specific annealing temperature for 30 seconds and 72°C for 30 seconds, followed by a melting curve. Primer sequences can be found in table 1. PCR data was analysed using Light Cycler software version 3.5.3, using the fit point method by setting the noise band to the exponential phase of the reaction to exclude background fluorescence. Expression of all genes was normalised to 18S levels and fold inductions were calculated using the comparative ΔCT method.

Table 1: Primer sequences for human genes.

Name	*Primer sequences*
18S	5'-CGGCTACCACATCCAAGGAA-3' 5'-GCTGGAATTACCGCGGCT-3'
OC	5'-GGCAGCGAGGTAGTGAAGAG-3' 5'-GATGTGGTCAGCCAACTCGT-3'
BSP	5'-TGCCTTGAGCCTGCTTCC-3' 5'-CAAAATTAAAGCAGTCTTCATTTTG-3'
OP	5'-CCAAGTAAGTCCAACGAAAG-3 5'-GGTGATGTCCTCGTCTGTA-3'
BMP-2 **RGS2** **GPRC5A** **BHLHE40**	Commercially bought (SA Biosciences)

cRNA synthesis and whole genome microarray analysis

Total RNA was isolated as described before, from biological triplicates of MSC-TCP or MSC-HA after 12 hours and 2 days of culturing. RNA concentration was determined by absorbence at 260 nm with the Nanodrop ND-1000 and quality and integrity were verified using the RNA 6000 Nano assay on the Agilent 2100 Bioanalyzer (Agilent Technologies). Next, 100 ng of total RNA was used for transcriptional profiling with Affymetrix 3Õ IVT microarray analysis (Affymetrix, Santa Clara, CA, USA) using the Affymetrix 3' IVT Express Kit (part nr. 901229) to generate Biotin-labeled antisense cRNA. cRNA quality was assessed using the Agilent 2100 Bioanalyzer. The labeled cRNA was used for hybridization to Affymetrix HT HG U133+ PM 16-Array Plate following the Affymetrix 3' IVT Express manual. After an automated process of washing and staining by the GeneTitan machine (Affymetrix, Santa Clara, CA, USA) using the Affymetrix HWS Kit for GeneTitan (part nr. 901530), absolute values of expression were calculated from the scanned array using the Affymetrix Command Console v3 software. Further analysis was performed using the RDN normalization toolbox (18). After normalization, genes were ranked based on their fold change difference between β-TCP and HA materials, for each separate time point. Using the RankProduct test [19], a combined list was created with genes that showed consistent high fold changes at both time points. The False Discovery Rate (FDR) was used to correct for multiple testing.

Statistical Analysis

Statistical analysis is indicated in the respective figure legends. Error bars indicate standard deviation. For all figures the following applies: * = $p < 0.05$; ** = $p < 0.01$; *** = $p < 0.001$.

Results

Ca^{2+} and $PO_4{}^{3-}$ release profile from β-TCP and HA

Figure 1 B depicts the results obtained on [Ca^{2+}] and $PO_4{}^{3-}$ concentration ([$PO_4{}^{3-}$]) by ICP-OES. Immersion of β-TCP in SPS resulted in a continuous increase of both [Ca^{2+}] and [$PO_4{}^{3-}$], to a level of 8 and 19 ppm respectively after 52 hours. Neither Ca^{2+} nor $PO_4{}^{3-}$ was detected in SPS after immersion of HA for the time points tested. Considering [Ca^{2+}] measured upon immersion of ceramics in α-MEM, initially, this was 31.6 and 33.6 ppm for β-TCP and HA respectively. In both β-TCP and HA incubation solutions, the [Ca^{2+}] increased to 32.5 to 34.1 ppm from 4 to 16 hours, respectively. After that [Ca^{2+}] dropped to approximately 28 ppm in both cases. Regarding $PO_4{}^{3-}$ dissolution, all values were close to 20 ppm at 4 and 16 hours. However the [$PO_4{}^{3-}$] decreased between 16 and 52 hours to approximately 17 ppm in both HA and β-TCP incubation solutions. Blank measurements in α-MEM showed a decrease in [$PO_4{}^{3-}$] from 16 to 52 hours. Measurements in SPS demonstrate the higher solubility of β-TCP versus HA. The decreasing values of [Ca^{2+}] and [$PO_4{}^{3-}$] in α-MEM in time possibly reflect supersaturation of Ca^{2+} and $PO_4{}^{3-}$ in solution and consequent precipitation on both β-TCP and HA.

FTIR spectra of HA and TCP

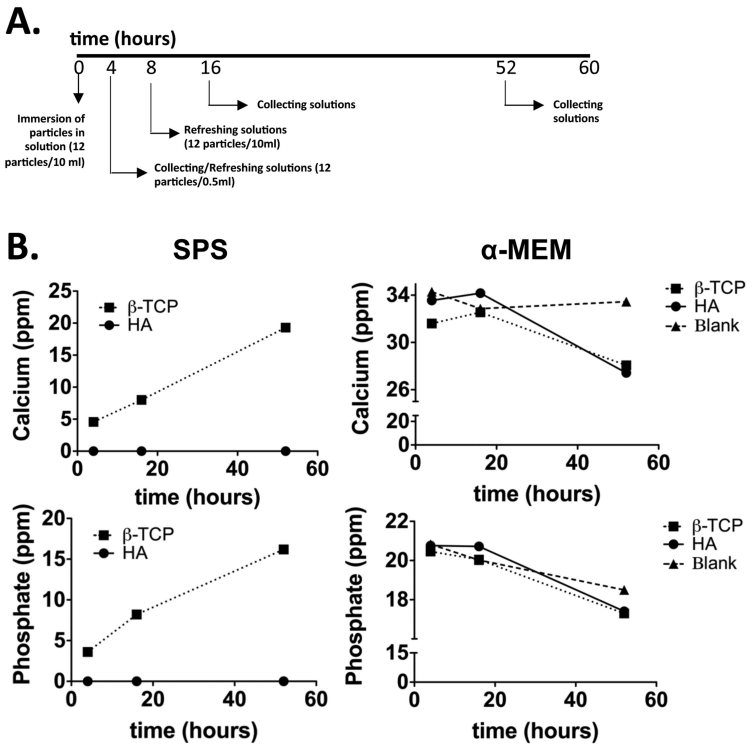

Figure 1: Ca^{2+} and $PO_4{}^{3-}$ dissolution from HA and β-TCP into SPS and α-MEM. A. HA and β-TCP particles were incubated for 52 hours in SPS and α-MEM. At 4, 16 and 52 hours, SPS and α-MEM were collected from the wells and B. Ca^{2+} and $PO_4{}^{3-}$ concentrations were measured by ICP-OES.

$[Ca^{2+}]$ and $[PO_4{}^{3-}]$ measurements in SPS suggested a continuous dissolution of ions, at least in the case of β-TCP, and measurements in α-MEM suggested precipitation of CaP salts on both ceramics. Therefore we hypothesized that the chemical composition of the ceramics was changing in time due to dissolution/precipitation events. Following a similar experimental setup depicted in figure 1A, but collecting the ceramics instead of the incubation solutions (figure S1A), FTIR analysis were performed on bulk ceramics immersed for 52 hours in SPS and α-MEM and in addition, on a sample immersed in BM. No obvious differences in the FTIR spectra were observed between the conditions tested.

HA and β-TCP surface imaging

To assess whether signs of dissolution/precipitation events were visible on HA and β-TCP, we imaged the surfaces before (blank) and after immersion in SPS, α-MEM or BM for 2 days (figure 2). In the blank images, it can be appreciated that the grains of HA surfaces are larger than those of β-TCP and that HA has fewer micropores, as was previously shown [14]. After 2 days of incubation in SPS, no considerable changes in surface morphology were observed in either ceramic. However, after immersion in α-MEM, surfaces of both HA and β-TCP

were covered with crystals, that grew perpendicular to the ceramic surface (figure 2, high magnification). Immersion in BM resulted in irregular precipitates of approximately 1 to 2 μm in size, heterogeneously distributed throughout β-TCP surface, while no obvious surface change was detected in BM-immersed HA. The surfaces of β-TCP and HA exhibited a new crystalline phase when immersed in α-MEM, but not when immersed in SPS or BM for 2 days.

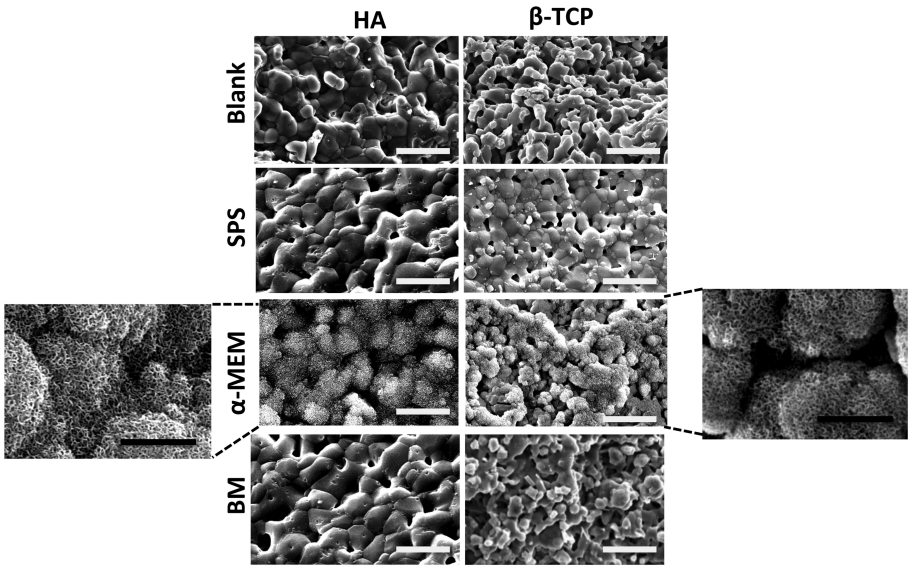

Figure 2: HA and β-TCP surfaces after immersion in different solutions. HA and β-TCP surfaces were imaged with SEM before and after incubation in SPS,α-MEM and BM for 2 days. A new crystalline phase can be observed in HA and β-TCP after immersion in α-MEM. BM and SPS did not significantly affect HA and β-TCP surfaces. White and black scale bars represent 5 and 2 μm, respectively.

MSC attachment and spreading at early time points

Next, we investigated MSC adhesion to the ceramic particles. We pre-wetted β-TCP and HA in BM for four hours and then seeded 600,000 MSC per 3 particles of either HA or β-TCP. After 4 hours, 2 ml of OM was added per sample. Four hours and 1 day later, samples were imaged with SEM (figure 3). After four hours, individual cells could be distinguished on HA. Their adhesion to the surface seemed to be less strong than that of MSC spread on β-TCP surface. After 1 day, similar images were obtained, showing that MSC were well spread on β-TCP (white arrow figure 3) whereas on HA patches of poorly adhered MSC were seen.

MSC-TCP vs MSC-HA osteogenic profile

It was shown in previous work that MSC-TCP express higher levels of OP, OC and BSP than MSC-HA after 7 days of culture [14]. Since our most recent work correlates Ca^{2+} to expression of the aforementioned genes and with that of BMP-2 [15], we analysed expression of all four genes in MSC-TCP and MSC-HA, to investigate the correlation of the expression of

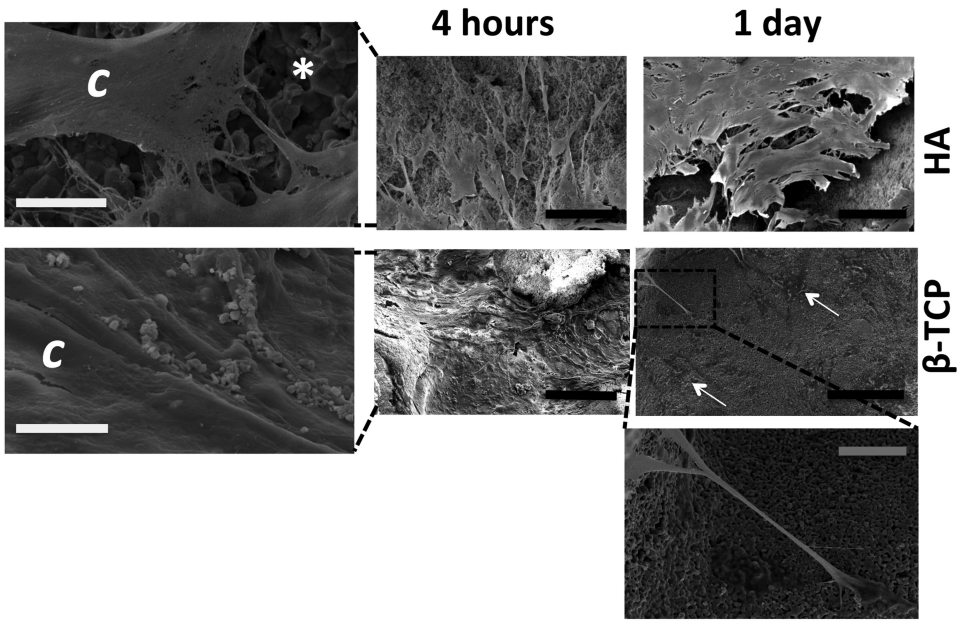

Figure 3: MSC attached and spread better on β-TCP than on HA. MSC were seeded on HA or β-TCP and cultured for 4 hours and 1 day. Cells attached to the ceramic surface were visualized with SEM. In β-TCP, MSC seemed attached and spread on the ceramic whereas in HA they loosely touched the surface at both time points. Far left images showing details of the cells (c) attached and spread on the ceramic surfaces (*) after 4 hours. White arrows point towards MSC spread on β-TCP surface and insert image provides details of filopodia-like structure. White, grey and black scale bars represent respectively 10, 20 and 100 μm.

osteogenic markers between β-TCP and high content Ca^{2+} medium, and HA and low content Ca^{2+} medium, respectively. Results from 2 donors show that expression of OC and OP was significantly higher in MSC-TCP than in MSC-HA (figure 4). Although differences between MSC-TCP and MSC-HA were not statistically significant for any donor in the case of BMP-2 or BSP, MSC-TCP exhibited a consistent higher expression of BMP-2 than MSC-HA. Next, we analysed the expression of the same genes at 12 hours, 2, 3, 5 and 7 days to see whether the gene expression differences between MSC-TCP and MSC-HA could be detected earlier then day 7. As shown in figure 5, differential gene expression between the two conditions was only visible after day 5. At this time point, however, MSC-TCP expressed 3 times more BMP-2 than MSC-HA, in line what was seen before (figure 4). At day 7, expression of OC, OP and BSP was always higher in MSC-TCP. Most profound was the expression of OP, which was 40 times higher in MSC-TCP than in MSC-HA. These experiments demonstrate that β-TCP promotes upregulation of OC, OP, BSP and BMP-2 expression in MSC, compared to HA. Before day 5, however, there was no statistical significant differential gene expression between MSC-TCP and MSC-HA for the markers analysed.

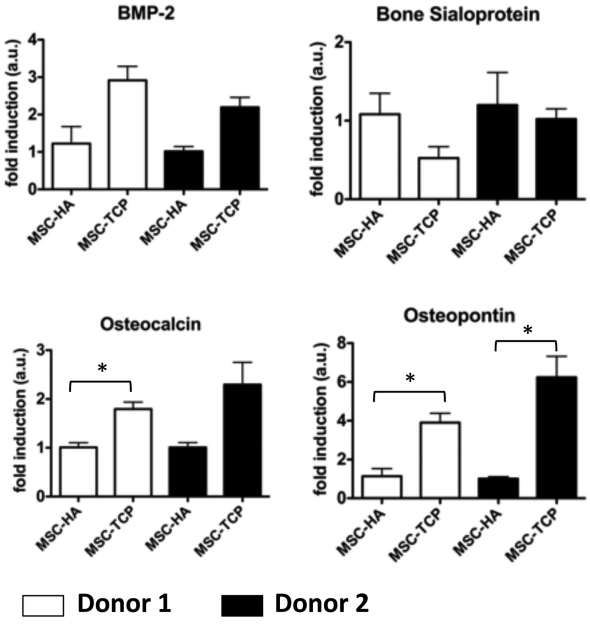

Figure 4: Gene expression profile of MSC-TCP vs MSC-HA is consistent among different donors. MSC from donor 1 (white bars) and donor 2 (black bars) were cultured on HA and β-TCP for 7 days in OM. At that time point, expression of BMP-2, osteopontin, osteocalcin and bone sialoprotein was analysed. MSC-TCP showed higher expression of those genes in both donors, except for BSP. Statistical analysis was done using a student t-test with Welch's corrections for the individual donors ($p<0.05$ and $n=3$).

MSC-TCP vs MSC-HA whole genome microarray

To further correlate extracellular signals provided by the ceramics to specific molecular and cellular responses at early stages of culturing, we performed a whole genome microarray. High fold changes in gene expression were investigated at both 12 hours and 2 days, between MSC-TCP and MSC-HA, in order to find those genes that were early, strongly and consistently affected by β-TCP over HA. In table 2, we report 70 genes that have a FDR of $\leq$0.10 as determined by the RankProduct test, that show the largest difference in expression between β-TCP and HA, at both timepoints. The genes here shown will be later discussed in terms of relevant signaling pathways and biological functions. Also to provide insight into biological functions regulated by β-TCP, analysis with Gene Ontology enrichment was performed, based on 145 probesets having a FDR <0.2. Enriched biological process terms were clustered on functional similarity to enhance their interpretability, using the method made available by DADIV [20]. Three clusters from the top 15 are presented in table 3, whereas all enriched clusters are shown as supplementary table 1 (ST1). Expression of genes in the top 3 of table 2 (RGS2, GPCR5A and BHLH40) was further confirmed by qPCR analysis. RGS2 and GPCR5A were upregulated in MSC-TCP compared to MSC-HA (figure 6) after 2 days, but not after 12 hours. For BHLHE40, results were consistent with the microarray, but not

statistically significant.

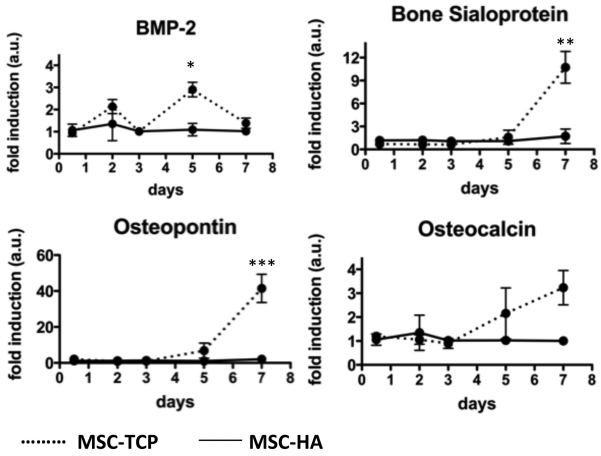

Figure 5: MSC-TCP exhibit stronger osteogenic profile than MSC-HA in time. MSC were cultured on HA and β-TCP for 12 hours, 2, 3, 5 and 7 days in OM. At each time point, expression of BMP-2, osteopontin, osteocalcin and bone sialoprotein was analysed. Statistical significant differences were observed on the late time points between MSC-TCP (dashed line) and MSC-HA (continuous line). Statistical analysis was done with Two-Way Analysis of Variance (ANOVA) and Bonferroni post-tests ($p< 0.05$ and $n=3$).

Discussion

In this manuscript, we analysed the expression of osteogenic markers in MSC grown on β-TCP and HA (figures 4 and 5) and using microarray analysis, we discovered novel genes whose expression is strongly evoked by β-TCP at early time points of culture (table 2 and figure 6). Furthermore, we tried to correlate the solubility of β-TCP and HA (figures 1, 2 and S1) with our biological findings, as based on our previous work, we hypothesized that this might be a key physico-chemical parameter in mediating the bioactivity of these ceramics.
We have shown in the past that MSC exhibit an osteogenic phenotype in culture medium containing high [Ca^{2+}] (CaM). BMP-2 expression is induced within 6 hours after exposing MSC to CaM and at later time points, OC, OP and BSP are induced as well [15]. Here, analysis of osteogenic marker genes also revealed higher expression of OC, OP, and BSP in MSC-TCP than in MSC-HA, consistent in all donors except for BSP. Furthermore, BMP-2 was also upregulated by MSC-TCP compared to MSC-HA (day 5) and earlier than the other genes. Although with a different timing, this resemblance in the osteogenic response between MSC-TCP and MSC cultured in CaM further suggests that the high solubility of β-TCP provides an enriched Ca^{2+} environment to MSC, which could be an important driving factor for the observed osteogenic differentiation.
This is also supported by an earlier reported effect of Ca^{2+} on osteogenic differentiation of human periosteal derived stem cells (PD-MSC). PD-MSC cultured in the presence of Ca^{2+},

Table2: Genes consistently upregulated by β-TCP after 12 hours and 2 days.

Gene symbol	*Gene description*	R_{FC1}	R_{FC2}	*FDR*
BHLHE40	basic helix-loop-helix family, member e40	1	24	0.0020
GPRC5A	G protein-coupled receptor, family C, group 5, member A	5	14	0.0020
RGS2	regulator of G-protein signaling 2, 24kDa	36	2	0.0017
DDIT3 /// NR1H3	DNA-damage-inducible transcript 3 /// nuclear receptor subfamily 1, group H, member 3	120	5	0.0178
HES1	hairy and enhancer of split 1, (Drosophila)	6	165	0.0280
GDF15 /// LOC100292463	growth differentiation factor 15 /// similar to growth differentiation factor 15	2	534	0.0252
SLC2A3	solute carrier family 2 (facilitated glucose transporter), member 3	137	9	0.0240
AMD1	adenosylmethionine decarboxylase 1	4	488	0.0371
CTGF	connective tissue growth factor	3	719	0.0368
ADM	adrenomedullin	22	99	0.0337
AREG	amphiregulin	2365	1	0.0335
SLC16A6	solute carrier family 16, member 6 (monocarboxylic acid transporter 7)	77	32	0.0326
ITPR1	inositol 1,4,5-triphosphate receptor, type 1	371	11	0.0495
GADD45B	growth arrest and DNA-damage-inducible, beta	32	136	0.0496
NEAT1	nuclear paraspeckle assembly transcript 1 (non-protein coding)	45	108	0.0517
RAB20	RAB20, member RAS oncogene family	19	273	0.0516
ERO1L	ERO1-like (S. cerevisiae)	275	21	0.0546
HNRNPAB	heterogeneous nuclear ribonucleoprotein A/B	7	830	0.0519
GADD45B	growth arrest and DNA-damage-inducible, beta	50	122	0.0516
ATF3	activating transcription factor 3	246	26	0.0515
PPP1R3C	protein phosphatase 1, regulatory (inhibitor) subunit 3C	41	158	0.0497
SIK1	salt-inducible kinase 1	14	464	0.0475
AMIGO2	adhesion molecule with Ig-like domain 2	8	878	0.0504
FAM98A	family with sequence similarity 98, member A	16	476	0.0539
C10orf10	chromosome 10 open reading frame 10	1912	4	0.0520
C13orf33	chromosome 13 open reading frame 33	312	25	0.0513
CDCA2	cell division cycle associated 2	78	113	0.0566
PTGS2	prostaglandin-endoperoxide synthase 2 (prostaglandin G/H synthase and cyclooxygenase)	191	49	0.0564
VEGFA	vascular endothelial growth factor A	150	64	0.0562
KYNU	kynureninase (L-kynurenine hydrolase)	60	162	0.0550
GPATCH4	G patch domain containing 4	27	376	0.0556
RYBP	RING1 and YY1 binding protein	47	243	0.0608
VEGFA	vascular endothelial growth factor A	126	92	0.0599
DUSP10	dual specificity phosphatase 10	142	83	0.0594
SLC2A14 /// SLC2A3	solute carrier family 2 (facilitated glucose transporter), member 14 /// solute carrier family 2 (facilitated glucose transporter), member 3	2008	6	0.0591
GADD45B	growth arrest and DNA-damage-inducible, beta	99	127	0.0598
NOP56	NOP56 ribonucleoprotein homolog (yeast)	31	457	0.0667
IRS2	insulin receptor substrate 2	90	169	0.0701
UHRF1	ubiquitin-like with PHD and ring finger domains 1	55	314	0.0779
IER3	immediate early response 3	108	160	0.0760
PITPNC1	phosphatidylinositol transfer protein, cytoplasmic 1	80	218	0.0749
CXCR4	chemokine (C-X-C motif) receptor 4	1499	13	0.0824
RRAGD	Ras-related GTP binding D	281	71	0.0810
C10orf10	chromosome 10 open reading frame 10	268	76	0.0810
RORA	RAR-related orphan receptor A	51	402	0.0800
UGP2	UDP-glucose pyrophosphorylase 2	318	67	0.0818
NEAT1	nuclear paraspeckle assembly transcript 1 (non-protein coding)	194	114	0.0837
CLEC2B	C-type lectin domain family 2, member B	2885	8	0.0863
EGLN3	egl nine homolog 3 (C. elegans)	118	220	0.0939
TFRC	transferrin receptor (p90, CD71)	12	2167	0.0924
SLC2A3	solute carrier family 2 (facilitated glucose transporter), member 3	219	119	0.0908
ABCE1	ATP-binding cassette, sub-family E (OABP), member 1	40	655	0.0897
RIPK4	receptor-interacting serine-threonine kinase 4	135	198	0.0900

RORA	RAR-related orphan receptor A	1578	17	0.0888
DSEL	dermatan sulfate epimerase-like	20	1354	0.0881
NAP1L3	nucleosome assembly protein 1-like 3	76	372	0.0888
SLC26A2	solute carrier family 26 (sulfate transporter), member 2	15	2008	0.0932
ELL2	elongation factor, RNA polymerase II, 2	996	31	0.0934
IL8	interleukin 8	10313	3	0.0921
STC2	stanniocalcin 2	98	322	0.0927
LOC729222 /// PPFIBP1	similar to PTPRF interacting protein binding protein 1 /// PTPRF interacting protein, binding protein 1 (liprin beta 1)	1026	33	0.0983
GPATCH4	G patch domain containing 4	46	738	0.0972
GALNTL2	UDP-N-acetyl-alpha-D-galactosamine:polypeptide N-acetylgalactosaminyltransferase-like 2	800	44	0.0997
IGFBP1	insulin-like growth factor binding protein 1	186	190	0.0987
NOP16	NOP 16 nuclear protein homolog (yeast)	44	841	0.1011
AKAP12	A kinase (PRKA) anchor protein 12	58	650	0.1015

R_{FC1}/ R_{FC2}: position in the rank of genes according to fold change on day 1 (FC1) or day 2 (FC2) (the larger the fold change, the lower in the rank)
FDR: false discovery rate

exhibited expression of BMP-2, OC, OP and BSP, in a dose dependent fashion [21, 22]. Furthermore, PD-MSC seeded onto Collagraft^{TM} and implanted subcutaneously in nude mice induced bone formation, whereas when Collagraft^{TM} was decalcified prior to cell seeding (i.e. removal of Ca^{2+} and $PO_4{}^{3-}$), bone formation was abrogated [23], suggesting the relevance of the construct's mineral composition.

The high solubility of β-TCP was demonstrated in SPS (figure 1). In α-MEM, however, which in addition to bioinorganics contains amino acids, $[Ca^{2+}]$ and $[PO_4{}^{3-}]$ decreased in time (figure 1B), suggesting supersaturation of these ions and precipitation both on HA and β-TCP surfaces. This was further confirmed by SEM analysis of the surface, where a new crystalline phase was observed (figure 2). Although β-TCP revealed the presence of irregular precipitates when immersed in BM, possibly of NaCl, no clear differences regarding a new crystalline phase were visible between the two HA and β-TCP (figure 2), perhaps due to adsorption of serum proteins. These are known to affect the original nucleation or crystal growth rate observed in CaP ceramics without proteins [24, 25]. Furthermore FTIR data did not reveal any significant differences in the chemical composition of samples analysed at day 2, perhaps because surface changes were of too low magnitude to be detected in the midst of the bulk.

Although we did not detect differences in the surface dynamics of HA and β-TCP when immersed in BM (FTIR and SEM), microarray data analysis, though, showed evidence of ongoing inorganic cation homeostasis and in particular Ca^{2+} homeostasis upregulation by β-TCP compared to HA (table 3), already 12 hours and 2 days after cell seeding. This could indicate that $[Ca^{2+}]$ in the vicinity of β-TCP is sufficient to affect cellular behavior without significantly altering the crystalline phase of the surface (figure 2) and that perhaps $[Ca^{2+}]$ increases in time, later inducing expression of OP, OC, BSP and BMP-2 (days 5 and 7). In fact, cluster 2 of the GO enrichment showed that ossification, skeletal development and bone development were upregulated functions in MSC-TCP compared to MSC-HA, suggesting that the microarray data are in line with later PCR observations on osteogenic markers expression. Thus, our biological data suggests that MSC-TCP experience higher $[Ca^{2+}]$ compared with MSC-HA.

Regarding the top genes in table 2, it is interesting to note that GPCR5A and regulator of G-

Table3: Selected enriched gene ontology clusters (following DAVID [20]) from the top 15 displayed in ST1, based on the set of consistently induced genes affected by β-TCP after 12 hours and 2 days (FDR<0.2).

AC	Biological process terms	FDR
2	***Enrichment Score: 2.27***	
	GO:0001503~ossification	0.0394
	GO:0060348~bone development	0.0485
	GO:0001501~skeletal system development	0.1911
13	***Enrichment Score: 1.27***	
	GO:0001569~patterning of blood vessels	0.0742
	GO:0048754~branching morphogenesis of a tube	0.1593
	GO:0001763~morphogenesis of a branching structure	0.1857
	GO:0035239~tube morphogenesis	0.1958
14	***Enrichment Score: 1.25***	
	GO:0055066~di-, tri-valent inorganic cation homeostasis	0.1456
	GO:0055080~cation homeostasis	0.2352
	GO:0030005~cellular di-, tri-valent inorganic cation homeostasis	0.2217
	GO:0006874~cellular calcium ion homeostasis	0.2620
	GO:0006873~cellular ion homeostasis	0.3333
	GO:0055074~calcium ion homeostasis	0.2761
	GO:0055082~cellular chemical homeostasis	0.3534
	GO:0030003~cellular cation homeostasis	0.3257
	GO:0006875~cellular metal ion homeostasis	0.3152
	GO:0019725~cellular homeostasis	0.4416
	GO:0055065~metal ion homeostasis	0.3604
	GO:0050801~ion homeostasis	0.4697

AC: annotation cluster number
FDR: false discovery rate
N.B.: the multiple testing correction is too conservative, as it does not take into account the similarity between many GO terms.

protein signaling (RGS2) are related with G-protein coupled receptor (GPCR) signaling [26]. Expression of these genes was further confirmed by PCR, showing that RGS2 and GPCR5A were expressed respectively 10 and 100 times more in MSC-TCP than in MSC-HA at day 2. At 12 hours differential expression was not confirmed by PCR. In particular, RGS2 has been linked with osteogenic differentiation and osteoblasts proliferation [27-29] and its expression can be regulated by cAMP [30]. Expression of GPCR5A, also known as retinoic acid inducible gene 1 (RAIG1), has been linked with differentiation and maintenance of homeostasis in epithelial cells and maturation of lung and kidney during embryonic development [31]. Furthermore GPCR5A expression has been associated with cancer development [32]. Overexpression of this gene also led to a decrease in cAMP accumulation and Gsα downregulation [33].

Genes coding for members of the Protein Kinase A (PKA) signaling cascade, regulated by cAMP cytosolic accumulation, which is downstream of GPCR signaling, also appear in table 2. For instance, A kinase anchor protein 12 (AKAP12) binds to PKA and drives its sub-

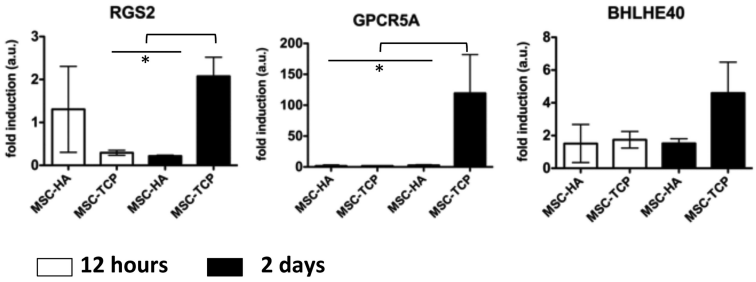

Figure 6: Genes differentially regulated between MSC-TCP and MSC-HA analysed by PCR. DNA microarray analysis showed that the top scored genes regulated by β-TCP were RGS2, GPCR5A and BHLHE40 (table 2). Fold induction of RGS2, GPCR5A and BHLHE40 measured by PCR shows that after 12 hours (white bars) there were no statistically significant differences between MSC-TCP and MSC-HA, whereas after 2 days there are in the case of RGS2 and GPCR5A. Statistical analysis was performed with One-Way ANOVA and Tukey's multiple comparison post-test ($p< 0.05$ and $n=3$).

units within the cell. Furthermore, both ATF3 and HES1 transcription is regulated by cAMP response element binding (CREB) [34, 35], supporting a strong upregulation of the PKA signalling pathway by β-TCP compared to HA. In addition, SIK1 is a PKA target protein (36) and GDF15, CTGF and amphiregulin expression are PKA dependent as well [37-39]. Future experiments will be aimed at looking in more detail at the involvement of PKA signaling in MSC-TCP induced gene expression and at identifying the molecules responsible for the induction. Furthermore other genes regulated by β-TCP have been previously linked to osteogenesis, such as GDF15 [40] and BHLHE40 [41, 42] and interestingly with angiogenesis, VEGFA [43] and IL-8 [44], further suggesting that β-TCP might not only have a pro-osteogenic effect but also a pro-angiogenic one. Indeed cluster 13 shows enrichment of terms related with blood vessel formation.
Although we suggest that Ca^{2+} dissolution plays a role in osteogenesis of MSC cultured in β-TCP, we do not exclude the effect of other physico-chemical parameters. We have also shown that MSC attachment and spreading is different between HA and β-TCP, as suggested by SEM analysis, which was not further explored here. Differences in cell attachment could be due to different microstructure or charge of these materials that lead to differential protein adsorption and consequent differential focal adhesion assembly.

Conclusions

We confirmed higher solubility of β-TCP in SPS when compared to HA, although a clear link between Ca^{2+} dissolution from β-TCP and osteogenesis of MSC could not be established. However, microarray analysis detected upregulation of Ca^{2+} homeostasis in MSC-TCP after 12 and 48 hours of culturing as compared to MSC-HA, and PCR analysis showed that β-TCP significantly increased expression of genes in MSC that are characteristic of high [Ca^{2+}] content medium, such as BMP-2, OP, OC and BSP. Furthermore, microarray analysis showed that GPCR signaling and PKA pathways are strongly upregulated by β-TCP over HA.

Acknowledgements

The authors gratefully acknowledge the technical support of the Katholieke Universiteit Leuven and financial support of the TeRM Smart Mix Program of the Netherlands Ministry of Economis Affairs and The Netherlands Ministry of Education, Culture and Science, BMM (ZT, AB) and STW Vernieuwingsimpuls Veni (PH, JdB, HF).

Supplementary Information

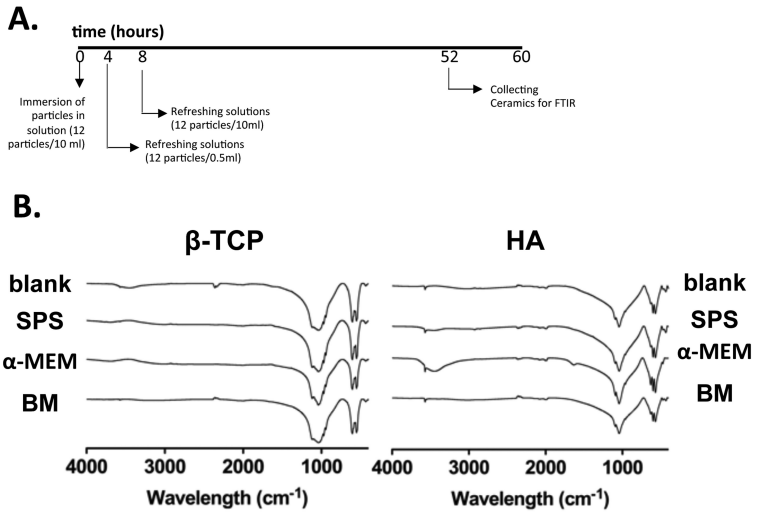

Figure S1: Changes in chemical composition after immersion in SPS, α-MEM or BM are detected by FTIR. Blank refers to ceramic particles before incubation. A. HA and β-TCP particles were incubated for 52 hours in SPS, α-MEM or BM. At 4 and 8 hours, solutions were refreshed. After 52 hours, particles were collected for FTIR analysis. B. There were no evident differences between the different spectra.

Table S1: Top 15 enriched gene ontology clusters (following DAVID [20]), based on the set of consistently induced genes affected by β-TCP after 12 hours and 2 days (FDR<0.2).

AC	Biological process terms	FDR
1	***Enrichment Score: 2.68***	
	GO:0040012~regulation of locomotion	0.0394
	GO:0051270~regulation of cell motion	0.0394
	GO:0030334~regulation of cell migration	0.0592
2	***Enrichment Score: 2.27***	
	GO:0001503~ossification	0.0394
	GO:0060348~bone development	0.0485
	GO:0001501~skeletal system development	0.1911
3	***Enrichment Score: 2.09***	
	GO:0019318~hexose metabolic process	0.0742
	GO:0006006~glucose metabolic process	0.0742
	GO:0005996~monosaccharide metabolic process	0.1163
4	***Enrichment Score: 2.02***	
	GO:0001837~epithelial to mesenchymal transition	0.0091
	GO:0014031~mesenchymal cell development	0.0933
	GO:0048762~mesenchymal cell differentiation	0.0933
	GO:0060485~mesenchyme development	0.0962
5	***Enrichment Score: 1.69***	
	GO:0042981~regulation of apoptosis	0.1824
	GO:0043067~regulation of programmed cell death	0.1911
	GO:0010941~regulation of cell death	0.1911
6	***Enrichment Score: 1.54***	
	GO:0030324~lung development	0.1400
	GO:0030323~respiratory tube development	0.1537
	GO:0060541~respiratory system development	0.1637
7	***Enrichment Score: 1.42***	
	GO:0030968~endoplasmic reticulum unfolded protein response	0.0742
	GO:0034620~cellular response to unfolded protein	0.0742
	GO:0034976~response to endoplasmic reticulum stress	0.1593
	GO:0006984~ER-nuclear signaling pathway	0.1637
8	***Enrichment Score: 1.42***	
	GO:0045892~negative regulation of transcription, DNA-dependent	0.2416
	GO:0051253~negative regulation of RNA metabolic process	0.0983
	GO:0016481~negative regulation of transcription	0.2416
	GO:0010558~negative regulation of macromolecule biosynthetic process	0.2937
	GO:0031327~negative regulation of cellular biosynthetic process	0.3333
	GO:0010629~negative regulation of gene expression	0.3604
	GO:0009890~negative regulation of biosynthetic process	0.3699
	GO:0045934~negative regulation of nucleobase, nucleoside, nucleotide and nucleic acid metabolic process	0.3887
	GO:0051172~negative regulation of nitrogen compound metabolic process	0.4127
	GO:0010605~negative regulation of macromolecule metabolic process	0.4500

9	***Enrichment Score: 1.41***	
	GO:0008643~carbohydrate transport	0.1316
	GO:0015758~glucose transport	0.1267
	GO:0008645~hexose transport	0.1316
	GO:0015749~monosaccharide transport	0.1385
10	***Enrichment Score: 1.37***	
	GO:0048609~reproductive process in a multicellular organism	0.1657
	GO:0032504~multicellular organism reproduction	0.1657
	GO:0007276~gamete generation	0.3794
11	***Enrichment Score: 1.29***	
	GO:0006351~transcription, DNA-dependent	0.2716
	GO:0006366~transcription from RNA polymerase II promoter	0.2620
	GO:0032774~RNA biosynthetic process	0.2761
12	***Enrichment Score: 1.28***	
	GO:0043255~regulation of carbohydrate biosynthetic process	0.0742
	GO:0010906~regulation of glucose metabolic process	0.1637
	GO:0010675~regulation of cellular carbohydrate metabolic process	0.1808
	GO:0006109~regulation of carbohydrate metabolic process	0.1857
13	***Enrichment Score: 1.27***	
	GO:0001569~patterning of blood vessels	0.0742
	GO:0048754~branching morphogenesis of a tube	0.1593
	GO:0001763~morphogenesis of a branching structure	0.1857
	GO:0035239~tube morphogenesis	0.1958
14	***Enrichment Score: 1.25***	
	GO:0055066~di-, tri-valent inorganic cation homeostasis	0.1456
	GO:0055080~cation homeostasis	0.2352
	GO:0030005~cellular di-, tri-valent inorganic cation homeostasis	0.2217
	GO:0006874~cellular calcium ion homeostasis	0.2620
	GO:0006873~cellular ion homeostasis	0.3333
	GO:0055074~calcium ion homeostasis	0.2761
	GO:0055082~cellular chemical homeostasis	0.3534
	GO:0030003~cellular cation homeostasis	0.3257
	GO:0006875~cellular metal ion homeostasis	0.3152
	GO:0019725~cellular homeostasis	0.4416
	GO:0055065~metal ion homeostasis	0.3604
	GO:0050801~ion homeostasis	0.4697
15	***Enrichment Score: 1.18***	
	GO:0051674~localization of cell	0.2937
	GO:0048870~cell motility	0.2937
	GO:0016477~cell migration	0.4214

AC: annotation cluster number
FDR: false discovery rate
N.B.: the multiple testing correction is too conservative, as it does not take into account the similarity between many GO terms.

References

[1] St John TA, Vaccaro AR, Sah AP, Schaefer M, Berta SC, Albert T, et al. American journal of orthopedics (Belle Mead, NJ). 2003;32(1):18-23.
[2] Damien CJ, Parsons JR. J Appl Biomater. 1991;2(3):187-208.
[3] Brandoff JF, Silber JS, Vaccaro AR. Am J Orthop. 2008;37(8):410-4.
[4] Giannoudis PV, Dinopoulos H, Tsiridis E. Injury. 2005;36(3, Supplement):S20-S7.
[5] Calori GM, Mazza E, Colombo M, Ripamonti C. Injury. 2011;42, Supplement 2(0):S56-S63.
[6] Van der Stok J, Van Lieshout EMM, El-Massoudi Y, Van Kralingen GH, Patka P. Acta Biomater. 2011;7(2):739-50.
[7] Barradas AMC, Yuan H, van Blitterswijk CA, Habibovic P. Eur Cell Mater. 2011;21:407-29.
[8] Daculsi G, Laboux O, Malard O, Weiss P. J Mater Sci Mater Med. 2003;14(3):195-200.
[9] Hoppe A, Guldal NS, Boccaccini AR. Biomaterials. 2011;32(11):2757-74.
[10] Matsushima A, Kotobuki N, Tadokoro M, Kawate K, Yajima H, Takakura Y, et al. Artif Organs. 2009;33(6):474-81.
[11] Tan Y, Wang G, Fan H, Wang X, Lu J, Zhang X. J Biomed Mater Res A. 2007;82A(1):152-9.
[12] Bernhardt A, Lode A, Peters F, Gelinsky M. Clin Oral Implants Res. 2011;22(6):651-7.
[13] Wang C, Duan Y, Markovic B, Barbara J, Howlett CR, Zhang X, et al. Biomaterials. 2004;25(13):2507-14.
[14] Yuan H, Fernandes H, Habibovic P, de Boer J, Barradas AM, de Ruiter A, et al. Proc Natl Acad Sci U S A. 2010;107(31):13614-9.
[15] Barradas AMC, Fernandes HAM, Groen N, Chai YC, Schrooten J, van de Peppel J, et al. Biomaterials. 2012;33(11):3205-15.
[16] Li S, de Wijn JR, Li J, Layrolle P, de Groot K. Tissue Eng. 2003;9(3):535-48.
[17] Alves H, Munoz-Najar U, De Wit J, Renard AJS, Hoeijmakers JHJ, Sedivy JM, et al. J Cell Mol Med. 2010;14(12):2729-[38]
[18] Hulsman M, Mentink A, van Someren EP, Dechering KJ, de Boer J, Reinders MJT. Bmc Bioinformatics. 2010;11.
[19] Tusher VG, Tibshirani R, Chu G. Proc Natl Acad Sci U S A 2001;98(9):5116-21.
[20] Huang DW, Sherman BT, Tan Q, Kir J, Liu D, Bryant D, et al. Nucleic Acids Res. 2007;35(suppl 2):W169-W75.
[21] Chai YC, Roberts SJ, Schrooten J, Luyten FP. Tissue Eng Part A. 2010;17(7-8):1083-97.
[22] Chai YC, Roberts SJ, Desmet E, Kerckhofs G, van Gastel N, Geris L, et al. Biomaterials. 33(11):3127-42
[23] Eyckmans J, Roberts SJ, Schrooten J, Luyten FP. J Cell Mol Med. 2009.
[24] Combes C, Rey C. Biomaterials. 2002;23(13):2817-23.
[25] Mann S. Nature. 1988;332(6160):119-24.
[26] Roy AA, Baragli A, Bernstein LS, Hepler JR, Hébert TE, Chidiac P. Cell Signal. 2006;18(3):336-48.
[27] Tsingotjidou A, Nervina JM, Pham L, Bezouglaia O, Tetradis S. Bone. 2002;30(5):677-84.
[28] Homme M, Schmitt CP, Himmele R, Hoffmann GF, Mehls O, Schaefer F. Endocrinology. 2003;144(6):2496-504.
[29] Teplyuk NM, Galindo M, Teplyuk VI, Pratap J, Young DW, Lapointe D, et al. J Biol Chem. 2008;283(41):27585-97.
[30] Xie Z, Liu D, Liu S, Calderon L, Zhao G, Turk J, et al. J Biol Chem. 2011;286(52):44646-58.
[31] Cheng Y, Lotan R. J Biol Chem. 1998;273(52):35008-15.
[32] Chen CH, Benjamin MS, Sun XD, Otto KB, Guo P, Dong XY, et al. Int J Cancer. 2006;118(6):1346-55.
[33] Hirano M, Zang L, Oka T, Ito Y, Shimada Y, Nishimura Y, et al. Biochem Biophys Res Commun. 2006;351(1):185-91.
[34] Watanabe H, Smith MJ, Heilig E, Beglopoulos V, Kelleher RJ, Shen J. J Biol Chem. 2009;284(20):13705-13.
[35] Mayer SI, Dexheimer V, Nishida E, Kitajima S, Thiel G. Endocrinology. 2008;149(12):6311-25.
[36] Berdeaux R, Goebel N, Banaszynski L, Takemori H, Wandless T, Shelton GD, et al. Nat Med. 2007;13(5):597-603.
[37] Ichikawa T, Horie-Inoue K, Ikeda K, Blumberg B, Inoue S. J Mol Endocrinol. 2007;39(4):239-47.
[38] Guo Y-s, Yuan W-j, Zhang A-p, Ding Y-h, Wang Y-x. Chin Med J (Engl). 2010;123(24):3671-6.
[39] Du B, Altorki NK, Kopelovich L, Subbaramaiah K, Dannenberg AJ. Cancer Res. 2005;65(13):5982-8.
[40] Vanhara P, Lincova E, Kozubik A, Jurdic P, Soucek K, Smarda J. Differentiation. 2009;78(4):213-22.
[41] Qian Y, Chen X. J Biol Chem. 2008;283(33):22410-6.
[42] Iwata T, Kawamoto T, Sasabe E, Miyazaki K, Fujimoto K, Noshiro M, et al. Eur J Cell Biol. 2006;85(5):423-31.

[43] Ferrara N, Gerber H-P, LeCouter J. Nat Med. 2003;9(6):669-76.
[44] Li A, Dubey S, Varney ML, Dave BJ, Singh RK. J Immunol. 2003;170(6):3369-76.

Chapter 5

The influence of genetic factors on the osteoinductive potential of calcium phosphate ceramics in mice

Ana M.C. Barradas, Huipin Yuan, Johan van der Stok, Bach Le Quang, Hugo Fernandes, Anindita Chatterjea, Marieke C.H. Hogenes, Kathy Shultz, Leah Rae Donahue, Clemens van Blitterswijk, Jan de Boer

Abstract

The efficacy of calcium phosphate (CaP) ceramics in healing large bone defects is, in general, not as high as that of autologous bone grafting. Recently, we reported that CaP ceramics with osteoinductive properties were as efficient in healing an ilium defect of a sheep as autologous bone graft was, which makes this subclass of CaP ceramics a powerful alternative for bone regeneration. Although osteoinduction by CaP ceramics has been shown in several large animal models it is sporadically reported in mice. Because the lack of a robust mouse model has delayed understanding of the mechanism, we screened mice from 11 different inbred mouse strains for their responsiveness to subcutaneous implantation of osteoinductive β-tricalcium phosphate (β-TCP). In only two strains (FVB and 129S2) the ceramic induced bone formation, and in particularly, in FVB mice, bone was found in all the tested mice. We also demonstrated that other CaP ceramics induced bone formation at the same magnitude as that observed in other animal models. Furthermore, VEGF did not significantly increase β-TCP induced bone formation. The mouse model here described can accelerate research of osteoinductive mechanisms triggered by CaP ceramics and potentially the development of therapies for bone regeneration.

Introduction

Porous calcium phosphate ceramics are frequently used in orthopaedic surgery as graft material to heal bone defects. Their chemical composition is similar to the natural mineral of the bone. In general, CaP-ceramics are considered osteoconductive, meaning that they are able to facilitate bone infiltration from the bone surrounding the defect. A subclass of CaP-ceramics also has been recognized as being osteoinductive [1-5]. We define osteoinductivity of a biomaterial by the potential of the material to induce bone formation while implanted in an animal at ectopic sites (e.g. subcutaneously or intramuscularly). The specific biological response triggered by osteoinductive materials that results in bone formation is, however, poorly known. Nonetheless, their osteoinductive capacity has been often linked with specific physico-chemical properties such as chemical composition, scaffold architecture and micro- and nano- structure.

We recently reported that ceramics with different physico-chemical properties induce bone formation in dogs with different degrees of efficacy: β-tricalcium phosphate (β-TCP) induced more bone formation than hydroxyapatite (HA). In the same study, we also demonstrated that β-TCP grafting of an ilium defect in sheep is as effective as the most frequently used therapies for human patients: autologous bone grafting and recombinant human BMP-2 (rhBMP-2). This finding strongly revealed the potential of osteoinductive ceramics to heal bone defects in clinical scenarios, overcoming the disadvantages of donor tissue morbidity and pain associated with autologous bone graft and issues related to cost and safety associated with the use of rhBMP-2 [6]. However, in order to bring these materials to the clinic, full understanding of the mechanism of action would help to determine their efficacy, efficiency and safety.

The immune system has been associated with the physiological response leading to CaP-ceramic induced bone formation. It is hypothesized, for instance, that materials with different surface characteristics, e.g. surface roughness or micro-topography, will induce different responses in macrophages. For instance, prostaglandin E2 (PGE2) was secreted by macrophages only when in contact with a micro rough- and not when in contact with a smooth surface. Furthermore, PGE2 enhanced chemotaxis and osteogenic differentiation of human bone barrow derived mesenchymal stromal cells [7]. In vivo, PGE2 enhances bone formation through the PGE receptor EP4 [8] and it can also induce osteoclast formation and bone resorption [9]. Harada and colleagues [10] also showed that among all different CaP granules tested, only HA dried at 110°C (HA110) induced expression of PGE2 by primary human macrophages/monocytes cells, whereas HA sintered at 900 and 1200°C did not. The authors from the study also noticed that although all granules were similar in size, HA110 presented a more irregular shape and sharper edges than the other CaP granules [10]. Similar studies have been conducted in vitro [11, 12] but the question of whether macrophages functionally contribute to in vivo bone formation by osteoinductive CaP biomaterials is not yet answered. Some authors have hypothesized though that the origin of the cells that deposit de novo bone is of vascular nature [13-15], based on the observation that cells of vascular origin appear in the vicinity of the ceramic implant. Therefore the role of blood vessels in osteoinduction could be more than the already essential transport of nutrients and gases to the tissue in the pores [16].

Although some progress has been made in the past 20 years, the mechanism of action of os-

teoinductive CaPs is not clear, partially due to limitations associated with the existent in vitro and in vivo models. Pre-clinical models with large animals, such as sheep, dogs and goats are more often used than small animal models, since osteoinduction by CaP ceramics in mice or rats is considered a sporadic event [17]. Nevertheless, a robust mouse model would be preferred over large animal models, since these are more expensive than smaller ones and require experienced surgeons. Mouse models could also accelerate research due to easy access to a wide variety of inbred strains, broader choice of complementary research tools, such as available drugs for functional assays, and antibodies for tissue characterization. Furthermore, there are many genetic tools available for mouse research, enabling gene identification via quantitative trait locus (QTL) coupled with genetic engineering to manipulate the mouse genome to prove causation of gene effects. Application of these methodologies in mice could potentially lead to identification of genetic loci associated with bone formation never before identified.

We previously obtained proof of principle that CaP-triggered osteoinduction is possible in mice [18]. Bone formation was observed in Swiss white mice implanted with biphasic calcium phosphate (BCP). The amount of bone formed was limited, with less than 1% of bone area per scaffold area and was only observed in 3/16 animals tested. Moreover, Swiss white is an outbred mouse strain, whereas inbred mice are preferred as mentioned before. More recently, Yang and colleagues [19] tested BCP ceramics in the muscle of the posterior legs of inbred Balb/C mice and found bone in all explants. Although a promising result, the distance between the leg muscle and native bone tissue in a mouse is short and it can be argued whether osteoconduction from bone tissue into the implant played a role or not.

These findings suggest that the induction of bone formation in mice induced by a CaP ceramic might be strain dependent. Indeed, Malusic and colleagues [20] reported that ectopic bone formation was dependent on genetic background, although in their case the implants were pieces of bone matrix. As BMPs are thought to be responsible for the osteoinductive potential of demineralized bone matrix, this further suggests that in addition to differences in osteoinduction by CaP in different strains there are also differences in BMP induction.

In the search for a suitable mouse model for the study of CaP osteoinductive ceramics, we investigated the response of 11 different mouse strains to subcutaneous implantation of CaP ceramics, based on the assumption that genetic background will influence the propensity of the materials to induce bone tissue.

Materials and Methods

Materials fabrication and sterilization

HA ceramics were prepared from HA powder (Merck) using the dual-phase mixing method and sintered at 1250°C for 8 h according to a previously described method [21]. BCP ceramics were fabricated using the H_2O_2 method using in-house made calcium-deficient apatite powder and sintered at 1150°C (BCP1150) and 1300°C (BCP1300), respectively [22]. The method used to synthesize the BCP ceramics was also used for preparation of β-TCP (for simplicity abbreviated to TCP). TCP ceramics were prepared from TCP powder (Plasma Biotal) and sintered at 1050°C. Ceramic blocks ($4\times4\times4$ mm) were cut, cleaned ultrasonically

with acetone, 70% ethanol and demineralized water (dH_2O), dried at 80°C and autoclaved for sterilization.

Growth factor incorporation into the ceramic blocks

Five μg of rh-BMP-2 dissolved in demineralized water (dH_2O) (Shanghai Rebone Biomaterials Co. Ltd) were pipetted per block of TCP (refered to as TCPb). TCPb was vacuum dried in a sterile environment for two days. In the case of rhVEGF (Invitrogen), 1.8 μg was loaded in 25 μl of dH_2O per block of TCP, just prior to implantation.

Ceramic implantation in mice

Ceramic blocks were implanted in 6 to 7 weeks old mice. Name and providers of mouse-inbred strains, as well as the respective abbreviations used throughout this manuscript, are given in table 1. Preoperative analgesia (Temgesic, Schering-Plough BV) was injected subcutaneously (s.c.) followed by general anesthesia consisting of a mix of 1-3% isoflurane (IsoFlo, Abbott Lab.) in oxygen (Linde Gas). After shaving the back and disinfection of the skin with ethanol, small incisions were created on the dorsal sides. Subcutaneous pockets were opened in these incisions with blunt scissors. Ceramic blocks were inserted into the pockets, which were then closed with sutures. Animals were allowed to recover from anesthesia before returning to the cages. Mice were killed with either CO_2 inhalation or cervical dislocation. Skin was immediately opened to retrieve the ceramic blocks (explants). All animal experiments were performed following approval of the Animal Experiments Committee Utrecht, The Netherlands.

Table 1: Mouse inbred strains and their respective providers.

Mice strain	*Abbreviations*	*Provider*
C3H/HeNHsd	C3H	Harlan Laboratories, Inc.
DBA/1OlaHsd	DBA1	
DBA/2OlaHsd	DBA2	
CBA/CaOlaHsd	CBA	
BALB/cOlaHsd	BALBc	
C57BL/6JOlaHsd	C57BL6	
FVB/NCrl	FVB	Charles River Laboratories International, Inc.
129S2/SvPasCrl	129S2	
SJL/JOrlCrl	SJL	
CB17/Icr-*Prkdc*^{scid}/IcrCrl	CB17	
A/J	A/J	The Jackson Laboratory

Femora extraction and micro-CT scanning

Three C3H, CBA, FVB and 129S2 mice, aged between 6 to 7 weeks, were selected for micro-CT scanning. The right femur of each mouse was extracted, cleaned from skin and soft tissue and fixed with 1.5% glutaraldehyde in 0.14 M cacodylate buffer, pH 7.3. Micro-CT scans were acquired using the SkyScan 1076 scanner (Kontich, Belgium) with a 9 μm-resolution

protocol (60 kV energy, 170 μA current, 1.0 mm Al filter). CT shadow projection images were converted into a three dimensional (3D) reconstruction of cross-sectional images in bitmap files using volumetric reconstruction software NRecon version 1.6 (SkyScan, Belgium). With Dataviewer 1.4, a segment of the distal metaphysis (10 mm) was selected as region of interest. To distinguish calcified tissue from non-calcified tissue and noise, the reconstructed grayscale images were segmented by an automated algorithm using local thresholds, resulting in a 3D dataset consisting of stacked black/white cross-sections. Cortical and trabecular bone were subsequently automatically separated using in-house software. Trabecular architecture of the metaphysic was characterized by determining the trabecular bone volume fraction (BV/TV), which is the ratio of trabecular bone volume over endocortical tissue volume, connectivity density, structural model index, trabecular thickness and trabecular separation were also calculated.

Histochemical stainings

After fixation with 1.5% v/v glutaraldehyde in 0.14 M cacodylate buffer, pH 7.3, explants were dehydrated with several microwave runs at 70°C for 1 hour. For each run, implants were immersed in either 70% ethanol in dH_2O, 80% ethanol in dH_2O, JFC (Milestone Medical Technologies S.r.l.) or 100% ethanol in dH_2O (2 times). After dehydration, samples were placed in glass jars, immersed in methyl methacrylate (MMA) for 16 hours at 4°C, and the next day MMA was refreshed. After 2 days in a water bath at 37°C, samples were removed from the glass jars and sectioned. Tissue sections of approximately 10 to 15 μm thickness were obtained with a Leica SP 1600 and stained with 1% methylene blue (Sigma-Aldrich) in 0.1 M borax (pH 8.5) and 0.3% basic fuchsin solutions (Sigma-Aldrich).

Bone quantification

Three nonconsecutive sections per sample per animal were digitally scanned and quantified using Adobe Photoshop CS5 Extended (version 12.0.4, Adobe Systems Inc.) as follows: bone and scaffold areas were differentially pseudo-colored and the ratio between pixels of each color converted to percentage of bone area per scaffold area (bA/sA). Figure S1 summarizes the number of implanted, explanted and analysed blocks.

Statistical Analysis

Statistical analysis performed for the individual experiments is specified in the figure legend. Error bars indicate standard deviation. For all figures the following applies: * = $p < 0.05$; ** = $p < 0.01$; *** = $p < 0.001$; ns = non significant.

Results

Bone induction by rhBMP-2 adsorbed onto TCP

To evaluate whether the mouse genetic background determines the efficacy of ectopic bone formation, we implanted rhBMP-2 adsorbed onto TCP subcutaneously in 11 different inbred mouse strains (table 1), since this cytokine has ectopic osteoinductive ability in different rodent models [23-27]. Prior to in vivo evaluation, however, the activity of rhBMP-2 adsorbed onto TCP was tested with C2C12 cells in vitro. C2C12 cells are known to express alka-

line phosphatase (ALP) in response to rhBMP-2 [28]. Therefore cells were cultured on TCP or TCPb in BM for three days, after which ALP activity and cell numbers were measured. In TCPb, C2C12 cells exhibited 18 times higher ALP activity per cell than when cultured in TCP alone, confirming that rhBMP-2 was still active while adsorbed onto the porous ceramics (figure S2). Next, TCPb was implanted subcutaneously in all mouse strains (table 1). Twelve weeks after implantation, animals were sacrificed, samples explanted, slides were cut and stained with basic fuchsin (mineralized tissue) and methylene blue (counterstaining). TCPb induced bone formation in every mouse of all strains. As can be seen in figure 1, representative for all strains, typical morphology of mature lamellar bone was observed in contact with the TCPb surface (for reference see figure S3). Mineralized bone matrix (stained pink) was observed, embedding osteoblasts resting in lacunae (osteocytes). The pores of the ceramic blocks were filled with bone marrow, characterized by the presence of nucleated heamatopoetic cells and large amounts of mature adipocytes. Interestingly, we observed differences in the amount of bone among the different mouse strains (figure 2), confirming that bone induction by rhBMP-2 is dependent on genetic background. Bone per scaffold area ranged from 7±3.2% (FVB) to 27±11% (C3H). Interestingly, strains with a close genetic background, such as DBA1 and DBA2 exhibited a large statistically significant difference (9 and 20% respectively). This result shows that all tested mouse strains can form bone in subcutaneous pockets and that furthermore, the efficacy of bone formation induced by TCPb depends on the genetic background.

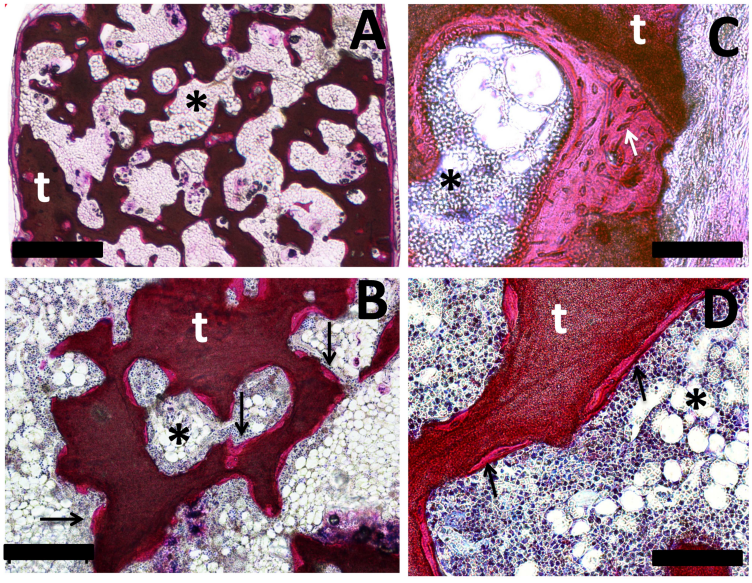

Figure 1: Representative images of bone formation induced by TCPb. A and B) Bright pink mineralized bone tissue (black arrows) was observed in contact with TCP (t) aligning the pores filled with bone marrow (*). C) Osteocytes (white arrows) were present in the mineralized bone matrix. D) Detail of bone marrow (*) and osteoblasts (black arrows). Scale bars represent 1 mm (A), 200 μm (B) and 100 μm (C and D).

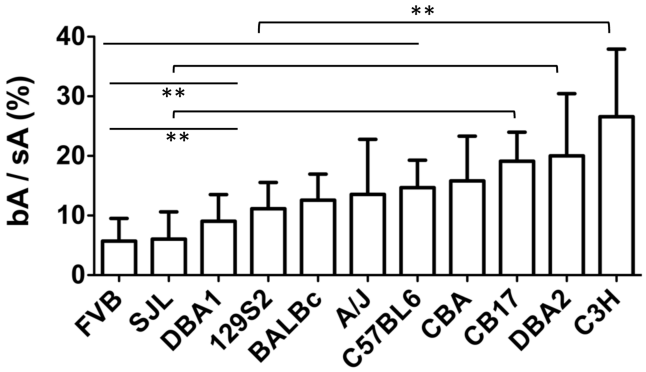

Figure 2: Bone formation induced by TCPb. TCP loaded with rhBMP-2 was implanted subcutaneously in mice from 11 different mouse strains. Twelve weeks later, samples were explanted, bone tissue quantified from tissue sections and presented as % bA/sA. FVB (7%) showed the lowest average amount of bone tissue whereas C3H the highest (27%). Statistical analysis was performed with One-Way Analysis of Variance (ANOVA) and Tukey's multiple comparison test ($p<0.05$).

Bone induction by TCP

In contrast with the results found for TCPb, but further confirming genetic background dependence, bone formation induced by TCP occurred in only two out of 11 mouse strains: FVB and 129S2. In both strains, bone tissue was mostly observed at the periphery of the ceramic block, and in contact with the scaffold (figure 3A). Similarly to results obtained with TCPb, mature lamellar bone had developed, with characteristic osteoblasts rimming the lamellar bone (figure 3B) and osteocytes within the lamellar bone (figure 3D). In a few cases, cavities filled with bone marrow were observed, in both mouse strains (figure 3C). Furthermore, we did not observe cartilage tissue in any of the explanted sections. Although mature lamellar bone tissue was found in both strains, the incidence was different. In FVB mice, TCP induced bone in all mice (6/6) whereas in 129S2 the incidence was lower: 4/5 (figure S1). TCP explants from FVB also showed an average bA/sA higher than that of 129S2: $2.8\pm4.6\%$ and $0.2\pm0.26\%$ respectively (figure 4). Thus, we successfully identified two mouse strains, FVB and 129S2, in which TCP induced bone formation subcutaneously, showing that the genetic background of individuals is a key element in the osteogenic response to synthetic materials.

Bone architecture

In order to investigate whether TCPb or TCP bone inductive capacity in specific mouse strains could be correlated with bone features inherent to each strain, femora from FVB (lowest induction by TCPb and highest by TCP), 129S2 (lowest induction by TCP), CBA and C3H (highest induction by TCPb) were extracted and evaluated by micro-CT scanning. Based on the distal metaphysis region from 3D reconstructed images of the femora, several parameters were evaluated: structural model index (prevalence of a particular trabecular shape), trabecular separation, trabecular thickness, connectivity density (number of redundant connec-

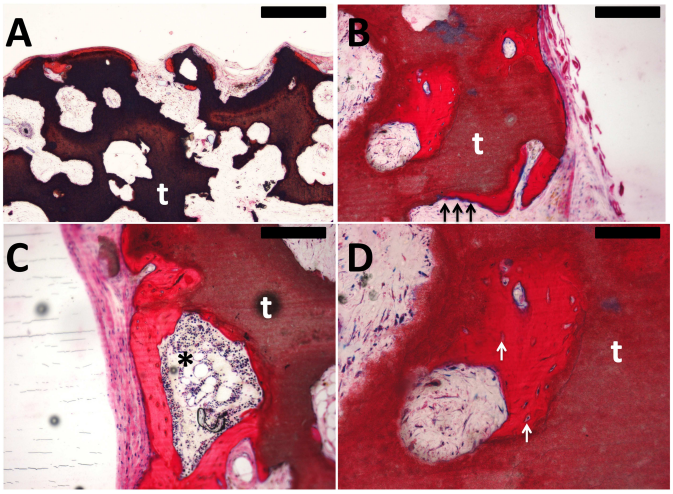

Figure 3: Representative images of bone formation induced by TCP in FVB and 129S2. Mineralized bone tissue (red) was observed mostly at the periphery of the implant (A) and in contact with the scaffold (t), aligned by osteoblasts (black arrows) (B). C) Detail of cavity filled with bone marrow (*). D) Detail of osteocytes (white arrows). Scale bars represent 400 μm (A), 200 μm (B and C) and 100 μm (D).

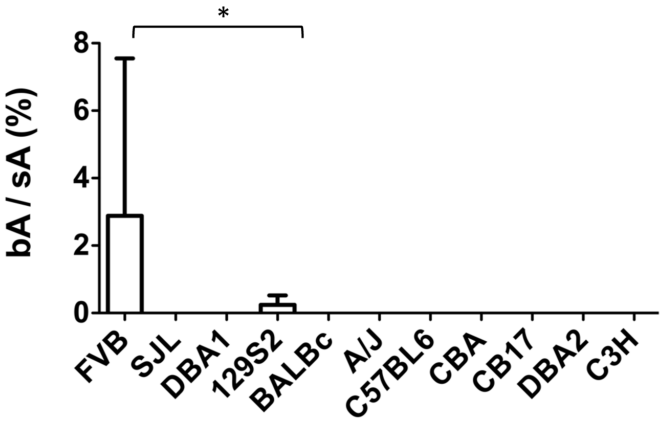

Figure 4: Bone formation induced by TCP. TCP was implanted subcutaneously in mice from 11 different mouse strains. Twelve weeks later, samples were explanted, bone tissue quantified from tissue sections and presented in the image as % relative to scaffold area. Bone formation was observed in FVB (2.8$\pm$4.6%) and 129S2 (0.2$\pm$0.26%) mice. Statistical analysis was performed with One-Way ANOVA and Tukey's multiple comparison test ($p<0.05$).

tions between trabecular structures per unit volume, which can be associated with trabecular strength [29]) and the percentage of bone in a defined volume of interest (% of bone volume, %BV), which can be seen as a true measurement of bone mineral density (BMD). Statistically significant differences were not observed for any of the parameters measured between the mouse strains (figure 5). This suggests that the genetic and molecular mechanisms that regulate bone induction by TCPb or TCP are not correlated with strain specific differences in bone parameters of 6 to 7 week old mice from these inbred strains.

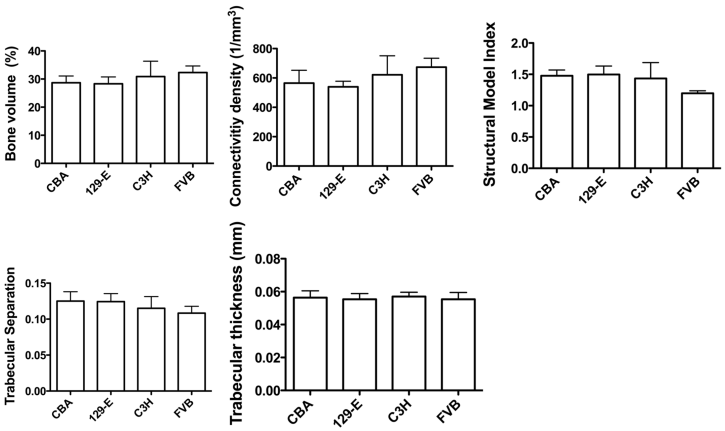

Figure 5: Micro-CT scan femoral analysis. Femora of CBA, 129S2, C3H and FVB/NCrl were scanned with Micro-CT. After 3D digital reconstruction of the scanned images, a segment of the distal metaphysis was selected and several parameters calculated. There were no statistically significant differences for any of the parameters shown between the mouse strains. Statistical analysis was performed with One-Way ANOVA and Tukey's multiple comparison test ($p<0.05$ and $n=3$).

Ectopic bone formation in response to different ceramics

After identifying the more responsive genetic background to TCP osteoinductivity, FVB, we implanted different CaP ceramics in these mice to evaluate whether any block shaped CaP ceramic would induce ectopic bone formation or whether that response was exclusive of a particular setting of physico-chemical characteristics. Therefore, this time, besides TCP, we also implanted HA, different in terms of chemistry and microstructural features, BCP1150 and BCP1300. The last two possess equal chemistry, though BCP1150 possesses more micropores and smaller grains than BCP1300. For a detailed characterization of these materials, the reader is referred to Yuan et. al. [3]. After 12 weeks of implantation, BCP1300 and HA did not induce bone formation in FVB mice. In contrast, BCP1150 and TCP induced bone formation. There were no statistically significant differences in the amount of bone tissue induced by TCP and BCP1150 (figure 6 B) though bone incidence, defined as the ratio between the number of explants with bone (Nb) and the number of total explants (Nt) (Nb/Nt), was different (3/4 and 5/5 for BCP1150 and TCP respectively, figure 6A). Similarly to what was previously described for TCP, bone was mainly found at the periphery of the implant but was also seen in contact with the scaffold (figure 6 C). Osteocytes and osteoblasts were also

observed in BCP1150 explants but bone marrow cavities were not. Furthermore, although all explants were perfused by blood vessels distributed throughout the implants, vascularization seemed to be more pronounced in the case of TCP and BCP1150, although no quantitative data is available to support these observations. Interestingly, in the case of BCP1150, blood vessels were often surrounded by adipocytes. In the pores of BCP1300 and HA explants, mainly fibrous tissue was observed (figure 7). TCP and BCP1150 induced ectopic bone formation in FVB mice whereas BCP1300 and HA did not. This suggests that the biological response that leads to bone formation in FVB mice is dependent on the materials' specific characteristics and not a random phenomenon of heterotopic ossification.

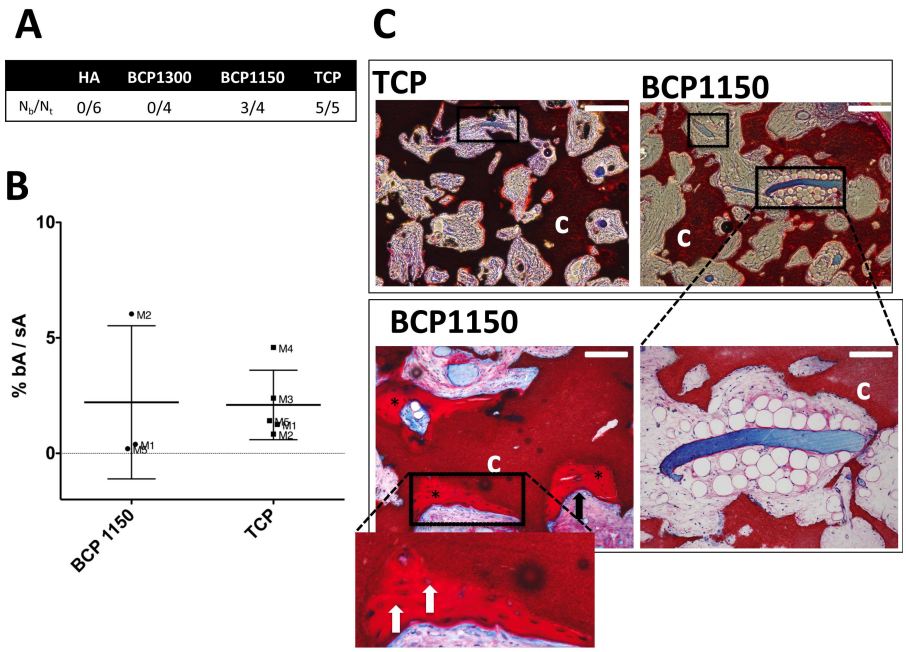

Figure 6: Analysis of TCP, BCP1150, BCP1300 and HA explants after subcutaneous implantation in FVB mice for 12 weeks. A. Bone incidence in the different CaP ceramics shows that bone was only found in BCP1150 and TCP. B. There were no statistical differences regarding % bA/sA between TCP and BCP1150, as calculated with One-Way ANOVA with Tukey's Multiple Comparison test ($p<0.05$). C. Representative images of tissue sections from TCP and BCP1150 explants. Top panel (scale bar represents 500 μm): notice presence of blood vessels (squares). Bottom left: mineralized bone tissue (asterisks) with osteoblasts (black arrow) and osteocytes (enlarged section);. Bottom right: blood vessels surrounded by fat, characteristic of BCP1150 tissue sections. C: ceramic block. Scale bars represent 200 μm (A and B) and 100 μm (C).

Role of vascularization in osteoinduction

Bone formation was observed in both TCP and BCP1150 explants, mainly at the periphery of the ceramic. Immediately after implantation, it is expected that the tissue at the periphery

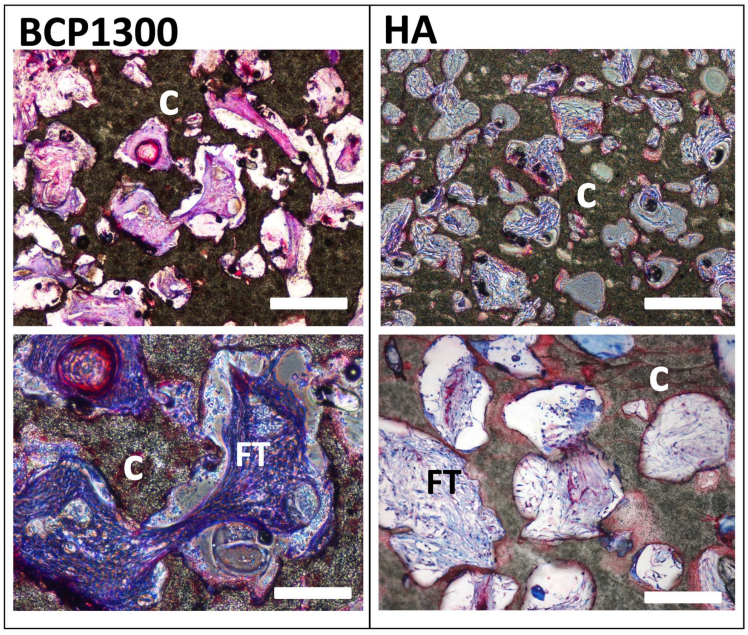

Figure 7: Detailed images of BCP1300 and HA tissue explants 12 weeks after subcutaneous implantation in mice. Tissue locates preferentially in the center of the pores, loosely connected with the surface of both ceramic types. C: ceramic block FT=fibrous tissue. Scale bars represent 400 μm (top row) and 200 μm (bottom row).

of the implant will be more vascularized than the tissue in the centre, since blood vessels do not immediately perfuse the whole implant. This led us to hypothesize that vascularization might be crucial (either triggering or sustaining) the biological mechanism that leads to osteoinduction by CaP ceramics in FVB mice. To address this hypothesis, we first investigated blood vessel formation occurring in TCP and BCP1150. Seven days after implantation, mature blood vessels were observed in explants of both ceramics, evidenced by the presence of erythrocytes in the lumen (figure 8). After confirming that vascularization occurs rather quickly in these ceramics, next we analysed whether enhancing this early vascularization through addition of vascular endothelial growth factor (VEGF) to TCP, would increase the amount of bone formed. For this, all mice received one block of TCP (-VEGF) and one block of TCP with adsorbed VEGF (+VEGF) and these were explanted 12 weeks later. Our results showed that all explants with VEGF induced bone formation whereas only 4/5 without VEGF did (figure 8B). There were no statistically significant differences in the amount of bone formed between the two groups (figure 8C). Whereas TCP explants were well vascularized after 7 days of implantation, addition of VEGF to TCP prior to implantation did not increase amounts of bone formation as analysed 12 weeks later.

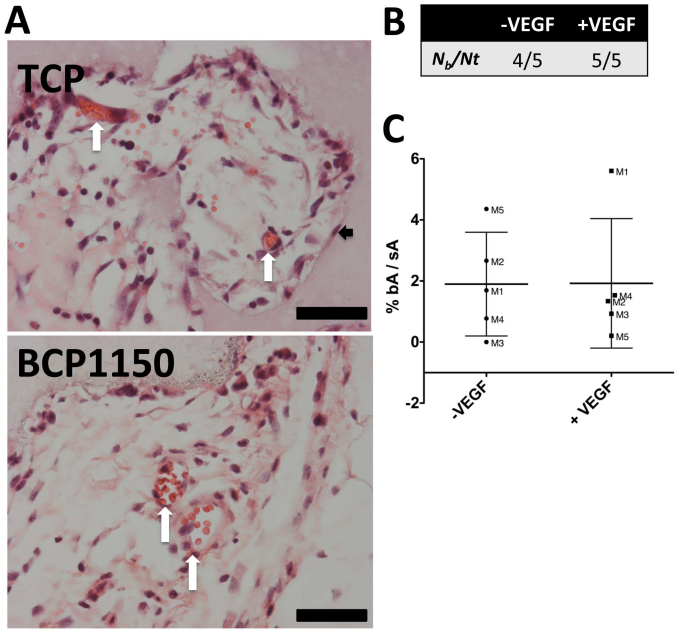

Figure 8: Analysis of blood vessel formation and enhancement of vascularization in bone formation. A. Blood vessel formation in TCP and BCP1150 after 7 days subcutaneous implantation in FVB (white arrows). Notice cell alignment with TCP (black arrow). Scale bar represents 50 μm. Twelve weeks after subcutaneous implantation in FVB, Nb/ Nt was higher in TCP (-VEGF) than in TCP with VEGF (+VEGF) (B) and there were no differences in % bA/sA (C). Statistical analysis was performed with One-Way ANOVA and Tukey's Multiple Comparison test ($p<0.05$).

Discussion

In the search for a mouse model to study osteoinductive CaP ceramics, we tested 6 to 7 weeks old mice from 11 different inbred mouse strains (table 1) for their responsiveness to subcutaneous implantation of TCP, based on the hypothesis that biomaterial-induced bone formation requires a particular genetic background.

Subcutaneous induction of bone formation by TCP was identified in two mouse strains: FVB and 129S2 (figure 4). Particularly in FVB, bone incidence (>80%) and amounts (2-3%) observed were never reported before [18], suggesting that this mouse strain is promising for the study of CaP osteoinductive ceramics. Furthermore, TCP loaded with rhBMP-2 induced subcutaneous bone formation in all mouse strains but with amounts varying among them (figure 2). Taken together these data demonstrate that the genetic background influences the response to osteoinductive stimuli. Also considering that these are inbred mice, which are or are not susceptible to material-induced osteoinduction, potentiates the identification of genetic loci correlated with the mechanism. Interestingly, FVB was the mouse strain in which bone formation induced by rhBMP-2 was lowest but when induced by TCP, highest, suggesting that

the physiological mechanism causing the strain to strain variance is different between TCP and rhBMP-2. Furthermore, although in both cases bone tissue contained osteocytes and osteoblasts (figures 1 and 3), bone with bone marrow was observed in virtually all pores of the TCPb explants whereas it was only visible in some TCP pores, which is likely related to the amount of bone tissue formed.

Bone fracture healing capacity was also correlated with mouse genetic background [30, 31]. Moreover, the bone regenerative capacity of different inbred mouse strains was strongly correlated with their BMD [31], although it was inversely correlated in another report [30]. Based on this, we analysed whether femoral BMD from different mouse strains was correlated to ectopic bone formation. However, femoral bone volume (figure 5) did not significantly differ among the strains tested, which could be due to the animals' age. We analysed femora from 1.5 months old mice and differences in BMD among different inbred strains have been reported at 2 months and thereafter [32].

Implantation of a series of CaP ceramics in FVB mice revealed that in order to observe bone formation after 12 weeks, a particular set of physico-chemical properties is required. HA, differing in terms of chemical composition and structural properties from TCP [3], did not induce bone formation. However, similar differences were observed between CaP ceramics with the same chemical composition but differing in terms of micro structural properties: whereas the more microporous BCP1150 induced bone formation, BCP1300 did not and moreover, the type of tissue found within the respective pores was very different (figures 6 and 7). These results suggest that microstructural properties determine attachment and spreading of cells in the pores and onto the surface, which might be determinant to whether bone will be deposited or not. Also, the osteoinductive potential revealed by the different CaP ceramics in FVB mice is similar to that seen in dogs, sheep and goats [2, 3] from previous studies. Therefore we conclude that this mouse strain can be used as a model to investigate novel bone-inducing CaP ceramics.

Histological observations suggested that TCP and BCP1150 were more vascularized than BCP1300 and HA explants. Besides their demonstrated pro-osteogenic effects, it could be that TCP and BCP1150 also exert pro-angiogenic ones. In fact, it was shown that TCP and BCP induce higher vessel density than HA, up to 30 days after subcutaneous implantation in rats [33]. Furthermore, the effect of Ca^{2+} on angiogenesis has been reported [34-37], which could further indicate some relationship between Ca^{2+} dissolution from the CaP ceramics and blood vessel perfusion. Although this would not sustain the differences observed between BCP1150 and BCP1300, which possess similar dissolution rates [3], quantitative data is needed in order to support these statements.

Angiogenesis is also crucial for the process of bone formation [38] and some authors have suggested that the cells that are stimulated to deposit bone tissue in osteoinductive CaP ceramics are pericytes [13-15]. Our results show that blood vessels perfused both TCP and BCP1150 as early as 7 days, however enhancing angiogenesis at an early stage of implantation did not increase the abundance of bone tissue 12 weeks later (figure 8). As to the nature of the cells contributing to bone formation, we observed cells aligning with the material as early as 7 days (figures 8 and S3), which may be the osteoprogenitor cells, but whether these are derived from the walls of neighbouring blood vessels needs to be investigated.

The effect of surface characteristics on the inflammatory response by biomaterials has been reported. More specifically, the behaviour of macrophages can be tuned according to size,

roughness or chemical composition of the biomaterials surface. For instance, Fellah and colleagues [11] showed that macrophage derived secretion of interleukin 6 and tumour necrosis factor α was dependent on BCP microparticle diameter in which they were cultured and that those cytokines could further induce osteogenic differentiation of MC3T3-E1 cells, suggesting a possible relation between inflammation and bone formation. Moreover, macrophages are susceptible to express BMP-2 in response to Ca^{2+} [39], which could also be correlated with the dissolution characteristics of these materials and their bone forming capacity. Although we did not address the functional role of macrophages in this study, we observed the presence of macrophages as early as 7 days in TCP (figure S3) and BCP1150. Some macrophages were also found in the vicinity of TCP and BCP1150 surfaces 12 weeks after implantation but higher amounts of these cells including numerous amounts of giant cells were found in the vicinity of HA and BCP1300 at that point in time (figure S3), suggesting that the innate inflammatory response towards HA and BCP1300 is more pronounced than the one towards TCP and BCP1150. Regarding the adaptive immune response, also lymphocytes appearance on the surface of CaP implants has been linked with specific physico-chemical properties of materials [40]. However, in this study, CD20-positive B-cells were only sporadically found in the pores of BCP1150 and TCP (figure S3). Unfortunately, due to cross reaction with the murine tissue, CD3-positive cells could not be identified.

Besides having a promising role in the field of osteoinductive biomaterials, the FVB model could also boost research on the acquired form of heterotopic ossification (HO). HO is a debilitating disorder, usually induced by trauma or surgery, where pathological bone growth occurs in e.g. muscle tissue, or close to joints, resulting in deformation and impediment of normal movements [41-43]. Current drugs cannot effectively eliminate these excessive bone masses and typically affect normal bone as well [44]. Furthermore, current animal models do not provide a basis for solid research. Since the biological mechanism leading to HO is not fully understood, researchers do not know which relevant parameters should be included in an in vivo setup. Key physiological parameters believed to have a role in HO development are the nervous and immune systems, blood Ca^{2+} levels, O_2 levels in the tissue and disequilibrium of hormone levels, such as parathyroid hormone or calcitonin [45]. TCP implanted under the skin requires surgery and dissolves into the surrounding tissue, releasing Ca^{2+} ions, which are factors associated with HO onset. We think that the subcutaneous bone induction by TCP in FVB may also serve as a model for the acquired form of HO and could therefore be used to, for instance, investigate drugs to counteract ectopic bone formation.

Conclusions

In this study, we identified FVB as a mouse strain that is suitable for the investigation of osteoinductive CaP ceramics. Our experiments further demonstrate that the capacity of CaP ceramics to induce bone formation is dependent on the mouse genetic background, confirming that genetic and molecular mechanisms are determinant for osteoinduction to occur. Seemingly, bone induction by rhBMP-2 loaded onto TCP yielded amounts of bone formation dependent on inbred strain. Amounts of bone formation observed in both cases did not correlate with bone structural features, such as % of bone volume, for any of the inbred strains tested. Bone induction by CaP ceramics in FVB is dependent on a specific set of physico-chemical

properties. Ceramics with the same chemical composition but different microstructural properties yielded different results: BCP1150 induced bone formation whereas BCP1300 did not. HA also did not induce bone formation. Furthermore, although invaded by blood vessels at as early as day 7 after implantation, enhancing vascularization with VEGF did not increase amounts of bone formation by TCP.

Acknowledgements

The authors gratefully acknowledge the financial support of the TeRM Smart Mix Program of the Netherlands Ministry of Economic Affairs and the Netherlands Ministry of Education, Culture and Science. We also wish to acknowledge Annette Gijsbers-Bruggink and collaborators (Biobank, UMC Utrecht) and Liliana Teixeira, Joyce Doorn and Karolina Janeczek-Portalska for technical assistance.

Supplementary Information

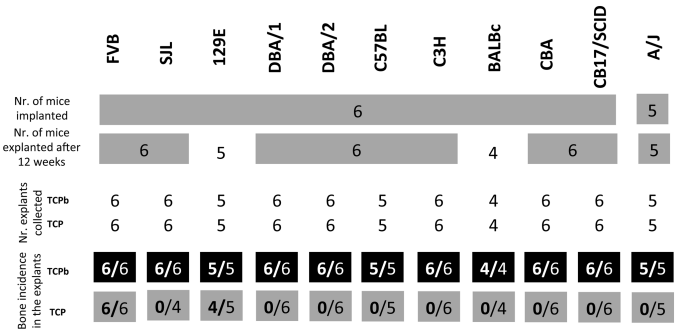

Figure S1: Schematic summary of implanted/explanted TCP and TCPb explants per mouse strain. Each TCPb or TCP was implanted in 6 to 7 weeks old males of each inbred mouse strain. During the 12 weeks period, one BALBc and two 129S2 mice died. Bone was found in all TCPb whereas TCP induced bone formation in only 2 mouse strains.

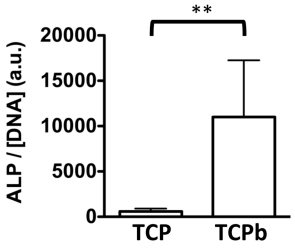

Figure S2: C2C12 cells ALP activity. C2C12 cells were cultured in either TCP or TCPb for three days. ALP activity and DNA concentration were measured. Data is presented as ALP activity corrected for cell numbers. C2C12 cells cultured in TCPb exhibited higher ALP/DNA, confirming the activity of adsorbed rhBMP-2.

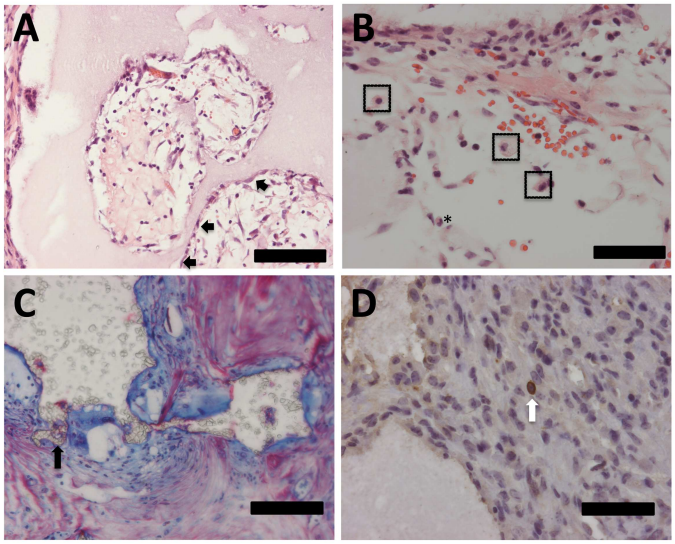

Figure S3: Representative images of tissue explants after subcutaneous implantation in FVB mice. Notice (A) cell alignment with TCP surface (black arrows), (B) macrophages (inside squares) and granulocytes (*) filling the pores of TCP, 7 days after implantation. Similar observations were done in BCP1150 C. Giant cell degrading BCP1300 surface, 12 weeks after implantation. D. CD3 positive cells (B lymphocytes) were sporadically observed in the tissue filling BCP1150 and TCP, 7 days after implantation. Scale bars represent 50 μm (B and D) and 100 μm (A and C).

References

[1] Huipin Y, Zongjian Y, Yubao L, Xingdong Z, Bruijn JDD, Groot KD. J Mater Sci Mater Med. 1998;9(12):723-6.
[2] Habibovic P, Yuan H, van der Valk CM, Meijer G, van Blitterswijk CA, de Groot K. Biomaterials. 2005;26(17):3565-75.
[3] Yuan H, Fernandes H, Habibovic P, de Boer J, Barradas AM, de Ruiter A, Walsh WR, et al. Proc Natl Acad Sci U S A. 2010;107(31):13614-9.
[4] Ripamonti U, Crooks J, Kirkbride AN. S Afr J Sci. 1999;95(8):335-43.
[5] Yamasaki H, Sakai H. 1992;13(5):308-12.
[6] Carragee EJ, Hurwitz EL, Weiner BK. Spine J. 2011;11(6):471-91.
[7] De Bruijn JD, Shankar K, Yuan H, P H. Osteoinduction and its evaluation. In: Bioceramics and their applications. T Kokubo ed. Woodhead Publishing Ltd, Cambridge; 2008.
[8] Yoshida K, Oida H, Kobayashi T, Maruyama T, Tanaka M, Katayama T, Yamaguchi K, et al. Proc Natl Acad Sci U S A. 2002;99(7):4580-5.
[9] Sakuma Y, Tanaka K, Suda M, Yasoda A, Natsui K, Tanaka I, et al. J Bone Miner Res. 2000;15(2):218-27.
[10] Harada Y, Wang JT, Doppalapudi VA, Willis AA, Jasty M, Harris WH, et al. J Biomed Mater Res. 1996;31(1):19-26.
[11] Fellah BH, Delorme B, Sohier J, Magne D, Hardouin P, Layrolle P. J Biomed Mater Res A. 2010;93A(4):1588-95.
[12] Thomsen P, Gretzer C. Curr Opin Solid St M.5(2-3):163-76.
[13] Ripamonti U, Klar RM, Renton LF, Ferretti C. Biomaterials. 2010;31(25):6400-10.
[14] Ripamonti U, Vandenheever B, Vanwyk J. Matrix. 1993;13(6):491-502.
[15] Yang Z, Yuan H, Tong W, Zou P, Chen W, Zhang X. Biomaterials. 1996;17(22):2131-7.
[16] Hartman EHM, Vehof JWM, Ruijter JEd, Spauwen PHM, Jansen JA. Biomaterials. 2004;25(27):5831-7.
[17] Barradas AMC, Yuan H, van Blitterswijk CA, Habibovic P. Eur Cell Mater. 2011;21:407-29.
[18] Yuan H, van Blitterswijk CA, de Groot K, de Bruijn JD. Tissue Eng. 2006;12(6):1607-15.
[19] Yang RN, Ye F, Cheng LJ, Wang JJ, Lu XF, Shi YJ, et al. J Zhejiang Univ SCI B. 2011;12(7):582-90.
[20] Marusic A, Katavic V, Grcevic D, Lukic IK. Bone. 1999;25(1):25-32.
[21] Li S, de Wijn JR, Li J, Layrolle P, de Groot K. Tissue Eng. 2003;9(3):535-48.
[22] Yuan H, van den Doel M, Li S, van Blitterswijk CA, de Groot K, de Bruijn JD. J Mater Sci Mater Med. 2002;13(12):1271-5.
[23] Crouzier T, Sailhan Fdr, Becquart P, Guillot R, Logeart-Avramoglou D, Picart C. Biomaterials. 2011;32(30):7543-54.
[24] Koyama N, Okubo Y, Nakao K, Osawa K, Bessho K. Br J Oral Maxillofac Surg. 2011;49(4):314-8.
[25] Hulsart-Billstrom G, Hu Q, Bergman K, Jonsson KB, Aberg J, Tang R, et al. Acta Biomater. 2011;7(8):3042-9.
[26] Takahashi Y, Yamamoto M, Tabata Y. Biomaterials. 2005;26(23):4856-65.
[27] Matsushita N, Terai H, Okada T, Nozaki K, Inoue H, Miyamoto S, et. al. J Biomed Mater Res A. 2004;70A(3):450-8.
[28] Li JZ, Li H, Sasaki T, Holman D, Beres B, Dumont RJ, et al. Gene Ther. 2003;10(20):1735-43.
[29] Odgaard A. Bone. 1997;20(4):315-28.
[30] Manigrasso M, O'Connor J. Calcif Tissue Int. 2008;82(6):465-74.
[31] Li X, Gu W, Masinde G, Hamilton-Ulland M, Rundle CH, Mohan S, et. al. Bone. 2001;29(2):134-40.
[32] Beamer WG, Donahue LR, Rosen CJ, Baylink DJ. Bone. 1996;18(5):397-403.
[33] Ghanaati S, Barbeck M, Detsch R, Deisinger U, Hilbig U, Rausch V, et al. Biomed Mater. 2012;7(1):015005.
[34] Andrikopoulos P, Baba A, Matsuda T, Djamgoz MBA, Yaqoob MM, Eccles SA. J Biol Chem. 2011;286(44):37919-31.
[35] Jung HJ, Kim JH, Shim JS, Kwon HJ. J Biol Chem. 2010;285(33):25867-74.
[36] Shen W-G, Peng W-X, Dai G, Xu J-F, Zhang Y, Li C-J. Cell Biol Int. 2007;31(2):126-34.
[37] Mukhopadhyay D, Akbarali HI. Biochem Biophys Res Commun. 1996;229(3):733-8.
[38] Zelzer E, Olsen BR. Curr Top Dev Biol; 2005;65:169-87.
[39] Honda Y, Anada T, Kamakura S, Nakamura M, Sugawara S, Suzuki O. Biochem Biophys Res Commun. 2006;345(3):1155-60.
[40] Klein C, Patka P, Denhollander W. Biomaterials. 1989;10(1):59-62.
[41] Shehab D, Elgazzar AH, Collier BD. J Nucl Med. 2002;43(3):346-53.
[42] Potter BK, Forsberg JA, Davis TA, Evans KN, Hawksworth JS, Tadaki D, et al. J Bone Joint Surg Am. 2010;92 Suppl 2:74-89.

[43] Kan LX, Kessler JA. J Biomed Biotechnol. 2011;2011:309289
[44] Cullen N, Perera J. J Head Trauma Rehabil. 2009;24(1):69-71.
[45] Baird EO, Kang QK. J Orthop Surg Res. 2009;4:12.

Chapter 6

Surface modifications by gas plasma control osteogenic differentiation of MC3T3-E1 cells

Ana M.C. Barradas, Kristina Lachmann, Gregor Hlawacek, Cathelijne Frielink, Roman Truckenmüller, Otto C. Boerman, Raoul van Gastel, Henk Garritsen, Michael Thomas, Lorenzo Moroni, Clemens van Blitterswijk, Jan de Boer

Abstract

Numerous studies have shown that physico-chemical properties of biomaterials can control cell activity. Cell adhesion, proliferation, differentiation as well as tissue formation in vivo can be tuned by properties such as porosity, surface micro- and nanoscale topography and chemical composition of biomaterials.This concept is very appealing for tissue engineering since instructive properties in bio-active materials can be more economical and time efficient than traditional strategies of cell pre-differentiation in vitro prior to their implantation. The biomaterial surface, which is easy to modify due to its accessibility, may provide the necessary signals to elicit a certain cellular behavior.

Here, we used gas plasma technology at atmospheric pressure to modify the physico-chemical properties of polylactic acid and analysed how this influenced pre-osteoblast proliferation and differentiation. Tetramethylsilane and 3-aminopropyl-trimethoxysilane with helium as a carrier gas or a mixture of nitrogen and hydrogen were discharged to polylactic acid discs to create different surface chemical compositions, hydrophobicity and micro-scale topographies. Such modifications influenced protein adsorption and pre-osteoblast cell adhesion, proliferation and osteogenic differentiation. Furthermore polylactic acid treated with tetramethylsilane enhanced osteogenic differentiation compared to the other surfaces. This promising surface modification could be further explored for potential development of bone grafts substitutes.

Introduction

Bone tissue engineering has emerged as a field providing alternatives to autologous bone grafts, which are still considered as the gold standard treatment to heal a bone defect [1-3]. Tissue engineering strategies focus on the development of scaffolds and/or on the combination of scaffolds with cells. Traditionally cells are pre-differentiated into the osteogenic lineage through addition of growth factors or steroids, such as bone morphogenetic proteins (BMPs) or dexamethasone [4-8]. Alternatively, cell differentiation may be controlled by the physico-chemical properties of the scaffold material [9-11]. This represents a more economic and expedite approach and has the additional advantage that biologically relevant molecular signals are still presented to the cells through cell-surface interactions after the graft has been implanted. For example, induction of bone formation is known to be influenced by the pore size of biphasic calcium phosphate ceramic granules [12], the depth of surface concavities in hydroxyapatite ceramic discs [13] and the chemical composition of the ceramic materials [14]. This demonstrates the relevance of material properties for clinical application.

Besides changing the biomaterial's bulk properties, one can also change those of the surface, such as topography or chemistry. For instance, it was noted that NH_2 enriched surfaces promoted osteogenesis of human bone marrow derived mesenchymal stromal cells (hMSCs) whereas chondrogenesis was favored by COOH and OH groups [15]. However, Phillips et. al. could not pertain the expression of chondrogenic markers to one specific group [16]. Changes in surface chemistry are accompanied by differences in material-protein interaction, which may account for the observed cell behavior [17, 18]. For instance, adsorption of fibronectin and vitronectin to polymeric scaffolds is affected by the polymer chemical composition [10, 19]. Moreover, fibronectin conformation attached to silica coated substrates depended on the size of silica sols used [20] and on the chemical groups present at the substrate surface [21]. Interestingly, when the central cell binding domain of fibronectin was blocked, the observed effects by NH_2 and OH coated surfaces on osteogenic differentiation of MC3T3-E1 cells was abrograted [22]. Furthermore, the authors of the study demonstrated that mineralization could be tailored by $\beta 1$ and $\beta 3$ integrin activity, which links cell adhesion to chemistry-dependent effects.

Thus, we consider chemical modification of surfaces as an efficacious strategy to control cell behavior. An efficient method to chemically modify surfaces is through gas plasma treatment. Gas plasma is a state of matter in which molecules of a gas are ionized due to an electric discharge, increasing the probability of interaction with surrounding molecules. Charged molecules as well as radicals are formed after applying a high voltage. These reactive species interact with material surfaces and lead to the incorporation of functional groups. Depending on the process parameters used (pressure, gas mixture, addition of film-forming agent, treatment time, applied power) different effects on the surface are observed. Gas plasma treatments applied to polymeric biomaterials modify not only their surface chemical composition but also roughness and wettability, which, as expected, can affect cell behavior as well [23-30]. For instance, adhesion of human umbilical vein endothelial cells (hUVECs) onto polylactic acid (PLA) improved upon plasma treatment with oxygen, argon or nitrogen [31]. Proliferation of fibroblasts was enhanced by treating polyetheretherketone (PEEK) with a plasma mixture of ammonia and argon, compared to the non-treated scaffold [27]. Similarly, treating poly(ethylene glycol)-terephthalate-poly(butylene terephthalate) (PEGT/PBT) block

co-polymer with argon plasma, increased cell numbers of chondrocytes [32]. Whereas adhesion and proliferation are often markedly affected by plasma treatments, effects on cellular differentiation have been reported less often. For instance expression of alkaline phosphatase (ALP) in osteoblast precursors cultured in PLA was not affected compared to cultures in PLA treated with gas plasma [27]. Similarly, expression of ALP and collagen type I by fibroblasts cultured on plasma treated PEEK did not change compared to cultures on the non-treated film. Conversely, plasma treatment enhanced collagen type II expression in chondrocytes to levels similar to those observed in a pellet system [32] and mildly affected expression of osteogenic markers in hMSCs [29], demonstrating the potential of this technology to alter cell fate.

Although most of these examples deal with gas plasma treatment at low pressure, atmospheric pressure is in general more advantageous since there is no need for vacuum and requires shorter processing times. In the past, we have reported on a method of gas plasma technology at atmospheric pressure used to incorporate amide and amine groups on polymers that improved cell adherence [25, 26]. In this manuscript, we applied this system in the field of bone tissue engineering by modifying the physico-chemical properties of PLA. PLA is a biodegradable material and one of the most tested for tissue engineering applications, including orthopedics [1, 16, 33-36]. We chose to use discs in order to eliminate cell seeding and nutrition inhomogeneity, frequently associated with three-dimensional (3D) scaffolds and thus address the sole effect of surface modifications on cellular behavior. Besides, discs could be easily obtained, disinfected and handled for cell culture. Plasma treatments resulted in PLA surfaces with different chemical composition, roughness and hydrophobicity and effects on adhesion, proliferation and differentiation of the pre-osteoblast cell line MC3T3-E1 were evaluated.

Materials and Methods

Gas plasma treatment of PLA samples

FDA approved poly (L,D-lactic acid) (PLA) transparent foil, with a thickness of 150 μm, was a kind gift from Folienwerk Wolfen GmbH (PLA-type 2002D). Disc-shaped samples of approximately 10 cm^2 were punched out of the PLA foil (PLAd) and placed in a grounded substrate carrier facing the high voltage electrode (HVE) in a dielectric barrier discharge configuration [37, 38]. In all cases, only one side of the PLAd was treated. An electric discharge was produced in the space between the HVE and the grounded substrate, charging the atmospheric molecules present in that space (gas plasma). PLAd were treated by adding the monomers 3-aminopropyl-trimethoxysilane (AP_{TMS}, > 97%, Sigma-Aldrich) or tetramethylsilane (TMS, >99,9%, abcr GmbH)) to the gas phase (helium, 5.0 Linde) or treated with a gas-mixtures of nitrogen and 3.4% hydrogen (N2/H2). An overview of the different treatments is given in Table 1.

PLAd disinfection and sterilization

PLAd were disinfected in 70% v/v ethanol in demineralized water (dH_2O) for 15 minutes, followed by 15 minutes in phosphate-buffered saline (PBS, Gibco). This procedure was performed twice. Ethanol solutions were filtered with a 0.22 μm pore size filter to remove

Table 1: Overview of PLAd gas plasma treatments at atmospheric pressure.

Process gas[a]	*Film-forming agent*	*Power [W]*	*Exposure time [s]*[b]	*Sample*[c]
He	APTMS[d]	50	20	P_{APTMS}
He	TMS[e]	50	40	P_{TMS}
N_2 + 3.4 % H_2	n/a[f]	150	36	$P_{N2/H2}$

[a]process gas can be the vapor phase of a monomer or a mixture of gases
[b]exposure time to the electric discharge
[c]resulting samples were named according to treatment received
[d]3-aminopropyl-trimethoxysilane
[e]tetramethylsilane
[f]non applicable

any particles in suspension that could adhere to the polymeric surfaces. Gamma-irradiation (GI) was performed at Membrana GmbH (D-42289 Wuppertal) with an irradiation dose of 30.5 kGy.

Water Contact Angle

After removal of samples from the different solutions in which they were incubated, samples were flushed in a stream of dry N_2. Afterwards, advancing contact angle measurements were performed on an OCA 20 L system (Dataphysics Instruments GmbH) with double-distilled water as test liquid and a dose rate of 0.06 μL s^{-1}. For each sample at least three drops were measured and approximately 150 points (4 values s^{-1}) were taken from each measurement.

Fourier Transform Infrared Spectroscopy-Attenuated Total Reflectance

Film composition was determined by Fourier Transform Infrared Spectroscopy-Attenuated Total Reflectance (FTIR-ATR) Spectroscopy on a Nicolet 5700 FTIR spectrometer (Thermo Scientific Inc.) equipped with a Mercury Cadmium Telluride detector and a DuraSamplIR single-reflection 45° diamond crystal. The spectra were taken with non-polarized light at a spectral resolution of 4 cm^{-1} and 64 scans were made. To identify characteristic absorption bands, spectra were achieved by subtracting the PLAd spectrum from the spectrum of P_{TMS}, P_{APTMS} or $P_{N2/H2}$. Coating thickness was roughly calculated based on the FTIR-ATR spectra and refractive index of the foil and coating. For this the coating was deposited on a polyethylene terephthalate foil (Mylar). The thickness was estimated by the attenuation of the characteristic C=O absorption band from the substrate, which is reduced by the deposited film. To estimate the film thickness the following formula was applied:

$$d = \frac{d_p}{2} \ln\left(\frac{a_{Sub}(0)}{a_{Sub}(d)}\right)$$

where aSub(0) is the area of the absorption band at 1720 cm^{-1} from an uncoated substrate, aSub(d) the area of the absorption band at 1720 cm^{-1} after film deposition and dp the penetration depth of the evanescent wave, which depends on the refractive index. The following assumptions were made: 1) the absorption is uniform on the whole substrate and 2) the refractive index of the film and the substrate are equal [39].

Atomic Force Microscopy
The topology of the surface was analysed with Atomic Force Microscopy (AFM, DI3100, Veeco Instruments Inc.) in tapping mode. Root mean squared roughness (Rq) was determined on an area of 5 x 5 μm2 in size, based on the following formula:

$$Rq = \left(\frac{1}{n}\sum_{1}^{n} y_i^2\right)^{1/2}$$

where n is the amount of points where sample height was measure and yi the height measured for each point.

Helium Ion Microscope
Samples for Helium Ion Microscopy (HIM) were fixed with 1.5% gluteraldehyde in 0.14 M cacodylate buffer (pH=7.4) followed by dehydration in an ethanol series (60, 70, 80, 90, 96 and 100% v/v in dH_2O) and critical point drying (CPD). Before inserting the samples in the CPD chamber, samples of approximately 1 cm^2 were cut with a sterile blade. After CPD, samples were gold sputtered and analyzed with HIM. HIM uses a He^+ beam with a diameter of less than 0.5 nm to scan the surface [40, 41]. Secondary electrons generated by the impinging He^+ are emitted and collected with an Everhart-Thornley detector. At the primary beam energy of 30-31 kV this results in a lateral resolution of 0.55 nm. The He+ dose used was 5x1012 cm^{-2} and 7x1013 cm^{-2} for the 50 μm and 5 μm field view images respectively (Figure 3B).

Bovine Serum Albumin quantification
Bovine Serum Albumin (BSA) was radio-iodinated using the iodogen-method [42]. Briefly, 60 μg BSA (Sigma-Aldrich Co.) was incubated with 11 MBq I-125 (PerkinElmer) in 100 μl of 50 mM phosphate buffer, pH 7.4 at room temperature (RT) in a vial coated with 100 μg iodogen. After 10 minutes the reaction was stopped by adding 100 μl saturated tyrosine solution. The reaction mixture was eluted on a PD-10 desalting column (Amersham Biosciences) with PBS and the 125I-labeled BSA (^{125}I-BSA) containing fractions were pooled. The radiochemical purity (RCP) as determined by instant thin layer chromatography (ITLC) using 0.1 M citrate pH 6.0 as mobile phase, exceeded 99%. The specific activity of ^{125}I-BSA was 124 kBq/μg. The ^{125}I-BSA was diluted in PBS and 4 mL (6.5 kBq; 53 ng BSA) were added to PLAd, P_{TMS}, P_{APTMS} and $P_{N2/H2}$, respectively. After 3.5 hours incubation at 37°C, the supernatant was removed and the samples were rinsed three times with PBS. Samples were measured in a well-type gamma counter (Wizard 1480, Wallac) along with a known fraction of the total activity added. The disc-associated activity was expressed as a fraction of the added activity.

Cell culturing
MC3T3-E1 cells (subclone 14) were expanded in basic medium (BM) consisting of α-MEM (Life Technologies Corporation), 10% foetal bovine serum (FBS, Lonza Group Ltd), 2 mM L-glutamine (Life Technologies Corporation) and 100 U/ml penicillin and 100 g/ml streptomycin (Life Technologies Corporation). During expansion phase, medium was refreshed every two days and cells were trypsinised upon reaching 80% confluency to subculture on

PLA discs. Subsequently a cell suspension was prepared in fresh BM and directly pipetted on the PLA discs placed in wells of 6 well plates having the non-treated side facing the bottom of the well. Cells were allowed to attach overnight (O/N) and medium was changed to either BM or Osteogenic differentiation medium (OM), comprising BM supplemented with 0.2 mM ascorbic acid (AA, Sigma-Aldrich Co., A8960) and 100 ng/ml of rh-BMP2 (Hangzhou Biodoor Biotechnology Co.). All cell culture experiments were performed at 37°C in a 5% CO_2 humid atmosphere.

Methylene blue staining
Cells were rinsed with PBS and then fixed in 10% formalin (Sigma-Aldrich Co.) for 15 minutes. After rinsing two times with dH_2O, 1% w/v methylene blue in 0.1 M borax (Sigma-Aldrich Co.) was added drop by drop until the samples' surface was covered. Samples were incubated for 1 minute in staining solution and afterwards rinsed several times with dH_2O until all excess staining solution was removed. Samples were analyzed with a stereomicroscope (Nikon SMZ-10A with Sony 3CCD camera).

Polymerase Chain Reaction
Samples were rinsed with PBS and transferred to new wells of 6 well plates. Total RNA was isolated using the NucleoSpin® RNA II isolation kit (Macherey-Nagel Gmbh & Co.) in accordance with the manufacturer's protocol. RNA was collected in RNAse-free water and the total quantity analyzed by spectrophotometry. cDNA was synthesized from 174 ng total RNA using iScript (Bio-Rad Laboratories Inc.). One μl of undiluted cDNA was used for quantitative Polymerase Chain Reaction (PCR) analysis, which was performed on a MyIQ single color real-time PCR detection system (BioRad). MyIQ data was analyzed using iQtm5 optical system software (Bio-Rad Laboratories Inc.). Ct values were normalized to the GAPDH housekeeping gene and the comparative ΔCt method (Ct control - Ct sample) was used to calculate fold inductions. Primer sequences are given in Table 2.

Table 2: Primer sequences for mouse genes.

Name	*Primer sequence*
GAPDH[a]	5'-TGGCAAAGTGGAGATTGTTGCC-3'
	5'-AAGATGGTGATGGGCTTCCCG-3'
Bone Sialoprotein	5'-ACTCGAGCCAGGACTGCCGA-3'
	5'-TCGAGAAAGCACAGGCCATTCCC-3'
Osteocalcin	5'- CAGACCTAGCAGACACCATGAGG-3'
	5'- AGGTCAGAGAGACAGAGCGCA-3'
Osterix	5´- ATGGCGTCCTCTCTGCTTG - 3
	5´- TGAAAGGTCAGCGTATGGCTT - 3
Runx-2	5'- CCCTGCCCGTGGCCTTCAAG -3'
	5'- AGGCATTTCGGAGCTCGGCG- 3'

[a]Glyceraldehyde 3-phosphate dehydrogenase

Statistical analysis

For each test, three replicates of each condition were used and statistical analysis performed using SPSS Statistics 18.0, with One Way ANOVA and Tukey's Multiple Comparison test or Student t-Test, in the case of Figure 5, between time points for each individual treatment. In all cases the following applies for description of statistical significance: * = $p < 0.05$; ** = $p < 0.01$; *** = $p < 0.001$.

Results

Gas plasma treatment changes the chemical composition of PLA surfaces

PLAd were treated with gas plasma at atmospheric pressure in a dielectric discharge barrier configuration (Table 1). By addition of TMS or APTMS a thin coating (50-150 nm) was deposited on the surface. In contrast, when treating the samples with N_2/H_2 ($P_{N2/H2}$), only the chemical composition of the original surface was modified and no coating was deposited. However, to confirm that all treatments effectively changed the PLAd surface chemical composition, FTIR-ATR was performed (Figure 1). Surface modification with N_2/H_2 led to incorporation of nitrogen-containing functional groups (e.g. primary and secondary amino groups, amides, imides), evidenced by the characteristic absorption band of the vibrational band N-H at wavenumbers larger than 3000 cm^{-1} as well as the C-N deformation vibration at 1650 cm^{-1}. Due to residual oxygen in the gas mixture hydroxyl groups were introduced on the surface as well. Primary amino groups were also achieved by film deposition of APTMS, as shown in Figure 1 (P_{APTMS}). The film is characterized by a Si-O-Si network, as well as Si-O-C-groups, which did not undergo a condensation reaction (absorption band at 1100 cm^{-1}). Hydrogen bonds, characterized by the broad band at wavenumbers larger than 3000 cm^{-1}, belong to Si-O-H and N-H vibrational band. Deposition of TMS led to a thin film mainly consisting of Si-(CH_3)x (x = 1, 2, 3). Characteristic absorption bands (2900-2800 cm^{-1} C-H, 1290-1850 cm^{-1} Si-(CH_3)x, Si-C) can be observed in the corresponding FTIR-spectrum. The small absorption at 2100 cm^{-1} shows that also Si-H bonds are formed during film deposition.

Altered biomaterial properties on the treated surfaces

Hydrophobicity was determined by measuring water contact angles on both non-treated samples (PLAd) and samples immediately after gas plasma treatment. In addition, wettability was assessed after the disinfection procedure (70% v/v ethanol in dH_2O) and O/N incubation in BM (Figure 2). P_{TMS} was the most hydrophobic surface after treatment, having a water contact angle of 119°, followed by PLAd, P_{APTMS} and $P_{N2/H2}$. Disinfection slightly affected wettability of P_{TMS} but after incubation in BM the water contact angle value was again 119°. After all steps, P_{TMS} was the most hydrophobic surface. Disinfection slightly decreased wettability of PLAd and P_{APTMS} but after incubation in BM there were no statistically significant differences between these two values: 82° and 80° respectively. $P_{N2/H2}$'s wettability was the most affected by disinfection (from 48° to 70°) but was not affected by incubation in BM. After incubation in BM, $P_{N2/H2}$ was the most hydrophilic sample. In a clinical scenario, ethanol will not be used as sterilization agent but γ-irradiation will more likely be. P_{TMS} and P_{APTMS} showed a slight increase in wettability after γ-irradiation: in the case of P_{TMS}, the

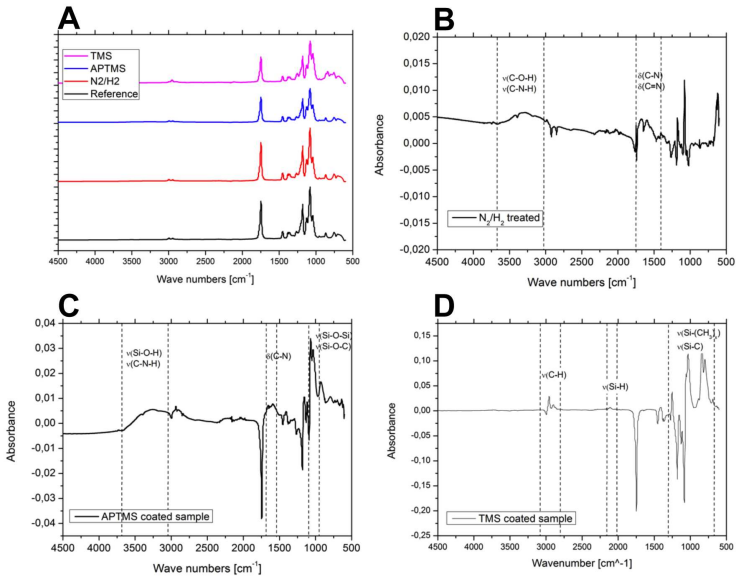

Figure 1: Gas plasma treatment at atmospheric pressure induces differences in surface chemical composition. A) Overview of all spectra obtained. Reference spectrum (PLAd) was subtracted to those of $P_{N2/H2}$, P_{APTMS} and P_{TMS}. Difference spectra are represented and characteristic functional groups indicated by the respective vibrational bands: B) N2/H2=$P_{N2/H2}$; C) APTMS=P_{APTMS}; D) TMS=P_{TMS}.

water contact angle changed from 118° to 114° and in the case of P_{APTMS} from 80° to 77°. A slight increase in wettability was also observed for PLAd. The water contact angle of $P_{N2/H2}$ increased after γ-irradiation from 48° to 55°. Based on AFM analysis, roughness was quantified as Rq. Treatment with N_2/H_2 increased Rq from 1.14 nm to 12.2 nm, whereas P_{TMS} and P_{APTMS} had lower Rq than that of PLAd (0.9 and 0.61 nm, whereas before the treatment it was 1.14 nm, see Figure 3A). Next, we used HIM to evaluate surface topology after incubation with FBS, the protein source in cell culture. Figure 3B shows that FBS roughens the surface of PLAd, relative to unexposed PLAd. Among the different samples, P_{TMS} exhibited the roughest surface.

BSA adsorption

After 3.5 hours of incubation at 37°C, excess ^{125}I-BSA was washed off the surface by rinsing the samples three times in PBS and the adhered protein was quantified (Figure 4). Adhesion of ^{125}I-BSA was highest on P_{APTMS} (67%) and lowest on $P_{N2/H2}$ (21%). Adsorption to PLAD and P_{TMS} was respectively 40 and 36% but the difference was not statistically significant. Overall the results demonstrated that differential protein binding occurs through surface treatment.

MC3T3-E1 adhesion and proliferation

We hypothesized that cellular behavior would be affected according to physico-chemical

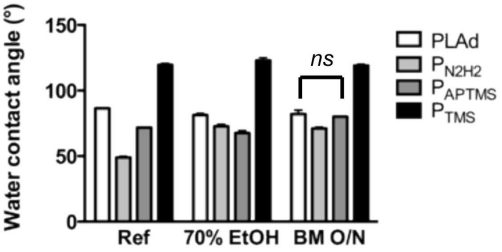

Figure 2: Hydrophobicity varies according to gas plasma treatment. Contact angle measurements were performed on PLAd, $P_{N2/H2}$, P_{TMS} and P_{APTMS} after three steps: at reference (ref; after gas plasma treatment), disinfection (70% EtOH) and O/N incubation in BM (BM O/N). Values are statistically significantly different ($p<0.001$), except when indicated by ns (not significant).

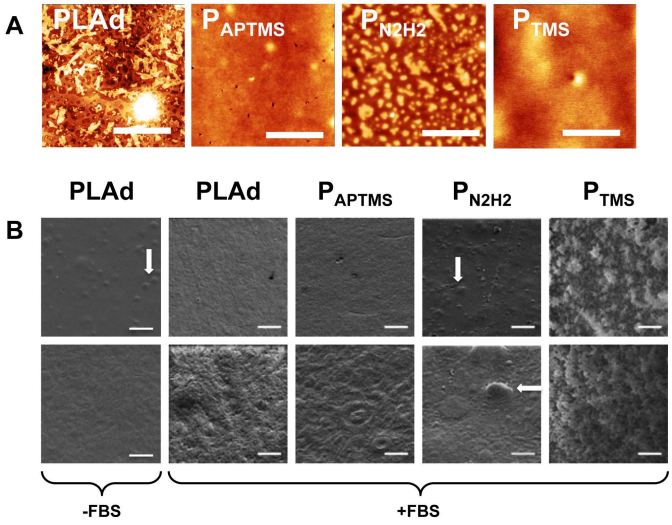

Figure 3: AFM and HIM visualization depict differences in the surface topography before and after protein adsorption. A. Surface topography of PLAd, $P_{N2/H2}$, P_{TMS} and P_{APTMS} was analysed with AFM immediately after treatment. Images illustrate surface roughness for each treatment in a heat map fashion, where lighter spots (yellow) represent higher feature height than darker ones (brown). Rq values are provided in section 3.2. Scale bar is 2 μm. B. PLAd surface after disinfection (-FBS) and PLAd, P_{APTMS}, $P_{N2/H2}$ and P_{TMS} surfaces after disinfection and incubation in FBS (+FBS) were analyzed with HIM. White arrows point towards characteristic topological features found in PLAd and $P_{N2/H2}$. Scale bar in top row is 10 μm and in bottom row is 1 μm.

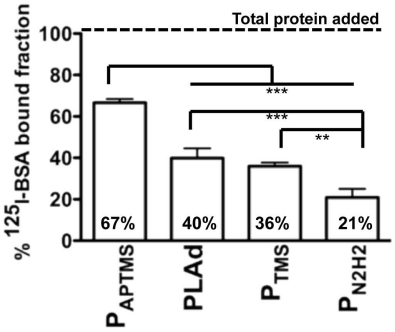

Figure 4: Adsorption of ^{125}I-BSA is tuned by surface properties. ^{125}I-BSA bound fraction (%) to PLAd, $P_{N2/H2}$, P_{TMS} and P_{APTMS} after 4 hours incubation at 37°C. Dashed line on top indicates total protein initially added. Values at the bottom of each bar represent percentage of bound ^{125}I-BSA for each sample.

properties of PLAd, $P_{N2/H2}$, P_{TMS} and P_{APTMS}. To investigate this, we chose the pre-osteoblast mouse cell line MC3T3-E1 as model cell because its transcriptional response to osteogenic signals is well documented. PLAd, P_{TMS}, P_{APTMS} and $P_{N2/H2}$ were incubated in BM overnight and the next day 50×10^3 MC3T3-E1 cells were seeded per sample and cultured for 24 and 48 hours. At both time points we qualitatively analyzed cell distribution on the surface by methylene blue staining. We chose early time points to describe the early molecular response of the cells to the surfaces, rather than to describe the downstream consequence on osteogenesis at a later time point. After 24 hours, MC3T3-E1 cells were homogenously distributed on $P_{N2/H2}$ and P_{APTMS} discs whereas on PLAd and P_{TMS} they were not (Figure 5A, top row). Characteristic of P_{TMS} was cell alignment in certain areas of the surface. Cell numbers decreased after 48 hours in the case of P_{TMS}, which was suggested by methylene blue staining and confirmed by DNA assay (Figure 5B). In contrast, cell density seemed higher after 48 hours in P_{APTMS}, consistent with DNA assay although in this case not statistically significant. Cell numbers did not seem to be significantly affected in the case of PLAd and $P_{N2/H2}$ within the time frame studied.

Osteogenesis of MC3T3-E1 cells

Two and four days after seeding MC3T3-E1 cells on PLAd, $P_{N2/H2}$, P_{TMS} and P_{APTMS}, gene expression of Runx-2, Osterix, osteocalcin (OC) and bone sialoprotein (BSP) was analysed by PCR. Overall, we observed that cells treated with OM exhibited higher expression of osteogenic markers than cells treated with BM, as expected (Figure 6). For all tested genes, cells cultured in BM on P_{APTMS} exhibited lower expression than cells cultured on control samples (PLAd), but not when cultured in OM, suggesting that rhBMP-2 and AA can rescue a possible negative effect of P_{APTMS} on osteogenesis of MC3T3-E1 cells. Cells cultured on $P_{N2/H2}$ showed levels of expression for all genes at both time points very similar to those of cells cultured on PLAd. In the case of P_{TMS}, expression of Osterix and Runx-2 genes was enhanced in OM when compared to the other treatments on day 2. Most notable were

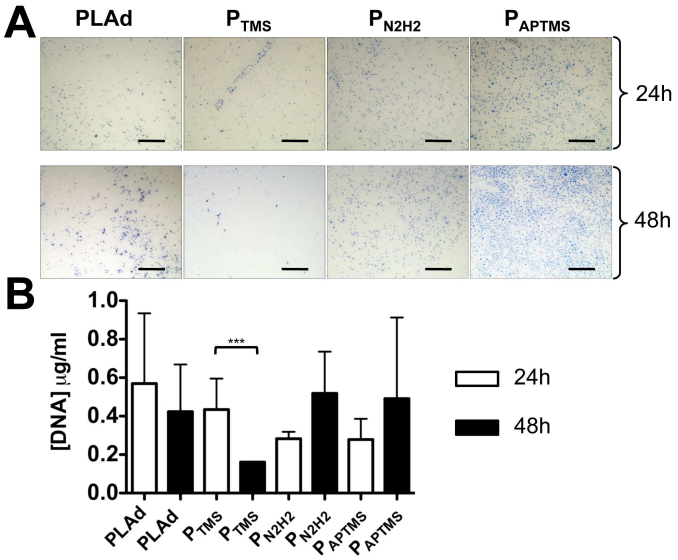

Figure 5: MC3T3-E1 cellular distribution and proliferation. A. Representative images (approximately 4x5 mm) of the cellular distribution pattern. MC3T3-E1 cells were stained with methylene blue after 24 and 48 hours of culturing on PLAd, $P_{N2/H2}$, P_{TMS} and P_{APTMS}. Scale bar is 1 mm. B. DNA quantification after 24 (white) and 48 (black) hours of cell culturing on PLAd, $P_{N2/H2}$, P_{TMS} and P_{APTMS} .

the levels of BSP and OC gene expression, for both BM and OM. Expression of BSP and OC genes were increased approximately 10 times in BM and 30 in OM, compared to cells cultured in PLAd in BM, on day 2. At day 4, differences in BSP expression between BM and OM were not visible but expression of OC, at this time point, was 100 fold higher in OM and approximately 20 fold higher in BM relative to cells cultured in PLAd in BM.

Discussion

Here we showed that gas plasma technology at atmospheric pressure could modify PLA to successfully enhance osteogenic differentiation of pre-osteoblasts cells. PLA discs were subjected to an electric discharge at atmospheric pressure in the presence of He containing tetramethylsilane (P_{TMS}), 3-aminopropyl-trimethoxysilane (P_{APTMS}) or N2/H2 ($P_{N2/H2}$). The surface of these samples was modified, as confirmed by FTIR-ATR (Figure 1), according to the treatment: in P_{TMS}, methylene (-CH_2-) and methyl (-CH_3) groups were mainly present; in $P_{N2/H2}$ amine groups (-NH- and -NH_2) and on P_{APTMS} silanol groups (Si-OH-) were detected, in addition to amine groups. Hydrophobicity of the discs differed and could be summarized from more hydrophobic to least as P_{TMS}> PLAd > P_{APTMS} > $P_{N2/H2}$, immediately after the treatment (Figure 2). Disinfection with ethanol altered hydrophobicity to P_{TMS}> PLAd > $P_{N2/H2}$> P_{APTMS}, but the original order was recovered after incubation

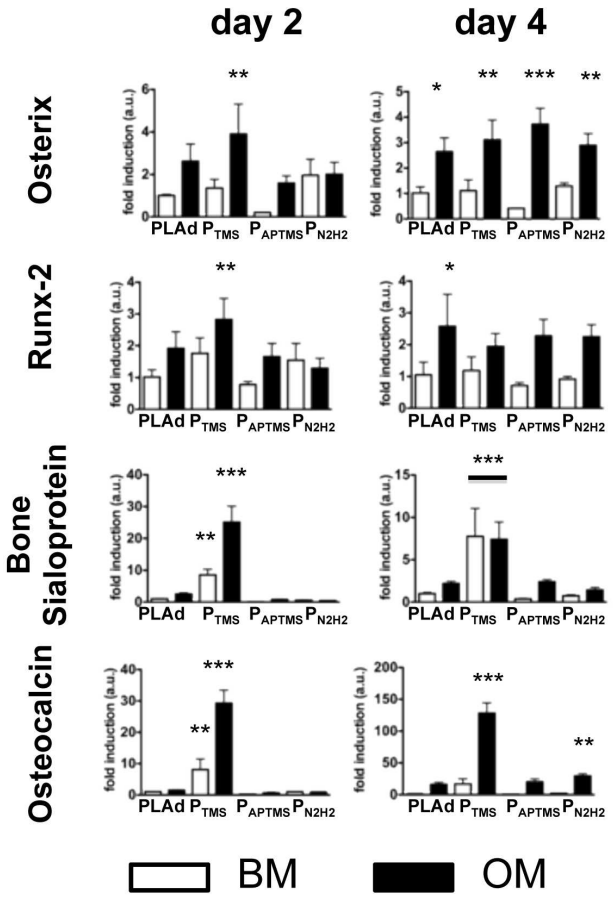

Figure 6: P_{TMS} enhances gene expression of Osteocalcin and Bone Sialoprotein in MC3T3-E1 cells. Gene expression of MC3T3-E1 cells cultured either in BM (white bars) or OM (black bars) in PLAd, $P_{N2/H2}$, P_{TMS} and P_{APTMS} for 2 and 4 days. Fold induction is relative to cells cultured in PLAd in BM. Statistical significance is shown relative to PLAd in BM.

in BM (Figure 2). Although used here as the disinfection agent, ethanol had an impact on the surface properties and so did O/N incubation in BM, possibly due to protein adsorption. Hence it is important to realize that biomaterials' properties do not remain unaffected once the treatment is finished. Instead subsequent steps can alter them before cells come into contact with the surface. In a clinical scenario, where more likely γ-irradiation will be used as sterilization agent instead of ethanol, the properties of these discs could be altered differently than what described so far. Therefore we also assessed wettability behavior after γ-irradiation and observed that γ-irradiation affected the wetting behavior in a similar fashion to ethanol by increasing wettability of P_{APTMS} and PLAd and decreasing that of $P_{N2/H2}$. However P_{TMS} became slightly more hydrophilic with γ-irradiation whereas with ethanol it became more hydrophobic. Nevertheless P_{TMS} remained after both ethanol and γ-irradiation steps, the most hydrophobic sample.

All treatments had an effect on surface roughness as measured by AFM (Figure 3A). Results showed the following trend from highest Rq to lowest: $P_{N2/H2}$>PLAd > P_{TMS}> P_{APTMS}. This suggests that film deposition smoothens the surface (Rq values close to PLAd), whereas treatment with N2/H2 not only changes chemical groups at the surface but also roughens it. However protein adsorption can again induce topographical changes, just as it did with wettability of some samples. For instance, although AFM showed that P_{APTMS} and P_{TMS} exhibited similar topographies after treatment, incubation in FBS changed this and Figure 3B suggests that P_{TMS} exhibited a rougher surface.

In respect to cellular adhesion, after 24 hours, representative images of cellular patterning suggest that there were less MC3T3-E1 cells adhered onto P_{TMS} than onto the other treatments. This treatment also had a negative effect on proliferation, as confirmed by DNA quantification (Figure 5B). It was also observed that MC3T3-E1 cells were heterogeneously distributed on P_{TMS}, forming characteristic cell lines (Figure 5A). Most likely this was not due to mechanical injury of the surface as if that would be the case, injuries in discs treated differently would be expected as well. It might be that with this particular treatment the distribution of chemical groups leads to uneven protein adsorption and consequently cell adhesion. Nonetheless, Philips et. al. also showed that adhesion of cells to -CH_3 surfaces was poor and could only be comparable to other surfaces when coated with fibronectin [16]. In addition, Curran et. al. showed that cells cultured on -CH_3 surfaces appeared in clusters and not homogeneously spread on the surface, similar to what we observed. By contrast, cells cultured on -NH_2 and -SH surfaces showed well spread morphology and by day 7 were well distributed on the surface [43]. We also observed homogeneous cell distribution in surfaces containing amine groups ($P_{N2/H2}$ and P_{APTMS}). Within the time points studied, none of the surfaces seemed to have had a profound positive effect on cell proliferation, although methylene blue staining of cells cultured on P_{APTMS} suggested an increase from 24 hours to 48 hours. Although not statically significant, observations were consistent with DNA quantification (Figure 5B). A note should be made though that some cells could have detached during washing steps, which was not evaluated, that could have led to an underrepresentation of cell amounts in figure 5.

Expression of osteogenic markers on MC3T3-E1 cells varied according to the sample in which they were cultured (Figure 6), implying that the specific gas plasma treatments changed PLA key physico-chemical properties that play a role in cell differentiation. Overall, gene expression in less pro-osteogenic surfaces seemed to be time dependent, since expression of

most markers is increased by day 4 compared to day 2. Thus osteogenic differentiation could be enhanced at later time points in the case of P_{APTMS} for instance. Such delay could prove beneficial as than it would combine high cell numbers with osteogenic differentiation in the same sample.

The combination of P_{APTMS} and BM had a negative effect on expression of all markers, rescued by AA and rhBMP-2. Cells cultured on $P_{N2/H2}$ exhibited similar levels of expression for all genes and time points as that of cells cultured on PLAd, suggesting that treatment with N2/H2 did not change surface key parameters that might regulate cell differentiation. Treatment with TMS had a positive effect on osteogenesis of MC3T3-E1 cells, since expression of BSP and OC genes was induced in cells cultured on P_{TMS} already in BM. Although these large fold inductions were not observed in the case of Osterix and Runx-2, P_{TMS} slightly enhanced expression of these genes at day 2 in OM. It is also interesting to note that treatment with TMS induced aggregation of cells on certain areas of the surface instead of an homogeneous distribution. A positive effect of cell aggregation on osteogenesis has been reported previously in hMSCs [44, 45].

If looking only at the chemical groups characteristic of these surfaces (and ignoring other surface characteristics), one could point out that -CH_2 and -CH_3 groups had a positive effect on osteogenesis of MC3T3-E1 cells. However, others have shown that osteogenesis of MC3T3-E1 cells was favored by -NH_2 and -OH groups [22], consistent with the effects observed on osteogenesis of hMSCs (also favored by -NH_2 groups) [15, 16]. In our work, -NH_2 and -OH were mainly found on $P_{N2/H2}$ (-NH_2) and P_{APTMS} (-NH_2) and these samples had a neutral or even negative effect on osteogenesis of MC3T3-E1 cells. Such contradictory results could be explained by the fact that the substrates used by others, silica or gold, were different than ours, PLA. Furthermore, other chemical groups besides the indicated ones were deposited by gas plasma, therefore a straightforward comparison is not possible. Also Curran et al. showed that introducing the same chemical group using different silane introducing chemistries can already lead to differences in the expression of some markers within the same cell type [46].

A clear link between physico-chemical properties of PLA modified surfaces and cellular responses of MC3T3-E1 cells could not be established. However, cellular adhesion was favored by surfaces with similar chemistry but different roughness ($P_{N2/H2}$ and P_{APTMS}) and furthermore, osteogenic differentiation was enhanced by P_{TMS}, whose roughness was comparable to P_{APTMS} but not the chemistry. These results suggest that the chemical composition of the PLA surface is more important in determining cellular adhesion and osteogenic differentiation of MC3T3-E1 cells than roughness. Interestingly, the relevance of chemistry over roughness effects was also highlighted on attachment, proliferation and viability of hUVECs when cultured on gas plasma treated PLA [31]. In Figure 4 we also showed that amounts of protein adsorption are dependent on the surface properties. Besides the quantity, the quality of adhered proteins might also change or even the domains of the same protein presented to the cells might vary according to the surface characteristics. This is relevant in the case of cell-adhesion proteins such as fibronectin, fibrinogen, vitronectin, laminin and collagen [20, 21, 47, 48], which could have a determinant effect in regulating cell adhesion, spreading and consequently fate.

Future work will include the response analysis of more clinically relevant cell types, such as hMSCs, to these surfaces and in 3D scaffolds, since the treatment can be easily applied to 3D structures. The easiness of gas plasma treatment makes it an appealing technique for quickly

transforming biomaterials properties and the results shown here make it a promising tool for the development of an effective generation of bone graft substitutes.

Conclusions

Gas plasma at atmospheric pressure was used to modify the physico-chemical properties of PLA discs. Chemical composition, hydrophobicity/hydrophilicity and topography of the surface changed according to treatment. MC3T3-E1 cell adhesion and proliferation was markedly influenced by the surface in which they were cultured. Treatment with TMS resulted in adhesion of few cells, aggregated heterogeneously throughout the surface and had a negative effect on proliferation. By contrast, APTMS treatment allowed cells to spread homogeneously throughout the surface and enhanced proliferation. Interestingly, TMS enhanced expression of OC and BSP genes whereas APTMS treatment had a negative effect on cell differentiation. Cells cultured on PLA without any treatment showed similar responses in terms of differentiation as cells cultured on surfaces treated with N2/H2. Modifications in PLA by gas plasma treatment at atmospheric pressure contributed to successfully guide osteogenesis in vitro. These results provide a solid basis to further investigate gas plasma modified 3D scaffolds as potential bone graft substitutes.

Acknowledgements

The authors gratefully acknowledge Jan Petersen for the technical support with AFM imaging, the financial support of the TeRM Smart Mix Program of the Netherlands Ministry of Economic Affairs and the Netherlands Ministry of Education, Culture and Science (AB) and the Dutch Technology Foundation STW, which is the applied science division of NWO, and the Technology Programme of the Ministry of Economic Affairs (GH).

References

[1] Kanzler B, Kuschert SJ, Liu YH, Mallo M. Development. 1998;125(14):2587-97
[2] Gorski JP. Crit Rev Oral Biol Med. 1998;9(2):201-23
[3] Van der Stok J, Van Lieshout EMM, El-Massoudi Y, Van Kralingen GH, Patka P. Acta Biomat. 2011;7(2):739-50
[4] Siddappa R, Fernandes H, Liu J, van Blitterswijk C, de Boer J. Curr Stem Cell Res Ther. 2007;2(3):209-20
[5] Fernandes H, Mentink A, Bank R, Stoop R, van Blitterswijk C, de Boer J. Tissue Eng Part A. 2009;16(5):1693-702
[6] Jorgensen NR, Henriksen Z, Sorensen OH, Civitelli R. Steroids. 2004;69(4):219-26
[7] AI-Aql ZS, Alagl AS, Graves DT, Gerstenfeld LC, Einhorn TA. J Dent Res. 2008;87(2):107-18
[8] Frank O, Heim M, Jakob M, Barbero A, Schafer D, Bendik I, Dick W, et al. J Cellular Biochem. 2002;85(4):737-46
[9] Anderson DG, Putnam D, Lavik EB, Mahmood TA, Langer R. Biomaterials. 2005;26(23):4892-7
[10] Neuss S, Denecke B, Gan L, Lin Q, Bovi M, Apel C, Wöltje M, et al. PLoS ONE. 2011;6(9):e23195
[11] Kumar G, Tison CK, Chatterjee K, Pine PS, McDaniel JH, Salit ML, Young MF, et al. Biomaterials. 2011;32(35):9188-96
[12] Habibovic P, Yuan H, Vandervalk C, Meijer G, van Blitterswijk C, de Groot K. Biomaterials. 2005;26(17):3565-75
[13] Ripamonti U, Crooks J, Kirkbride AN. S Afr J Sci. 1999;95(8):335-43
[14] Yuan H, De Bruijn JD, Li Y, Feng J, Yang Z, De Groot K, Zhang X. J Mater Sci Mater Med. 2001;12(1):7-13
[15] Curran JM, Chen R, Hunt JA. Biomaterials. 2006;27(27):4783-93
[16] Kim S, Koga T, Isobe M, Kern BE, Yokochi T, Chin YE, Karsenty G, et al. Genes Dev. 2003;17(16):1979-91
[17] Bale M, Wohlfahrt L, Mosher D, Tomasini B, Sutton R. Blood. 1989;74(8):2698-706
[18] Fabrizius-Homan DJ, Cooper SL. J Biomater Sci Polym Ed. 1992;3(1):27-47
[19] Mahmood TA, Miot S, Frank O, Martin I, Riesle J, Langer R, van Blitterswijk CA. Biomacromolecules. 2006;7(11):3012-8
[20] Lord MS, Cousins BG, Doherty PJ, Whitelock JM, Simmons A, Williams RL, Milthorpe BK. Biomaterials. 2006;27(28):4856-62
[21] Keselowsky BG, Collard DM, Garcia AJ. J Biomed Mater Res A. 2003;66A(2):247-59
[22] Keselowsky BG, Collard DM, Garcia AJ. Proc Natl Acad Sci. 2005;102(17):5953-7
[23] Pavlica S, Piscioneri A, Peinemann F, Keller M, Milosevic J, Staeudte A, Heilmann A, et al. Biomaterials. 2009;30(33):6514-21
[24] Siow KS, Britcher L, Kumar S, Griesser HJ. Plasma Process Polym. 2006;3(6-7):392-418
[25] Lachmann K, Dohse A, Thomas M, Pohl S, Meyring W, Dittmar KEJ, Lindenmeier W, et al. Eur Phys J Appl Phys. 2011;55(1):13812-9
[26] Griesser HJ, Chatelier RC, Gengenbach TR, Johnson G, Steele JG. J Biomater Sci Polym Ed. 1994;5(6):531-54
[27] Chim H, Ong JL, Schantz J-T, Hutmacher DW, Agrawal CM. J Biomed Mater Res A. 2003;65A(3):327-35
[28] Briem D, Strametz S, Schroder K, Meenen NM, Lehmann W, Linhart W, Ohl A, et al. J Mater Sci Mater Med. 2005;16(7):671-7
[29] Mwale F, Wang HT, Nelea V, Luo L, Antoniou J, Wertheimer MR. Biomaterials. 2006;27(10):2258-64
[30] Woodfield T, Miot S, Martin I, Vanblitterswijk C, Riesle J. Biomaterials. 2006;27(7):1043-53
[31] Shah A, Shah S, Mani G, Wenke J, Agrawal M. J Tissue Eng Regen Med. 2011;5(4):301-12
[32] Woodfield TBF, Miot S, Martin I, van Blitterswijk CA, Riesle J. Biomaterials. 2006;27(7):1043-53
[33] Middleton JC, Tipton AJ. Biomaterials. 2000;21(23):2335-46
[34] Navarro M, Michiardi A, Castano O, Planell JA. J R Soc Interface. 2008;5(27):1137-58
[35] Athanasiou KA, Agrawal CM, Barber FA, Burkhart SS. Arthroscopy. 1998;14(7):726-37
[36] Brown SA, Rohrich RJ, Baumann L, Brandt FS, Fagien S, Glazer S, Kenkel JM, et al. Plast Reconstr Surg. 2011;127(4):1684-92
[37] Klages C-P, Hoepfner K, Klaeke N, Thyen R. Plasmas Polym. 2000;5(2):79-89
[38] Klages C-P, Eichler M. Vakuum in Forschung und Praxis. 2002;14(3):149-55
[39] Tompkins HG. Appl Spectrosc. 1974;28(4):335-41
[40] Hill R, Notte J, Ward B. The ALIS He ion source and its application to high resolution microscopy. In: Munro ERJ, editor. Proceedings of the Seventh International Conference on Charged Particle Optics2008. p. 135-41.
[41] Notte J, Ward B, Economou N, Hill R, Percival R, Farkas L, McVey S. An introduction to the helium ion microscope. In: Seiler D, Diebold A, McDonald R, Garner C, Herr D, Khosla R, Secula, E, editors. Frontiers of Characterization and Metrology for Nanoelectronics: 2007. p. 489-96.

[42] Fraker PJ, Speck JC. Biochem Biophys Res Commun. 1978;80(4):849-57
[43] Curran JM, Chen R, Hunt JA. Biomaterials. 2005;26(34):7057-67
[44] Unadkat HV, Hulsman M, Cornelissen K, Papenburg BJ, Truckenmueller RK, Post GF, Uetz M, et al.Proc Natl Academ Sci U S A. 2011;108(40):16565-70
[45] Dalby MJ, Gadegaard N, Tare R, Andar A, Riehle MO, Herzyk P, Wilkinson CD, et al. Nat Mater. 2007;6(12):997-1003
[46] Curran JM, Pu F, Chen R, Hunt JA. Biomaterials. 2011;32(21):4753-60
[47] Denis F, Hanarp P, Sutherland DS, Gold J, Mustin C, Rouxhet PG, Dufrene YF. Langmuir. 2002;18(3):819-28
[48] Nygren H, Stenberg M, Karlsson C. J Biomed Mater Res. 1992;26(1):77-91

Chapter 7

General discussion and main conclusions

In the field of Bone Tissue Engineering, scientists search for alternatives to the current therapies for healing bone fractures and defects [1-5]. Recent work showed that biomaterials' physico-chemical properties can regulate cell fate [6-11], hence **it would be ideal to orchestrate bone defect healing through the biomaterials' own set of instructions captured by the surrounding host**. Biomaterials of synthetic origin are therefore a subject of raising interest in the field, as they overcome the need of additional surgeries (as autologous bone graft do), can be produced in large quantities (overcoming the shortage of bone graft availability) and overall lower the health care associated costs. **To govern cell fate through biomaterials'physico-chemical properties, the underlining interactions between the biomaterial and the cells that lead to a particular cellular phenotype must be understood**. To do so, first of all one has to acknowledge the complexity of the system and second, work hard to break it into pieces.

In the work here described, the interaction between biomaterials and the biological responses they elicit in cells or tissues was explored. In this chapter, it will be discussed the results of this thesis relating the material specific physico-chemical properties and how these influence the osteogenic response of the cells. This will be discussed on the basis of the *in vitro* work developed in *Chapters 3*, *4* and *6* and *in vivo* work reported in *Chapter 5*.

Surface properties

Pre-osteoblast cells (MC3T3-E1) were cultured on polylactic acid (PLA) substrates modified with different gas plasma treatments (*Chapter 6*). MC3T3-E1 cells attachment was enhanced on P_{APTMS} and $P_{N2/H2}$, expressing alongside lower amounts of osteocalcin (OC) and bone sialoprotein (BSP), when compared to cultures in P_{TMS}. In the first case, $P_{N2/H2}$'s surface was rougher than that of P_{APTMS} but the chemistry of these two surfaces was similar, differing mainly at the 1000 cm^{-1} vibrational band, due to the Si network of the APTMS molecule. In the case of P_{TMS} the roughness was similar to that of P_{APTMS} but the chemical composition of the surface different. P_{TMS} contained methyl groups whereas P_{APTMS} not. These results suggest that the respective chemical composition of P_{APTMS} and P_{TMS} dictated phenotypical differences, regardless of the surface roughness. Here one could speculate that this occurs

through differential protein adsorption onto the different substrates, which induces a particular cellular shape/conformation that leads to osteogenic differentiation. In that respect, it was shown that P_{APTMS} adsorbs double the amount of bovine serum albumin (BSA) compared to P_{TMS}, indicating that proteins will bind differently in quantity, and possibly quality, to the different surfaces. Further work should identify the nature of these differentially adsorbed proteins.

In *Chapter 4*, the interaction of bone marrow derived mesenchymal stromal cells (MSCs) with different calcium phosphate (CaP) ceramics was studied. **Scanning Electron Microscopy analysis revealed close contact of MSCs to β-tricalcium phosphate (β-TCP), whereas on hydroxyapatite (HA) they were loosely attached.** This differential cellular adhesion was further confirmed in a different cellular context. Twelve weeks after subcutaneous implantation of β-TCP and HA in FVB/NCrl mice (*Chapter 5*) led to marked histological differences in the ceramic pores. In HA, the tissue, mainly fibrotic, was poorly connected to the surface leaving large empty areas between the tissue and the scaffold surface. In contrast, in β-TCP, the pores were filled with connective tissue and as observed *in vitro*, cells were aligning the ceramic surface. **Furthermore, it was observed that cell alignment to β-TCP occurs as early as 7 days upon subcutaneous implantation in FVB/NCrl mice, remaining throughout the implantation period.** These cells might be osteoblast precursors that will deposit bone in β-TCP, but the origin and identity of these cells remains elusive and needs to be verified.

HA and β-TCP differ in chemical composition and microstructure, namely grain size and, consequently, roughness. In the past it was shown that β-TCP surface adsorbs fewer proteins per m^{-2} than HA [12]. Therefore, differences in MSCs attachment and spreading may again be due to differential protein binding, which was not investigated here. It was demonstrated that expression of a panel of osteogenic-related genes was higher in β-TCP than in HA, which could also possibly be linked to differences in cell conformation [10]. However, in contrast with the PLA substrates discussed before, in the case of β-TCP vs HA, CaP ceramics are soluble materials (*Chapter 4*). Therefore the release of ions from these materials will play a role in cell behaviour.

Soluble Factors

In saline physiological solution (SPS), a solution that contains only NaCl and a pH adjusted to that of human body fluids (pH=7.4), β-TCP is a more soluble ceramic than HA, hence releasing more Ca^{2+} and $PO_4{}^{3-}$. It was demonstrated that when immersed in α-MEM, Ca^{2+} and $PO_4{}^{3-}$ will precipitate on the surface of these ceramics, resulting in a new crystalline phase deposited on their surface. When serum proteins were added to α-MEM, we did not detect differences between HA and β-TCP surfaces and their respective blanks after 2 days. This suggests that serum proteins adsorbed on the surface influence nucleation and crystal formation. Although Ca^{2+} concentration ($[Ca^{2+}]$) and $PO_4{}^{3-}$ concentration ($[PO_4{}^{3-}]$) were not quantified in the medium bulk, it is possible that locally, on the surface vicinity, these concentrations are different for β-TCP and HA, due to their different dissolution rates. It was shown that bone formation induced by β-TCP and biphasic calcium phosphate sintered at 1150°C (BCP1150) was observed in contact with the ceramic surface growing towards

the pore but not on HA (*Chapter 5*). **This suggests that a specific [Ca^{2+}] is required to trigger osteogenesis and that is only found in the vicinity of the CaP ceramic surface.** Furthermore, microarray analysis revealed that β-TCP regulates inorganic cation homeostasis and in particular Ca^{2+} homeostasis in MSCs (*Chapter 4*). MSCs cultured in high [Ca^{2+}] culture medium (CaM) expressed osteoblasts-specific genes, such as OC, and furthermore, osteopontin (OP), BSP and bone morphogenetic protein 2 (BMP-2). The same genes were also highly expressed when MSCs where cultured on β-TCP vs HA (*Chapter 3*). Notably OP was upregulated 2000 fold by CaM and 40 fold by β-TCP, compared to control medium (CM) and HA, respectively, suggesting a strong effect of Ca^{2+} on regulation of OP. As mentioned before, β-TCP induced expression of BMP-2 in MSCs *in vitro* more than HA, and also induced bone formation *in vivo*, whereas HA did not. BMP-2 is a growth factor that can induce cartilage and bone formation *in vivo* [13, 14]. Furthermore it is one of the first growth factors to be induced following bone fracture [15] and is indispensable for fracture repair [16]. **It is plausible to hypothesize that Ca^{2+} dissolution from β-TCP is sufficient to induce BMP-2 expression and secretion, thus leading to bone formation *in vivo*.**

The effect of Ca^{2+} on osteogenic differentiation of several cell types is indisputable. It has been demonstrated that Ca^{2+} induces an osteogenic program in different cell types [17-19]. However, in the case of CaP ceramics, Ca^{2+} dissolution alone does not explain their bone forming ability. BCP1150 and BCP sintered at 1300°C (BCP1300), having similar solubility in SPS [12], induced a completely different cellular behaviour *in vivo* (*Chapter 5*). Tissue inside BCP1300 was loosely connected to the ceramic surface, similarly to what was observed in HA. In contrast, in BCP1150, cells were well connected to the surface and the tissue homogenously distributed in the pores. These differences in cell attachment can again, as discussed previously, be related to protein adsorption. BCP1150 adsorbs less proteins than BCP1300 (per m^2) [12], demonstrating a differential binding in terms of quantity and possibly quality. **Therefore, the effects of Ca^{2+} dissolution from CaP ceramics on osteogenesis might only be exerted when cells display a certain conformation/shape, which can partially result from differential protein adsorption.**

MSCs treated with CaM were more spread on tissue culture polystyrene than cells treated with CM, 12 hours after treatment (*Chapter 3*). In this case, a soluble factor induced conformational changes when MSCs were cultured on the same substrate. **Taken together the data suggests that Ca^{2+} might have an effect on specific cellular conformations but it is also able to induce cell conformational changes.** Here possible differences in cell shape were determinant for cell fate and soluble factors did not compensate for it. However, in *Chapter 6*, P_{APTMS} negatively regulated expression of osterix and runt related transcription factor 2 (Runx-2) in MC3T3-E1 cells when compared to PLAd, the control sample, cultured in the same culture medium. However, in contrast to BCP1150 and BCP1300, when the culture medium was supplemented with ascorbic acid (AA) and recombinant human BMP-2 (rhBMP-2), there were no differences in the expression of these two genes between MC3T3-E1 cultured on the two surfaces. **In this case, soluble factors, AA and rhBMP-2, rescued the effect exerted by the surface alone on osterix and Runx-2 expression.** It would be interesting to see, for instance, if MSCs cultured on HA in medium supplemented with Ca^{2+} would express OP, OC, BSP and/or BMP-2 at similar levels as MSCs cultured on β-TCP. Surface properties and soluble factors can be controlled *in vitro*. However, the physiological/systemic dimension is added only in *in vivo* systems, where cell types and soluble factors

can be experimentally controlled up to a certain and very limited level.

In vivo understanding of cell-materials interactions

In *Chapter 5*, CaP ceramics with different physico-chemical properties led to different cellular outcomes subcutaneously in FVB/NCrl mice. The histological features of the tissue observed in BCP1150 and BCP1300 were similar but different than those in HA and BCP1300. Tissue found inside HA and BCP1300 explants was mainly fibrotic and poorly connected to the ceramics surface. Blood vessels were observed but in general, the vessels' diameter in these ceramics seemed smaller than those found in BCP1150 and β-TCP. Also the overall amount of blood vessels seemed higher in the case of BCP1150 and β-TCP, although these parameters were not quantitatively evaluated. In *Chapter 4*, microarray analysis also revealed positive regulation of the vascular endothelial growth factor A (VEGFA) and interleukin-8 (Il-8) genes, by β-TCP in MSCs, when compared to cultures in HA, two molecules that can induce angiogenesis [20, 21]. Furthermore, cluster analysis showed enrichment of terms related with blood vessel formation in MSCs cultured on β-TCP when compared to HA. However these differences were not confirmed by PCR. A protein assay (e.g. ELISA), could further reveal whether these molecules were secreted or not. **These results suggest a pro-angiogenic effect exerted by β-TCP in BM-MSCs.**

Analysis of β-TCP and BCP1150 explants 7 days after implantation, showed that the inner regions of both material types were already perfused with functional blood vessels (*Chapter 5*). It would be interesting to know whether early blood vessel formation also occurs in BCP1300 and HA, to further comment on the possible pro-angiogenic effects of β-TCP and BCP1150 when compared to the other ceramics tested. Nonetheless, in line with these findings, the number of blood vessels was higher in β-TCP and BCP than in HA, 30 days after subcutaneous implantation in rats [22]. Furthermore, He and co-workers [23] found that the higher the HA content in a composite scaffold, the more vascularized it was eight weeks after subcutaneous implantation in rats.

In both β-TCP and BCP1150, bone was found at the periphery of the implants. This could indicate a potential positive role for nutrients and oxygen supply on bone formation, where at least early after implantation, cells have more access. The effect of VEGF on bone formation and repair is well established [24, 25] and its incorporation into CaP ceramics has shown to be beneficial to bone formation [26]. However, addition of VEGF to β-TCP at the time of implantation did not have any detectable consequences on bone formation after 12 weeks. Another possible explanation for the fact that bone was only found at the periphery of the explant could be related with the excessively high $[Ca^{2+}]$ in the centre of the blocks that made the environment non permissive for osteogenic differentiation. Proliferation and osteogenic differentiation of osteoprogenitor cells are $[Ca^{2+}]$ dependent [18]. It could be that in the case of mouse cells, $[Ca^{2+}]$ at the periphery of the implant is optimal for osteogenesis. In the past, however, bone formation was induced by CaP ceramics in the centre of these materials and not at the periphery (using a different animal model though) [27, 28]. To further understand this "inhomogeneous" osteoinductive effect throughout the material, it would be interesting to use the *in vitro* model reported in *Chapter 4* to test whether cells at the periphery of the scaffold express different levels of osteogenic markers than cells at the centre.

Although bone tissue was found in both BCP1150 and β-TCP, the number of β-TCP explants with bone was higher than that of BCP1150, but there was no statistical significant difference in terms of bone amounts between the two ceramic types. The quality of the bone found in BCP1150 and β-TCP was similar, with osteocytes and bone lining cells observed in both cases. **However bone marrow cavities were occasionally found in β-TCP and never in BCP1150, suggesting that bone in β-TCP was in a later developmental stage than the one found in BCP1150.**

Physiological responses to osteoinductive stimuli are genetically determined (*Chapter 5*). Eleven inbred mouse strains were tested for their responsiveness to CaP ceramics and rhBMP-2 and only two were susceptible to develop bone formation induced by β-TCP. Although all strains were prone to rhBMP-2 bone induction, amounts of bone formation also varied among the strains. It would be interesting to investigate why such differences in genetic background led to differences in bone formation. Through QTL analysis [29], for instance, genetic loci related with osteoinduction could be potentially identified [30]. That would help to understand the chances of success with β-TCP among human patients to heal bone defects or even develop therapies that specifically deliver or target a gene or a set of genes that have a certain function for bone development and formation.

Osteoinduction by CaP: proposed mechanism

Chapters 2, 3, 4 and 5 are related with bioactivity of CaP ceramics. Physico-chemical properties can dictate the lower or higher osteoinductive capacity of these materials. Based on the findings of this thesis and on the hypothesis here generated, a schematic mechanism for osteoinduction by CaP ceramics is proposed in figure 1.

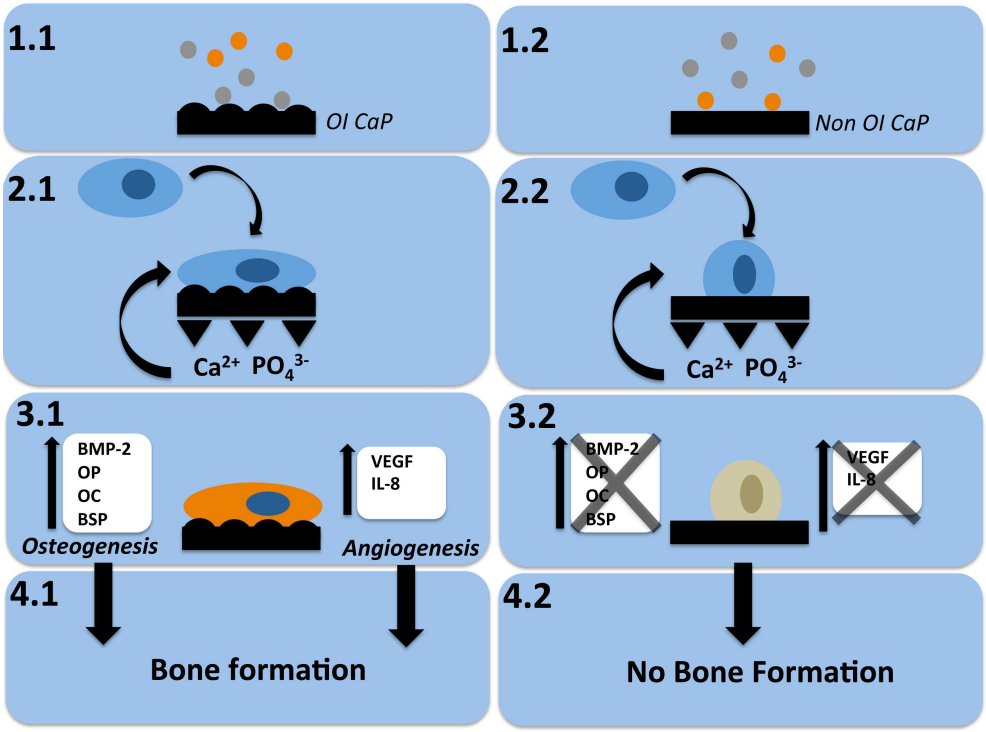

Figure 1: Schematic representation of the hypothetical physico-chemico-biological mechanism underlining a CaP ceramic (non)osteoinductivity. The surface physico-chemical properties, such as roughness or hydrophobicity/hydrophilicity, account for a specific protein adsorption (1.1 and 1.2). When cells in the body of the host reach the material, they will align to the surface according to its properties, adopting a specific cellular conformation (2.1 and 2.2). This cellular conformation will dictate whether the cell is permissive (3.1) or not (3.2) to the pro-osteogenic and pro-angiogenic effects of Ca^{2+} and possibly PO_4^{3-} released from the CaP during chemical or cellular degradation. Expression of osteoinductive growth factors (BMP-2) and components of the bone extracellular matrix (OP, OC, BSP) together with the effects of an enhanced vascularization will support bone formation (4.1). A CaP that does not induce a specific cellular conformation, even if it possesses a similar degree of solubility to a CaP that does, will not support bone formation (BCP1150 vs BCP1300) (4.2). On the other hand, if both CaPs support a specific cellular conformation but have different degrees of solubility, bone formation will start earlier in the more soluble ceramic (β-TCP vs BCP1150).

References

[1] Calori GM, Mazza E, Colombo M, Ripamonti C. Injury. 2011;42, Suppl 2:S56-63.
[2] De Long WG, Einhorn TA, Koval K, McKee M, Smith W, Sanders R, Watson T. J Bone Joint Surg Am. 2007;89A(3):649-58.
[3] Giannoudis PV, Dinopoulos H, Tsiridis E. Injury. 2005;36 Suppl 3:S20-7.
[4] Habal M. and Reddi A. (eds). Bone grafts & bone substitutes. W. B. Saunders, New York, 1992.
[5] Damien CJ, Parsons JR. J Appl Biomater. 1991;2(3):187-208.
[6] Kumar G, Tison CK, Chatterjee K, Pine PS, McDaniel JH, Salit ML, Young MF, et al. Biomaterials. 2011;32(35):9188-96.
[7] Kilian KA, Bugarija B, Lahn BT, Mrksich M. Proc Natl Acad Sci. 2010;107(11):4872-7.
[8] Oh S, Brammer KS, Li YSJ, Teng D, Engler AJ, Chien S, Jin S. Proc Natl Acad Sci. 2009;106(7):2130-5.
[9] Dalby MJ, Andar A, Nag A, Affrossman S, Tare R, McFarlane S, Oreffo RO. J R Soc Interface. 2008;5(26):1055-65.
[10] McBeath R, Pirone DM, Nelson CM, Bhadriraju K, Chen CS. Dev Cell. 2004;6(4):483-95.
[11] Unadkat HV, Hulsman M, Cornelissen K, Papenburg BJ, Truckenmueller RK, Post GF, Uetz M, et al. Proc Natl Acad Sci USA. 2011;108(40):16565-70.
[12] Yuan H, Fernandes H, Habibovic P, de Boer J, Barradas AM, de Ruiter A, Walsh WR, et al. Proc Natl Acad Sci USA. 2010;107(31):13614-9.
[13] Urist MR. Science. 1965;150(3698):893-9.
[14] Urist MR, Iwata H. Journal of Theoretical Biology. 1973;38(1):155-67.
[15] Gerstenfeld LC, Cullinane DM, Barnes GL, Graves DT, Einhorn TA. Journal of cellular biochemistry. 2003;88(5):873-84.
[16] Tsuji K, Bandyopadhyay A, Harfe BD, Cox K, Kakar S, Gerstenfeld L, Einhorn T, et al. Nat Genet. 2006;38(12):1424-9.
[17] Honda Y, Anada T, Kamakura S, Nakamura M, Sugawara S, Suzuki O. Biochem Biophys Res Commun. 2006;345(3):1155-60.
[18] Chai YC, Roberts SJ, Schrooten J, Luyten FP. Tissue Eng Part A. 2010;17(7-8):1083-97.
[19] Chai YC, Roberts SJ, Desmet E, Kerckhofs G, van Gastel N, Geris L, Carmeliet G, et al. Biomaterials. 2012;33(11):3127-42
[20] Li A, Dubey S, Varney ML, Dave BJ, Singh RK. J Immunol. 2003;170(6):3369-76.
[21] Ferrara N, Gerber H-P, LeCouter J. Nat Med. 2003;9(6):669-76.
[22] Ghanaati S, Barbeck M, Detsch R, Deisinger U, Hilbig U, Rausch V, Sader R, et al. Biomed Mater. 2012;7(1):015005
[23] He J, Genetos DC, Leach JK. Tissue Eng Part A. 2010;16(1):127-37.
[24] Zelzer E, Olsen BR. Current Topics in Developmental Biology: Academic Press; 2005;65:169-87
[25] Street J, Bao M, deGuzman L, Bunting S, Peale FV, Ferrara N, Steinmetz H, et al. Proc Natl Acad Sci. 2002;99(15):9656-61.
[26] Wernike E, Montjovent MO, Liu Y, Wismeijer D, Hunziker EB, Siebenrock KA, Hofstetter W, et al. Eur Cells Mater. 2010;19:30-40.
[27] Habibovic P, Yuan H, Vandervalk C, Meijer G, van Blitterswijk C, de Groot K. Biomaterials. 2005;26(17):3565-75.
[28] Habibovic P, de Groot K. J Tissue Eng Regen Med. 2007;1(1):25-32.
[29] Keane TM, Goodstadt L, Danecek P, White MA, Wong K, Yalcin B, Heger A, et al. Nature. 2011;477(7364):289-94.
[30] Hunter KW, Crawford NPS. Annu Rev Genet. 2008;42(1):131-41.

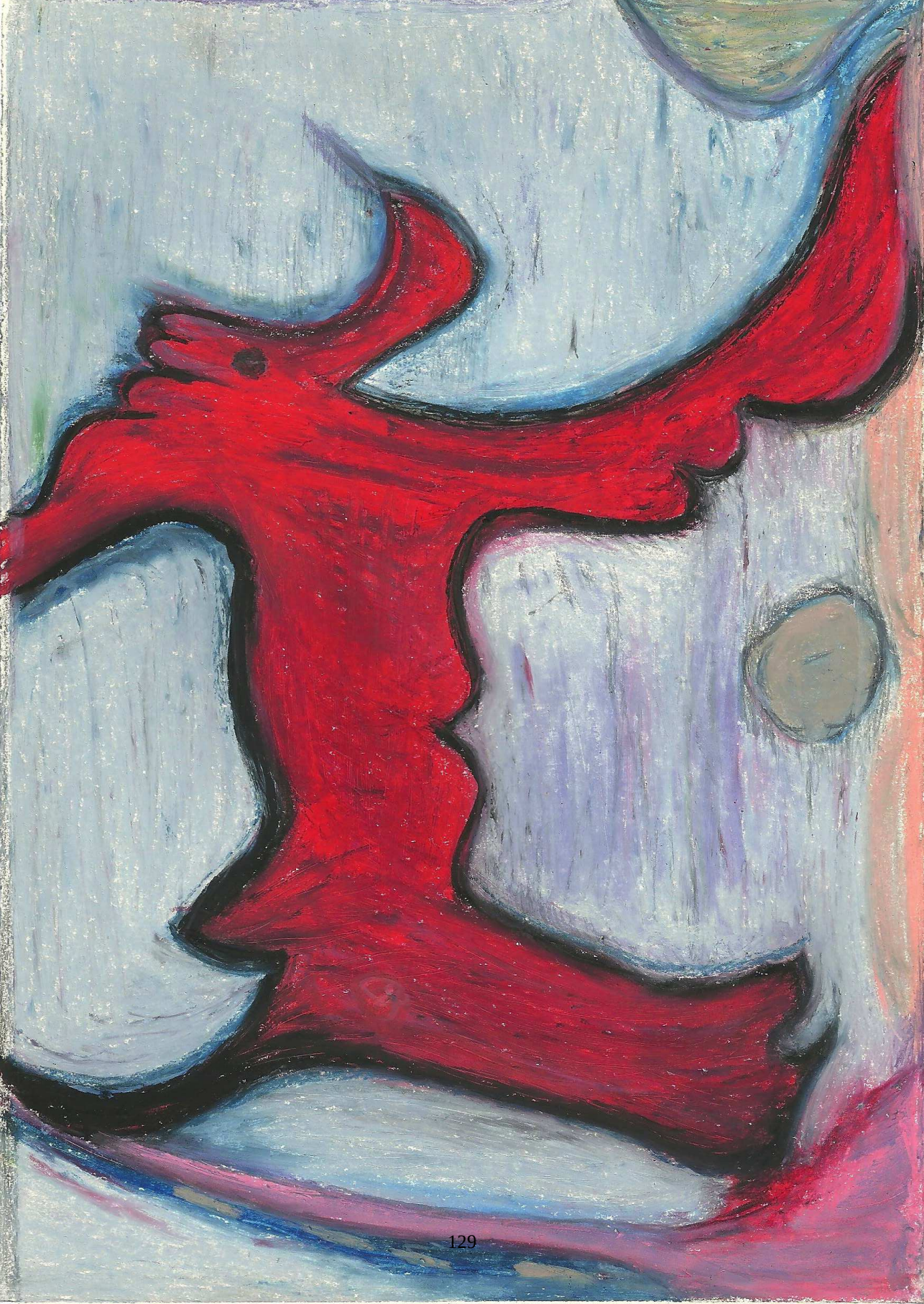

Biosketch

Ana was born on the 9^{th} February 1984 in Vila Viçosa, Portugal. She lived there with her parents and younger sisters, Beatriz and Teresa, until she graduated from Liceu Públia Hortênsia de Castro, at the age of 18. She then moved to Lisbon to enrol the Biomedical Engineering BSc/MSc programme at Instituto Superior Técnico but she spent the last academic year of her MSc at the University of Twente, as an ERASMUS student. During this period she performed research at the lab of Prof. Clemens van Blitterswijk, under supervision of Prof. Jan de Boer, the outcome of which resulted in her MSc thesis, entitled "A Bioluminescent imaging system to detect nutrient availability in Tissue Engineering".

In January 2008 she joined the Department of Tissue Regeneration as a PhD student, with Prof. Jan de Boer. During the past 4 years, she explored the mechanisms occurring at the interface of stem cells and biomaterials for bone regeneration, the results of which are described in this thesis.

Ana currently lives in Enschede with Hugo Fernandes, to whom she is married since 11^{th} January 2012.

List of Publications

Ana M.C. Barradas, Huipin Yuan, Johan van der Stok, Bach Le Quang, Hugo Fernandes, Anindita Chaterja, Marieke C.H. Hogenes, Kathy Shultz, Leah Rae Donahue, Clemens A. van Blitterswijk, Jan de Boer; *The influence of genetic factors on the osteoinductive potential of calcium phosphate ceramics in mice*; Biomaterials *(accepted for publication)*

Ana M.C. Barradas, Kristina Lachmann, Gregor Hlawacek, Cathelijne Frielink, Roman Truckenmüller, Otto C. Boerman, Raoul van Gastel, Henk Garritsen, Michael Thomas, Lorenzo Moroni, Clemens A. van Blitterswijk, Jan de Boer; *Surface modifications by gas plasma control osteogenic differentiation of MC3T3-E1 cells*; Acta Biomaterialia *(accepted for publication)*

Ana M.C. Barradas, Hugo Fernandes, Nathalie Groen, Yoke Chin Chai, Jan Schrooten, Jeroen van de Peppel, JPTM van Leeuwen, Clemens A. van Blitterswijk, Jan de Boer; *A calcium-induced signalling cascade leading to osteogenic differentiation of human bone marrow-derived mesenchymal stromal cells*; Biomaterials; 2012; 33(11):3205-15

Ana M.C. Barradas, Huipin Yuan, Clemens A. van Blitterswijk, Pamela Habibovic; *Osteoinductive biomaterials: current knowledge of properties, experimental models and biological mechanisms*; Eur Cell Mater; 2011; 21:407-29

Huipin Yuan, Hugo Fernandes, Pamela Habibovic, Jan de Boer, **Ana M.C. Barradas**, Ad de Ruiter, William R Walsh, Clemens A. van Blitterswijk, de Bruijn JD; *Osteoinductive ceramics as a synthetic alternative to autologous bone grafting*; Proc Natl Acad Sci USA; 2010;107(31):13614-9

Ferry P Melchels, **Ana M.C. Barradas**, Clemens A van Blitterswijk, Jan de Boer, Jan Feijen, Dirk W Grijpma; *Effects of the architecture of tissue engineering scaffolds on cell seeding and culturing*; Acta Biomater; 2010;6(11):4208-17

Jun Liu, **Ana M.C. Barradas**, Hugo Fernandes, Frank Janssen, Bernke Papenburg, Dimitris Stamatialis, Anton Martens, Clemens A. van Blitterswijk, Jan de Boer; *In vitro and in vivo bioluminescent imaging of hypoxia in tissue-engineered grafts*; Tissue Eng Part C Methods; 2010;16(3):479-85

Bernke J. Papenburg, Jun Liu, Gustavo A. Higuera, **Ana M.C. Barradas**, Jan de Boer, Clemens A. van Blitterswijk, Mathias Wessling, Dimitris Stamatialis; *Development and analysis of multi-layer scaffolds for tissue engineering*; Biomaterials; 2009;30(31):6228-39

Manuscripts submitted for publication

Ana M.C. Barradas, Veronica Monticone, Marc Hulsman, Charlène Danoux, Hugo Fernandes, Zeinab Thamasebibirgani, Florence Barrère-de Groot, Huipin Yuan, Marcel Reinders, Pamela Habibovic, Clemens van Blitterswijk, Jan de Boer; *Molecular analysis of biomaterial-driven osteogenesis in human mesenchymal stromal cells*

Anandkumar Nandakumar, **Ana M.C. Barradas**, Jan de Boer, Lorenzo Moroni, Clemens van Blitterswijk, Pamela Habibovic; *Combining technologies to create bioactive hybrid scaffolds for bone tissue engineering*

Anindita Chatterjea, **Ana M.C. Barradas**, Henk Garritsen, Huipin Yuan, Nicolas Rivron, Auke Renard, Clemens A. van Blitterswijk, Jan de Boer; *Cell aggregation enhances bone formation by human mesenchymal stromal cells*

Hemant V. Unadkat, Nathalie Groen, Joyce Doorn, Bart Fischer, **Ana M.C. Barradas**, Marc Hulsman, Lorenzo Moroni, Marcel J. T. Reinders, Clemens A. van Blitterswijk, Jan de Boer; *High content imaging as a novel tool for automated analysis of biomaterial-induced cellular responses*

Patent Application

University of Twente; Jan de Boer, **Ana Margarida Cravo Barradas**; Mouse models for osteoinduction and heterotopic ossification; EP12152861.6

Acknowledgements

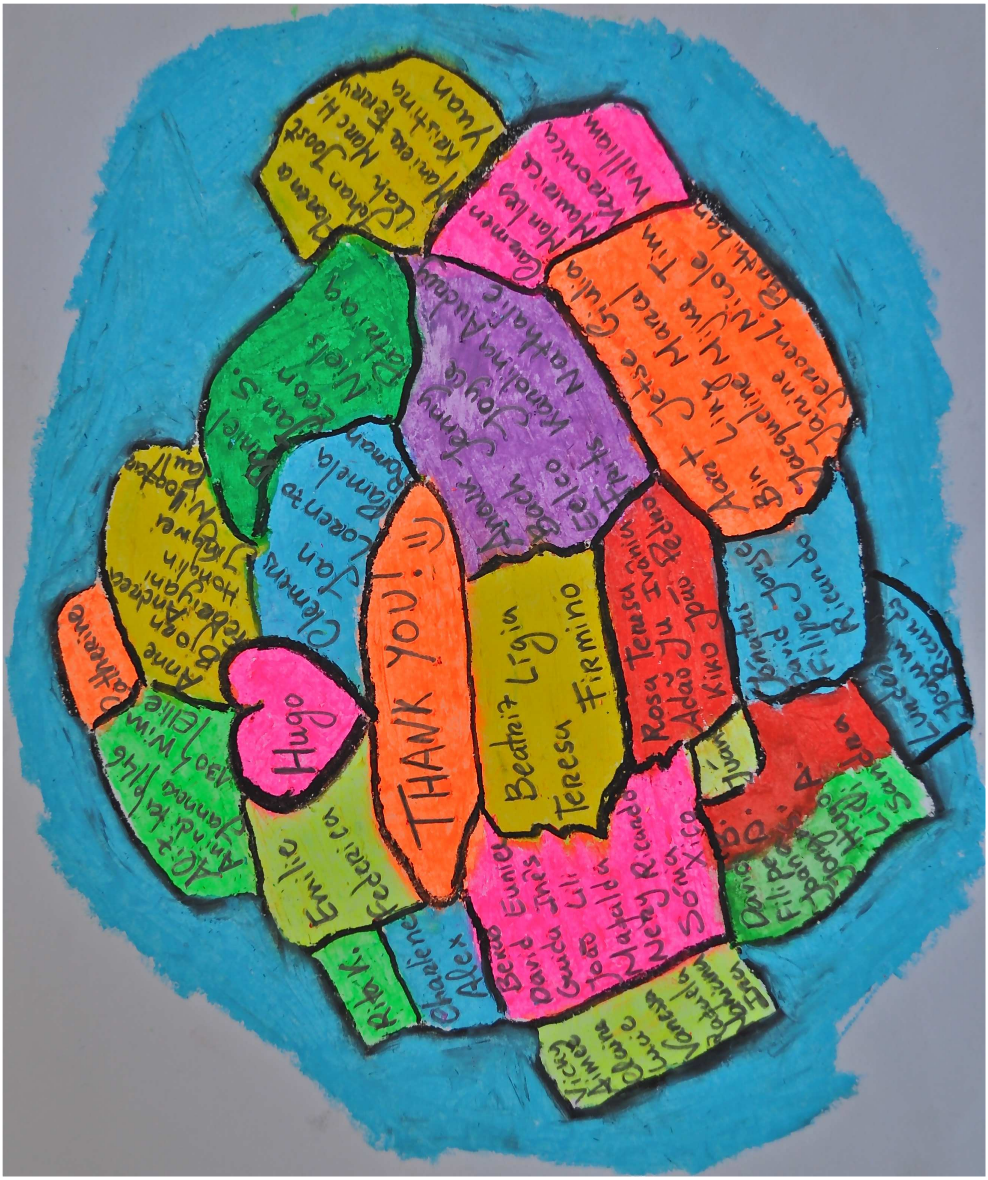
THANK YOU!
Hugo